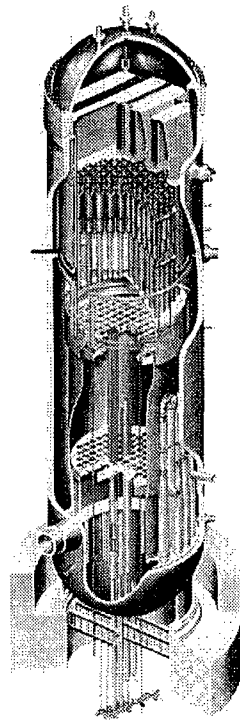


BWVRVIP-99NP-A, BWR Vessel and Internals Project

Crack Growth Rates in Irradiated Stainless Steels in BWR Internal Components



NON-PROPRIETARY INFORMATION

NOTICE: This report contains the non-proprietary information that is included in the proprietary version of this report. The proprietary version of this report contains proprietary information that is the intellectual property of BWVRVIP utility members and EPRI. Accordingly, the proprietary report is available only under license from EPRI and may not be reproduced or disclosed, wholly or in part, by any licensee to any other person or organization.

BWRVIP-99NP-A: BWR Vessel and Internals Project

Crack Growth Rates in Irradiated Stainless Steels in
BWR Internal Components

1016566NP

Final Report, January 2009

EPRI Project Manager
R. Pathania

DISCLAIMER OF WARRANTIES AND LIMITATION OF LIABILITIES

THIS DOCUMENT WAS PREPARED BY THE ORGANIZATION(S) NAMED BELOW AS AN ACCOUNT OF WORK SPONSORED OR COSPONSORED BY THE BWR VESSEL AND INTERNALS PROJECT (BWRVIP) AND ELECTRIC POWER RESEARCH INSTITUTE, INC. (EPRI). NEITHER BWRVIP, EPRI, ANY MEMBER OF EPRI, ANY COSPONSOR, THE ORGANIZATION(S) BELOW, NOR ANY PERSON ACTING ON BEHALF OF ANY OF THEM:

(A) MAKES ANY WARRANTY OR REPRESENTATION WHATSOEVER, EXPRESS OR IMPLIED, (I) WITH RESPECT TO THE USE OF ANY INFORMATION, APPARATUS, METHOD, PROCESS, OR SIMILAR ITEM DISCLOSED IN THIS DOCUMENT, INCLUDING MERCHANTABILITY AND FITNESS FOR A PARTICULAR PURPOSE, OR (II) THAT SUCH USE DOES NOT INFRINGE ON OR INTERFERE WITH PRIVATELY OWNED RIGHTS, INCLUDING ANY PARTY'S INTELLECTUAL PROPERTY, OR (III) THAT THIS DOCUMENT IS SUITABLE TO ANY PARTICULAR USER'S CIRCUMSTANCE; OR

(B) ASSUMES RESPONSIBILITY FOR ANY DAMAGES OR OTHER LIABILITY WHATSOEVER (INCLUDING ANY CONSEQUENTIAL DAMAGES, EVEN IF BWRVIP, EPRI OR ANY EPRI REPRESENTATIVE HAS BEEN ADVISED OF THE POSSIBILITY OF SUCH DAMAGES) RESULTING FROM YOUR SELECTION OR USE OF THIS DOCUMENT OR ANY INFORMATION, APPARATUS, METHOD, PROCESS, OR SIMILAR ITEM DISCLOSED IN THIS DOCUMENT.

ORGANIZATION(S) THAT PREPARED THIS DOCUMENT

General Electric Nuclear Energy

NON-PROPRIETARY INFORMATION

NOTICE: This report contains the non-propriety information that is included in the proprietary version of this report. The proprietary version of this report contains proprietary information that is the intellectual property of BWRVIP utility members and EPRI. Accordingly, the proprietary report is available only under license from EPRI and may not be reproduced or disclosed, wholly or in part, by any Licensee to any other person or organization.

NOTE

For further information about EPRI, call the EPRI Customer Assistance Center at 800.313.3774 or e-mail askepri@epri.com.

Electric Power Research Institute, EPRI, and TOGETHER...SHAPING THE FUTURE OF ELECTRICITY are registered service marks of the Electric Power Research Institute, Inc.

Copyright © 2009 Electric Power Research Institute, Inc. All rights reserved.

CITATIONS

This report was prepared by

Electric Power Research Institute
3420 Hillview Avenue
Palo Alto, CA 94304

Principal Investigator
R. Pathania

This report describes research sponsored by the Electric Power Research Institute (EPRI) and its participating BWRVIP members.

The report is a corporate document that should be cited in the literature in the following manner:

BWRVIP-99NP-A: BWR Vessel and Internals Project, Crack Growth Rates in Irradiated Stainless Steels in BWR Internal Components. EPRI, Palo Alto, CA: 2008. 1016566NP.

This report is based on the following previously published report:

BWRVIP-99: BWR Vessel and Internals Project, Growth Rates in Irradiated Stainless Steels in BWR Internal Components. EPRI, Palo Alto, CA: 2001. 1003018.

Prepared by

General Electric Nuclear Energy
175 Curtner Avenue
San Jose, California 95125

General Electric Nuclear Energy Principal Investigators
R. B. Davis
R. M. Horn

General Electric Corporate Research and Development Laboratory Principal Investigators
P. L. Andresen
J. L. Nelson

REPORT SUMMARY

The BWR Vessel and Internals Project (BWRVIP) has developed methodologies to evaluate crack growth in internal components of stainless steel and nickel-base alloys in the BWR vessel. One BWRVIP report—BWRVIP-14—developed an approach to evaluate crack growth by intergranular stress corrosion cracking in austenitic stainless steel core shrouds exposed to a limited amount of neutron irradiation. Subsequently another report—BWRVIP-99—was prepared to provide a crack growth methodology applicable to irradiated BWR stainless steel internal components for fluence levels from 5×10^{20} n/cm² to 3×10^{21} n/cm², serving as an extension of BWRVIP-14 for this irradiation regime. This report (BWRVIP-99-A) incorporates changes proposed by BWRVIP in response to U.S. Nuclear Regulatory Commission (NRC), Requests for Additional Information, recommendations in the NRC Safety Evaluation, and other necessary revisions identified since the previous publication of the report. All changes are marked with margin bars. In accordance with the NRC request, the Safety Evaluation is included here as an appendix: and the report number includes an “A” indicating the version of the report accepted by the NRC staff.

Background

The NRC has accepted the approach proposed in BWRVIP-14 (EPRI report TR-105873), as documented in the NRC initial and final safety evaluation reports. However, the NRC limited the application of the BWRVIP-14 crack growth correlation to fluences of less than 5×10^{20} n/cm². As plants age, certain locations in the mid-plane of the core shroud experience fluence levels exceeding this limit. With increasing fluence, the materials become susceptible to irradiation assisted stress corrosion cracking (IASCC). Consequently, there is a need to develop a method to evaluate crack growth in irradiated stainless steels at fluence levels above 5×10^{20} n/cm².

Objective

To provide crack growth rates that are applicable to BWR internal components of stainless steel irradiated to fluence levels of 5×10^{20} n/cm² to 3×10^{21} n/cm².

Approach

Investigators first reviewed the mechanistic basis for the effects of irradiation on crack growth behavior. Next, they assembled and analyzed data from crack growth measurements on core shrouds in several BWRs. They also summarized the available laboratory data on crack growth in irradiated stainless steels in BWR environments. Their third step was to discuss the significant role of irradiation-induced stress relaxation, which tends to counteract the effect of irradiation on IASCC susceptibility. Based on this collective understanding, investigators developed crack growth curves that can be applied under normal water chemistry (NWC) and hydrogen water chemistry (HWC) conditions in the fluence range of 5×10^{20} n/cm² to 3×10^{21} n/cm².

Results

A review of the field data indicates that crack growth rates decrease as a function of core shroud thickness. This is consistent with the shape of the stress intensity (**K**) distribution developed for BWRVIP-14, where the **K** first increases and then decreases as a function of thickness. This finding supports the decreasing stress intensity distribution currently recommended for use in evaluating shroud welds that experience fluence levels below 5×10^{20} n/cm².

Screening of the laboratory crack growth data eliminated data not applicable to stress and chemistry conditions relevant to BWR core shrouds. The **K**-dependent crack growth curves developed for this project provide a reasonable bound to laboratory data under NWC and HWC conditions. It should be noted that the HWC curve was a factor of three lower than the NWC curve. This report includes significant discussion of the basis for data screening as well as additional crack growth rate data from unirradiated materials that further strengthen the proposed curves. The report recommends the most appropriate **K**-distribution consistent with the field crack growth data. The report concludes with an example evaluation of flaw growth in a core shroud under NWC and HWC conditions.

EPRI Perspective

This BWRVIP report provides the technical basis for evaluation of flaw growth in core shroud welds in the fluence range of 5×10^{20} n/cm² to 3×10^{21} n/cm². Such information will be valuable for plants where core shroud welds have exceeded a fluence of 5×10^{20} n/cm², or may do so in the future as they extend operation from 40 to 60 years.

Keywords

BWR Vessel and Internals Project
Crack growth rates
Irradiated stainless steel
BWR
Core shroud welds

ACKNOWLEDGMENTS

The members of the BWRVIP Focus Group on Irradiated Crack Growth, listed below, are gratefully acknowledged for their efforts which led to the successful completion of the original version of this document.

Robin Dyle, SNOC
George Inch, NIMO
Lew Willertz, PP&L
Guy Deboo, Exelon
Larry Yemma, CP&L
John Wilson, Amergen
Jai Brihmadessam, Entergy
Bob Carter, EPRI,
Raj Pathania, EPRI,
Larry Steinert, EPRI

General Electric Nuclear Energy Principal Investigators:

R. B. Davis
R. M. Horn

General Electric Corporate Research and Development Laboratory Principal Investigators:

P. L. Andresen
J. L. Nelson

RECORD OF REVISIONS

Revision Number	Revisions
BWRVIP-99	Original Report (1003018)
BWRVIP-99-A	<p data-bbox="451 737 1398 940">This report (BWRVIP-99-A) is based on a previous report (BWRVIP-99) that was reviewed by U.S. Nuclear Regulatory Commission (NRC). It the incorporates changes proposed by BWRVIP in response to NRC Requests for Additional Information, recommendations in the NRC Safety Evaluation, and other necessary revisions identified since the previous publication of the report. All changes, except corrections to typographical errors, are marked with margin bars. Non-essential format changes were made to comply with current EPRI publication Guidelines.</p> <p data-bbox="451 982 948 1010">Appendix A added: NRC Safety Evaluation.</p> <p data-bbox="451 1052 899 1079">Appendix B added: Details of revisions.</p>

EXECUTIVE SUMMARY

The purpose of this report is to provide a crack growth methodology that is applicable to irradiated BWR stainless steel internal components for fluence levels from 5×10^{20} to 3×10^{21} n/cm². It serves as an extension of BWRVIP-14 to this regime of irradiation. This report (BWRVIP-99-A) is based on a previous report (BWRVIP-99) that was reviewed by U.S. Nuclear Regulatory Commission (NRC). It incorporates changes proposed by BWRVIP in response to NRC Requests for Additional Information, recommendations in the NRC Safety Evaluation, and other necessary revisions identified since the previous publication of the report. All changes are marked with margin bars. The basis for these rates requires significant background and understanding of the effects of irradiation on stainless steel. It also requires information on measured crack growth behavior of irradiated materials tested in laboratories and of actual core components in operating plants. To convey this understanding and to provide the disposition crack growth rates, the report covers several topics in detail.

The report first reviews the understanding of the irradiation assisted stress corrosion cracking phenomena along with its direct relationship to stress corrosion cracking of austenitic structural materials. All structural materials exhibit an inherent SCC susceptibility in high temperature water. Specifically, for stainless steels, cold work, sensitization, neutron fluence, corrosion potential, water purity, temperature, and loading all affect crack growth rates. Additionally, there is a large benefit of changing to low potential conditions, which leads to a significant reduction in crack growth rate.

Content Deleted - EPRI Proprietary Information

The next sections present the existing proprietary crack growth rate data that has been measured in irradiated materials, tested in BWR-type high temperature water environments by GENE or in the Halden Research Test Reactor. The data, screened to remove non-representative measurements, are later used as the basis for two disposition curves, one for NWC environments and one for HWC environments. These curves are based on bounding the data while maintaining a stress intensity dependence that is consistent with the crack growth behavior of other austenitic materials. The report includes significant discussion on the basis for data screening as well as additional crack growth rate data from un-irradiated materials that provide further strength to the proposed curves. The report also provides the basis for incorporating radiation-induced stress relaxation into the evaluation methodology. The factor is validated through comparison with the field data. The report concludes with an example evaluation.

CONTENTS

1 INTRODUCTION AND BACKGROUND	1-1
2 UNDERSTANDING OF IRRADIATED CRACK GROWTH	2-1
2.1 Major Findings of the Last Fifteen Years of IASCC Research	2-2
2.2 The Beneficial Effect of Reduced Corrosion Potential on the Stress Corrosion Crack Growth Rates of Irradiated Stainless Steel	2-3
2.3 Status of Current Understanding of Irradiated Crack Growth Rate Behavior	2-4
3 FIELD EVALUATIONS OF CRACK GROWTH RATES IN HIGH FLUENCE STAINLESS STEEL WELDMENTS BASED ON ULTRASONIC MEASUREMENTS	3-1
3.1 Background of Field Data Approach	3-1
3.2 Actual Plant Data.....	3-1
3.2.1 KKM Weld 11 (H4): 1994 through 1995 (from BWRVIP-14)	3-1
3.2.2 Susquehanna Unit 1 and Unit 2 Weld H4: 1995 through 2000.....	3-2
3.2.3 Peach Bottom Unit 3 Weld H4: 1995 through 1999.....	3-3
3.2.4 Brunswick Unit 2 Weld H4: 1995 through 1999.....	3-3
3.3 Summary of Field Data.....	3-3
4 SUMMARY OF IRRADIATED CRACK GROWTH RATE DATA FROM LABORATORY TESTING OF IRRADIATED STAINLESS STEEL MATERIALS	4-1
4.1 GE/JAPEIC Irradiated Crack Growth Testing (GENE-VNC)	4-1
4.1.1 CT Tests-Specimens	4-2
4.1.2 CT Tests-Experimental.....	4-3
4.1.3 Notched 4-Point Bend Tests-Specimens.....	4-3
4.1.4 Notched 4-Point Bend Tests-Experimental	4-4
4.2 HALDEN Irradiated Crack Growth Tests.....	4-5
4.2.1 CT Specimens	4-5
4.2.2 Experimental.....	4-6
4.3 Overview of Other Data.....	4-7

4.4 Summary of Relevant Data	4-8
5 IMPORTANCE OF PLASTICITY AND OTHER TESTING FACTORS ON LABORATORY TEST DATA	5-1
5.1 Background	5-1
5.2 Application to Unirradiated Materials.....	5-3
5.3 Application to Irradiated Materials	5-3
5.4 IASCC Data from Halden Test Reactor.....	5-5
5.5 Nine Mile Point Unit 1 In-Core IASCC Growth Rate Data	5-6
6 SUMMARY OF UN-IRRADIATED STAINLESS STEEL DATA RELEVANT TO IRRADIATED BEHAVIOR.....	6-1
6.1 Introduction	6-1
6.2 Experiments	6-2
6.3 Results and Discussion.....	6-3
6.4 Relevance to IASCC and Supporting Evidence for Corrosion Potential Benefits	6-7
6.5 Summary.....	6-7
7 DEPENDENCY OF SCC ON STRESS INTENSITY AND THE ROLE OF RADIATION CREEP RELAXATION	7-1
7.1 Background	7-1
7.2 Observed K Dependencies in Unirradiated and Irradiated Data	7-2
7.3 Summary of Stress Intensity Dependency	7-3
7.4 Radiation Creep Relaxation	7-3
7.5 Proposed Stress Intensity Dependency and Weld Residual Stress Relaxation Levels.....	7-4
8 PROPOSED DISPOSITION RATES AS A FUNCTION OF FLUENCE AND WATER CHEMISTRY	8-1
8.1 Review of Approach to Disposition Curves	8-1
8.2 Applicable Range of Fluence	8-2
8.3 Proposed Disposition Curves	8-2
8.3.1 Normal Water Chemistry (NWC)	8-2
8.3.2 Hydrogen Water Chemistry (HWC)	8-3
8.4 Comparison with Field derived data.....	8-3
8.5 Summary	8-4

9 EXAMPLE EVALUATIONS OF CRACK GROWTH ASSESSMENT: CORE SHROUD MATERIAL IRRADIATED TO A FLUENCE BETWEEN 5×10^{20} N/CM² AND 3×10^{21} N/CM²	9-1
9.1 Evaluation Procedure Review	9-1
9.2 Examples of Crack Growth Depth Predictions in a Irradiated Core Shroud H4 Weld for NWC, Action Level 1 Operating Conditions	9-2
9.3 Examples of Crack Growth Depth Predictions in a Irradiated Core Shroud H4 Weld for HWC, Action Level 1 Operating Conditions	9-2
10 SUMMARY AND CONCLUSIONS	10-1
11 REFERENCES	11-1
A NRC SAFETY EVALUATION	A-1
B RECORD OF REVISIONS	B-1

LIST OF FIGURES

Figure 2-1 Illustration of engineering factors (stress, environment, and microstructure), underlying fundamental phenomena (mass transport, oxide rupture, and repassivation), and primary effects of radiation on crack advance processes	2-5
Figure 2-2 Dependence of IASCC on fast neutron fluence for creviced control blade sheath in high conductivity BWRs [2-10].....	2-5
Figure 2-3 Dependence of IASCC on fast neutron fluence in slow strain tests at $3.7 \times 10^{-7}/s^{-1}$ on pre-irradiated type 304 stainless steel in 288°C water [2-12]. The inset shows the effect of corrosion potential via changes in dissolved oxygen at a fluence of $2 \times 10^{21} n/cm^2$	2-6
Figure 2-4 Comparison between observed [2-24] and predicted time-to-failure for the effect of fast neutron fluence on pre-irradiated type 304 stainless steel tested at constant load in the laboratory in oxygen saturated, 288°C water	2-6
Figure 2-5 The large points show the effect of corrosion potential on the crack growth rate of unsensitized stainless steels in very high purity, 288°C water [2-13, 2-14]. The smaller points are for sensitized type 304 stainless steel under the same test conditions. The curves represent the predicted response of sensitized type 304 stainless steel for different water purity levels.....	2-7
Figure 2-6 Observed and predicted relationships of crack growth rate vs. Corrosion potential for furnace sensitized type 304 stainless steel at a constant K of $\approx 27.5 MPa\sqrt{m}$. The observed data were obtained in water of conductivity between 0.1 to 0.3 $\mu S/cm$. The predicted relationships show the sensitivity of the crack growth rate to changes in combinations of corrosion potential and water purity (0.1 to 0.5 $\mu S/cm$) [2-9, 2-10, 2-11]. The circled points above 0.1 V_{she} (and at $-0.42 V_{she}$) were obtained in-core in a BWR or under proton irradiation simulating BWR core exposure	2-8
Figure 2-7 Compositional profiles across grain boundaries obtained by dedicated STEM from a low strain, high purity 348 stainless steel swelling tube specimen irradiated to $3.4 \times 10^{21} n/cm^2$ at 288°C in a BWR [2-25]. The depletion of Cr and Fe, and enrichment of Ni and Si are characteristic of irradiated stainless steels	2-9
Figure 2-8 Comparison of predicted and observed crack length vs. time for fracture mechanics specimens of furnace sensitized type 304 stainless steel in the peak flux region of the core and in the recirculation line of a commercial BWR [2-1 through 2-3]. The high corrosion potential in core caused significantly higher crack growth rates than in the specimen exposed in the recirculation system (neutron fluence did not reach consequential levels early in core exposure). Specimens were pre-cracked and wedge loaded to an initial stress intensity factor of $27.5 MPa\sqrt{m}$	2-10

Figure 2-9 Comparison between observed and predicted crack growth rate vs. solution conductivity for statically loaded type 316L and sensitized type 304 stainless steels in 288°C water containing 200 ppb O ₂ [2-16 through 2-18].....	2-11
Figure 2-10 The similarity in the effects of solution conductivity for unirradiated and irradiated BWR components is shown in the field correlations of the core component cracking behavior vs. average plant water purity for (a) stainless steel IRM/SRM instrumentation dry tubes, (b) creviced stainless steel safe ends, and (c) creviced inconel 600 shroud head bolts, which also shows the predicted response vs. conductivity [2-11, 2-26]	2-12
Figure 2-11 Effect of temperature on stress corrosion crack growth rate of stainless steel cool worked by 20% at +140°C and tested in H ₂ -deaerated, near-theoretical purity water [2-13, 2-14].....	2-13
Figure 2-12 Effect of temperature on SCC of irradiated stainless steel in PWR water [2-27]	2-14
Figure 3-1 Comparison of the 1994 and 1995 KKM UT determined crack depths of the different ID indications in weld 11 (H4). (shroud thickness of 31.2 mm equivalent to 1.25 inches).....	3-4
Figure 3-2 Average crack growth rates plotted as a function of azimuthal location along with the predicted fluence levels for KKM weld 11	3-5
Figure 3-3 Average crack growth rates determined from 1994/95 inspections of KKM weld 11 plotted as a function of initial 1994 depth	3-5
Figure 3-4 UT scans for the 1995/96 and 2000 inspections of the lower ID H-4 weld in plant susquehanna unit 1 with relative location and growth shown	3-6
Figure 3-5 Average crack growth rates as a function of azimuthal position are shown along with fluence estimates for the H4 weld in susquehanna unit 1.....	3-6
Figure 3-6 UT scans for the 1995 and 1999 inspections of the lower ID of H-4 weld in susquehanna unit 2 with relative location and growth shown	3-7
Figure 3-7 Average crack growth rates as a function of azimuthal position are shown along with fluence estimates for susquehanna unit 2.....	3-7
Figure 3-8 Average crack growth rates determined based on UT inspection data for susquehanna units 1 and 2, plotted as a function of initial depth.....	3-8
Figure 3-9 UT scans for the 1995 and 1999 inspections of the upper and lower ID of H-4 weld in peach bottom unit 3 with relative location and growth shown	3-9
Figure 3-10 Average crack growth rates as a function of azimuthal position for peach bottom unit 3	3-10
Figure 3-11 UT scans for the 1996 and 1999 inspections of the ID of H-4 weld in brunswick unit 2 along with relative location and growth shown	3-10
Figure 3-12 Average crack growth rates as a function of azimuthal position for brunswick unit 2	3-11
Figure 3-13 The field derived crack growth rate data is re-plotted based on the average normalized depth crack growth rates decrease with increasing depth.....	3-12
Figure 4-1 0.3 X 0.5T – CT specimen used in crack growth tests conducted by GE	4-15
Figure 4-2 Notched 4-point bend specimen used in crack growth tests conducted by GE.....	4-16

Figure 4-3 CT specimen (with unirradiated arm extensions) used in crack growth tests conducted by Halden	4-17
Figure 4-4 Updated valid Halden data and the BWRVIP-99 NWC disposition curve (a corrected version of figure 8-2) displayed with the data binned by fluence. The curve also details the position of the data points with respect to the curve. (fluence values in Halden Tests are starting values)	4-18
Figure 4-5 Updated Halden data and the BWRVIP-99 HWC disposition curve displayed with the data binned by fluence. The curve also details the position of the data points with respect to the curve. (fluence values in Halden tests are starting values)	4-19
Figure 4-6 Effect of HWC environment (leading to reduction of oxygen levels to ~0 ppb) on crack growth rates. The rates are reduced by a factor greater than 20	4-20
Figure 5-1 Example from GE/JAPEIC data of rapid increase in crack growth rate for type 304 stainless steel BWR irradiated to 3×10^{21} n/cm ² as the specimen exceeded the K/Size criteria for IASCC testing	5-7
Figure 5-2 The DCB specimen design used in early Halden tests. This GE CRD design was about 4.2 inches long and 0.8 inch nominal thickness, and used a tapered ligament (the side grooves varied with crack depth) and tapered height (1 inch near the initial crack depth) to produce a constant K crack depth on a wedge loaded specimen.....	5-8
Figure 5-3 Example of crack length vs. time for the wedge-loaded DCB design used in the early Halden test reactor program. The specimens were loaded to about 35 ksi√in, which is a severe violation of the K/Size validity criteria	5-9
Figure 5-4 Example of crack length vs. time for the wedge-loaded DCB design used in the early Halden test reactor program. The specimens were loaded to about 35 ksi√in, which is a severe violation of the K/Size validity criteria	5-10
Figure 5-5 Crack growth rate vs. corrosion potential for the wedge-loaded DCB design used in the early Halden test reactor program. The specimens were loaded to about 35 ksi√in, which is a severe violation of the K/Size validity criteria	5-11
Figure 5-6 SCC growth rate vs. corrosion potential of sensitized and cold worked stainless steel and alloy 600 tested under linear elastic K/Size conditions.....	5-12
Figure 5-7 Response of irradiated stainless steel tested under valid linear elastic K/Size conditions, as evaluated elsewhere in this report. data cover a range of fluences from 1 – 4 dpa, and differ markedly from irradiated crack growth data where the K/Size criteria are violated	5-13
Figure 5-8 Crack length vs. time response for in-core, wedge-loaded DCB specimens installed in the nine mile point unit 1 BWR.....	5-14
Figure 5-9 Crack length vs. time response for recirculation, wedge-loaded DCB specimens installed in the nine mile point unit 1 BWR.....	5-14
Figure 5-10 Crack growth rate vs. corrosion potential for sensitized stainless steel tested in 288°C water at 25 – 30 ksi√in. The solid lines are the predicted response. most data are from laboratory specimens of thermally sensitized CT specimens, but the "Asterisk" points (at about 3.3×10^{-8} and 1.4×10^{-7} mm/s) are shown that represent the nine mile point unit 1 DCB specimens exposed in the recirculation system and in-core	5-15
Figure 6-1 SCC growth rate vs. corrosion potential for stainless steels tested in 288°C high purity water containing 2000 ppb O ₂ and 95 – 3000 ppb H ₂	6-8

Figure 6-2 Crack length vs. time for a 0.5TCT specimen of unsensitized type 316L stainless steel "Cold" worked at -55°C to 20% reduction in area	6-9
Figure 6-3 Crack length vs. time for a 0.5TCT specimen of unsensitized type 316L stainless steel "Cool" worked at $+140^{\circ}\text{C}$ to 20% reduction in area	6-9
Figure 6-4 Crack length vs. time for a 0.5TCT specimen of unsensitized type 316L stainless steel "Cool" worked at $+140^{\circ}\text{C}$ to 20% reduction in area	6-10
Figure 6-5 Crack length vs. time for a 0.5TCT specimen of unsensitized type 316L stainless steel "Cool" worked at $+140^{\circ}\text{C}$ to 50% reduction in area	6-10
Figure 6-6 Crack length vs. time for a 0.5TCT specimen of unsensitized type 347 stainless steel "Cool" worked at 140°C to 20% RA	6-11
Figure 6-7 Crack length vs. time for a 0.5TCT specimen of unsensitized type 304L stainless steel "Cool" worked to $\approx 50\%$	6-11
Figure 6-8 Crack length vs. time for a 0.5TCT specimen of unsensitized type 316L stainless steel "Cool" worked to $\approx 50\%$	6-12
Figure 6-9 Crack length vs. time for a 1TCT specimen of unsensitized alloy 600 cold worked at 25°C to 20% reduction in area.....	6-12
Figure 6-10 IG morphology observed in cold worked materials. (a) annealed + 20% cold work (-55°C) type 304L SS. (b) annealed + 20% cold work alloy 600.....	6-13
Figure 6-11 Hydrogen permeation vs. time and coolant H_2 fugacity unsensitized type 304L stainless steel.....	6-13
Figure 6-12 Hydrogen permeation rate (measured as a pressure increase or decrease) vs. crack growth rate and vs. coolant H_2 (and O_2) concentration in unsensitized 304L SS.....	6-14
Figure 6-13 Effect of yield strength and martensite on the stress corrosion crack growth rate on stainless steel and alloy 600 in 288°C , high purity water ($<0.10 \mu\text{S}/\text{cm}$ outlet) containing 2000 ppb O_2	6-14
Figure 6-14 Effect of yield strength and martensite on the stress corrosion crack growth rate on stainless steel and alloy 600 in 288°C , high purity water ($\approx 0.06 \mu\text{S}/\text{cm}$ outlet) containing 95 or 1580 ppb H_2	6-15
Figure 6-15 Effect of gentle unloading cycles on environmental crack advance on stainless steel whose yield strength is elevated by cold work.....	6-15
Figure 7-1 Calculated default residual stress profile for BWR core shroud belt-line weld based on alternate side welding passes (a ≈ 0.5 ksi stress from differential pressure also exists). some local shifts in this average residual stress profile must exist because of fit-up stresses, location of the last welding pass, statistical deviations in residual stresses, etc.	7-5
Figure 7-2 Measured residual stress data for large diameter BWR pipe weld. variations about the average may be associated with fit-up stresses, location of the last welding pass, statistical deviations in residual stresses, etc.	7-6
Figure 7-3 Stress corrosion crack growth rate data for alloy 182 weld metal from the literature [7-4, 7-7]. Similar examples of irreproducible SCC data exist for stainless steel, low alloy steel, and irradiated stainless steel, and are due primarily to flaws in testing.....	7-7

Figure 7-4 Crack growth rate vs. stress intensity for sensitized stainless steel in water of varying purity and corrosion potential. These variations change the K dependency from about K^2 to over K^3	7-8
Figure 7-5 Crack growth rate vs. crack tip strain rate (proportional to K^4) for sensitized stainless steel in water of varying purity. This variation changes the dependency on crack tip strain Rate (i.e., stress intensity) markedly	7-9
Figure 7-6 The effect of stress intensity on SCC growth rate of alloy 182 weld metal in 288°C water containing 100 ppb sulfate as H_2SO_4 [7-12].....	7-10
Figure 7-7 Crack length vs. time and the effect of stress intensity on SCC growth rate of cold worked 316L stainless steel in 288°C pure water at high corrosion potential [7-7, 7-13,7-14].....	7-11
Figure 7-8 The effect of stress intensity on SCC growth rate of 316NG stainless steel irradiated to 0.9×10^{21} n/cm ² in 288°C pure water at high corrosion potential [7-15, 7-16].....	7-12
Figure 7-9 The effect of stress intensity on SCC growth rate of 347 stainless steel irradiated to 1.5×10^{21} n/cm ² in 288°C pure water at high corrosion potential [7-15, 7-16].....	7-12
Figure 7-10 The effect of stress intensity on SCC growth rate of 304 stainless steel irradiated to 9×10^{21} n/cm ² in 288°C pure water at high corrosion potential [7-15,7-16]	7-13
Figure 7-11 Creep strain of 20% cold worked 316 stainless steel with and without radiation (about 10^{15} n/cm ² -s, E >0.1 MeV) [7-8, 7-19]. Following a short-term transient, the creep strain at constant load is very linear with fluence (integrated flux over time)	7-13
Figure 7-12 Stress relaxation in bolts of 20% cold worked 316 stainless steel initially stressed to 250 MPa and exposed at temperatures between 60 and 400°C [7-19, 7-20]	7-14
Figure 7-13 Radiation creep relaxation of shear stresses in springs of 20% cold worked 316 stainless steel, along with modeling curves [7-21]	7-14
Figure 7-14 Constant curvature bent beams exposed at 60 – 300°C in the chalk river reactor on pure nickel with 50% relaxation occurring at or before the 1 dpa point.....	7-15
Figure 7-15 Constant curvature bent beams of X-750 exposed at 60 – 300°C in the chalk river reactor	7-15
Figure 7-16 stress relaxation in 20% cold worked 316 stainless steel four-point bend beams at 370°C in EBR-II ranging from 4 to 54 ksi and up to 1 dpa. relaxation is independent of stress level	7-16
Figure 7-17 Stress relaxation in wedge-loaded DCB specimens at Halden that exhibited minimal or no crack growth [7-22]	7-16
Figure 8-1 Proposed NWC curve for stainless steel irradiated between 5×10^{20} to 3×10^{21} n/cm ² . applicable to normal operation at or below action level 1 parameters limits	8-5
Figure 8-2 Proposed HWC curve for stainless steel irradiated between 5×10^{20} to 3×10^{21} n/cm ² . Applicable to normal operation with verified reduction in corrosion potential at or below action level 1 parameter limit.....	8-6

Figure 8-3 Comparison of calculated K-dependent rates as a function of average normalized depth with the field data plotted against average depth. note that the K level varies based on the actual shroud thickness. The legend indicates the core shroud thickness	8-7
Figure 9-1 Stress intensity profile for a 1.5 in thick core shroud based on combined stress distribution which serves as the basis for the crack growth rate determination in example evaluations shown in figure 9-2	9-6
Figure 9-2 Normalized stress intensity profile for a core shroud versus normalized crack depth	9-7
Figure 9-3 Predictions for crack deepening under NWC and HWC conditions. Calculations made for recommended stress intensity distributions based on (1) combination of 1.6 ksi membrane and BWRVIP-NRC agreed upon weld residual stresses which are relaxed 30%. Predictions are applicable over 5×10^{20} to 3×10^{21} n/cm ² fluence range.....	9-8

LIST OF TABLES

Table 4-1 GENE/JAPEIC NWC data measured in type 304 stainless steel irradiated to a fluence of $2.7\text{-}3.0 \times 10^{21}$ n/cm ²	4-10
Table 4-2 Initial and updated Halden NWC data measured in types 304, 316 and 347 stainless steel irradiated to a starting fluence of 8×10^{20} to 1.5×10^{21} n/cm ²	4-11
Table 4-3 GENE/JAPEIC HWC data measured in type 304 stainless steel irradiated to a fluence of $2.7\text{-}3.0 \times 10^{21}$ n/cm ²	4-13
Table 4-4 Initial and updated Halden HWC data measured in type 316 and 347 stainless steel irradiated to a starting fluence of 8×10^{20} to 1.0×10^{21} n/cm ²	4-14
Table 9-1 Depth versus time for NWC crack growth rates and recommended K conditions for 1.5 inch thick shroud	9-3
Table 9-2 Depth versus time for HWC (FOI=3) crack growth rates and recommended K conditions for 1.5 inch thick shroud	9-5
Table B-1 Revision details	B-2

1

INTRODUCTION AND BACKGROUND

In earlier efforts, the BWR Vessels and Internals Project (BWRVIP) has developed crack growth disposition methodologies for evaluating intergranular stress corrosion cracking (IGSCC) in the internal components of BWRs [1-1, 1-2]. The focus of these efforts have been the primary austenitic materials used in the core region. Specifically, these methodologies have been directed at the stainless steel core shroud [1-1] and the Alloy 600/Alloy 182 materials used in the construction of the shroud support and the reactor pressure vessel attachment welds[1-2]. The first of these efforts resulted in the issuance of BWRVIP-14 [1-1], which developed the methodology for evaluating IGSCC crack indications in the core shroud. The report addressed all the different elements of the disposition methodology including the appropriate crack growth rates, the stresses that provided the driving force for crack advance and the role of environmental parameters on crack advance. The approach proposed in BWRVIP-14 [1-1] has been accepted by the NRC. The NRC initial and final safety evaluation reports (SERs) documents this acceptance [1-3, 1-4]. However, the specific relationships to be used for material and environmental condition are dependent on many parameters.

**Content Deleted -
EPRI Proprietary Information**

The purpose of this report is to provide new crack growth rates that can be used for irradiated stainless steel that has been exposed to a fluence greater than 5×10^{20} n/cm². The proposed crack growth rates will be developed based on several inputs which are presented in this report. First, the report provides an overview of the fundamental basis for the effects of irradiation on crack growth behavior. This is directly tied to the fundamental understanding of stress corrosion cracking processes in austenitic structural materials. With this understanding as the primary building block, the report presents supporting data from crack growth measurements made on core shrouds through ultrasonic inspections. The report next summarizes the useful laboratory crack growth rate data that have been measured in irradiated stainless steel. These data, developed by GENE and Halden in test facilities with BWR water environments, establish the effects of stress and environment on the measured rates. The summary data is based on detailed evaluation of the proprietary testing efforts that are reported in supporting EPRI/GE Report [1-6]. The report also provides a summary of other relevant data on un-irradiated stainless steel that have provided valuable insights into crack growth rate behavior of stainless steel following irradiation. The final topic discussed is the very important role of irradiation-induced stress relaxation. This factor will significantly reduce crack growth rates in irradiated components where the residual stresses adjacent to welds account for the majority of the driving force through the thickness.

Based on this understanding and these data, the report will propose disposition crack growth rate curves for use with stainless steel core components such as the beltline H4 core shroud weld irradiated in the range of 5×10^{20} to 3×10^{21} n/cm². These curves will be capable of being applied to both normal water chemistry (NWC) and hydrogen water chemistry (HWC) conditions. They also will be shown to produce predictions that bound the existing field shroud crack growth database.

Implementation Requirements

In accordance with the implementation requirements of Nuclear Energy Institute (NEI) 03-08, Guideline for the Management of Materials Issues, the crack growth rate curves described in Sections 8.3.1 and 8.3.2 along with the stress intensity factor distribution described in Section 9.1 are considered “needed” when performing flaw evaluations for core shroud welds in the fluence range of 5×10^{20} to 3×10^{21} n/cm². For evaluations of flaws in other irradiated components in this fluence range the crack growth rate disposition curves in Section 8.3.1 and 8.3.2 are considered “needed” when used with stress intensity factor distributions appropriate to the component to be evaluated. The remaining sections of the report are provided for information only.

2

UNDERSTANDING OF IRRADIATED CRACK GROWTH

Irradiation assisted stress corrosion cracking (IASCC) is the sub-critical intergranular cracking of materials exposed to ionizing irradiation [2-1 through 2-8], although it sometimes is viewed more restrictively to represent environmentally assisted cracking of irradiated materials (not unirradiated materials exposed to radiolytic environments). IASCC is most often associated with light water reactor (LWR) environments involving high temperature water and neutron irradiation exposure, which alters many material properties and causes radiolysis of water. While initially viewed as a unique and very complex form of cracking, IASCC is now broadly interpreted as a radiation accelerated process within the spectrum of environmental cracking [2-1 through 2-3] (Figure 2-1).

**Content Deleted -
EPRI Proprietary Information**

Among the various factors that alter IGSCC (and IASCC) susceptibility, corrosion potential is among the most potent and most important, because it can be controlled in existing plants. The strong contribution of the oxidizing water chemistry produced by radiolysis is indicated in the inset of Figure 2-3 by the effect of corrosion potential on cracking of irradiated stainless steel at a fluence of $\approx 2 \times 10^{21}$ n/cm², in Figure 2-6 for unirradiated, sensitized stainless steel, and in Figure 2-5 for unirradiated, unsensitized, cold worked stainless steel.

IASCC has been extensively observed, despite the use, e.g., of solution annealed materials and low design stresses. As summarized in several references [2-1 through 2-9], initial reports of IASCC occurred in the early 1960s in fuel elements, where high stresses associated with fuel swelling were considered an essential and unusual ingredient. However, IASCC was subsequently reported in a variety of high and low stress core components and in-situ test specimens in boiling water reactors (BWR), commercial pressurized water reactors (PWR), U.S. Navy test PWRs, and steam generating heavy water reactors (SGHWR). Evaluation of IGSCC in cold worked, irradiated stainless steel baffle bolts in PWRs has shown that low corrosion potential does not provide immunity to IASCC, although the higher temperature in PWRs is the key parameter responsible for the significant increase in SCC susceptibility and corresponding growth rates.

IASCC concerns also exist in applications such as high level radioactive waste containers and fusion reactors. In all cases, IASCC poses special concerns related to difficulties in inspection, and repair or replacement. In 1986 an International Cooperative Group on IASCC was formed [2-4] with the primary objective of developing fundamental understanding and life prediction capability for IASCC, which is crucial to LWR plant management and life extension.

2.1 Major Findings of the Last Fifteen Years of IASCC Research

Even though there is a very large amount of literature on the effects of irradiation on SCC behavior, the critical findings can be summarized. Based on both laboratory and field experience, these critical findings of the last 15 years of research into IASCC are as follows:

1. There is inherent SCC susceptibility in high temperature water of all structural materials and alloy types under almost all conditions, although very dramatic differences in kinetics also occur.
2. Major contributing factors to SCC susceptibility include neutron fluence, cold work, corrosion potential, water purity, temperature, and loading.
3. The interactive nature of the influential parameters makes their individual contribution to SCC appear complex, and changes the apparent threshold in any one parameter. This, coupled with the obvious importance of test/exposure time on the appearance of IASCC makes any “threshold” uncertain and even of dubious significance. A reasonable “working threshold” fluence of about 2×10^{20} n/cm² can be used for annealed components in high purity oxidizing environments, but some radiation enhancement (esp. in sensitized stainless steels) can be expected at lower fluences. Conversely, under low potential conditions (e.g., BWR NobleChem™, HWC or PWR primary water chemistry), the kinetics of SCC are dramatically reduced and the “working threshold” is $\approx 3 \times 10^{21}$ n/cm² at 288°C ($\approx 10^{21}$ n/cm² at 325 °C).
4. The quality and reproducibility of most IASCC (indeed, all SCC) measurements is not consistently high, and data must be carefully compared and verified against other observations. The origins of these problems include the complexity of the experiments and number of disciplines that must be mastered, as well as the nature of SCC.
5. Radiation promotes SCC via several phenomena:
 - Radiolysis can produce an oxidizing environment that increases the corrosion potential (this is suppressed by the high H₂ fugacity in PWRs)
 - Radiation induced segregation (RIS, or RS) produces compositional differences very near to grain boundaries (Figure 2-7). While into the mid-1990s there was a heavy preoccupation with the possible effects of impurities like P, S, Si, N, and B, there is now a broader acceptance of the primary importance of Cr depletion. Cr depletion is most important in oxidizing environments (that produce a pH-shifted crevice and crack chemistry); in low potential BWR and PWR environments, its role is secondary.
 - Radiation hardening (RH) causes dramatic increases in yield strength by generating point defect damage and small diameter vacancy and interstitial loops. These are very strong barriers to initial dislocation motion, but once a few dislocations move along a slip plane, they clear the point defects and most of these very fine obstacles. This creates a “dislocation channel” of softened material in which subsequent dislocation motion readily occurs. Thus, in almost all cases, highly irradiated materials are not brittle, but highly ductile on a local scale. This also results in strain softening

(not strain hardening), and necking often develops at low strains, leading to low uniform elongation but high reduction in area near the fracture. Because strain softening occurs, ASTM fracture mechanics stress intensity, K_{Ic} /size criteria [2-14] must be interpreted and applied with caution. It is believed that radiation hardening acts in a similar fashion to cold work, as both processes increase the yield strength and enhance SCC growth rates at high and low corrosion potential [2-1 through 2-3, 2-12, 2-13].

- Radiation creep/relaxation is a relatively well behaved, consistent process that tends to enhance SCC by promoting dislocation motion. Under constant displacement conditions (e.g., for weld residual stresses or baffle bolts), radiation creep produces substantial stress relaxation within a few dpa, which is an important factor in understanding and predicting the behavior of core components.

2.2 The Beneficial Effect of Reduced Corrosion Potential on the Stress Corrosion Crack Growth Rates of Irradiated Stainless Steel

Early investigators suggested that IASCC was a unique phenomenon, largely because of its supposedly unusual characteristics (e.g., its occurrence in solution annealed stainless steel) and the myriad of hypothetical radiation effects on cracking. However, as new data have been generated and critical experiments performed, the basis for viewing IASCC as a radiation-enhanced form of environmental cracking have increased and become very compelling. A summary of these findings that support these ties follows:

- There are consistent observations of similar dependencies among cracking of unirradiated materials in the laboratory, and irradiated materials in the laboratory, test reactor, and in-plant [2-1, 2-2, 2-8, 2-9, 2-16 through 2-18], including effects of corrosion potential (Figures 2-5 and 2-6 vs. Figures 2-3, 2-6, and 2-8 – with other examples to be given later) and water purity (Figure 2-9 vs. Figure 2-10).
- There is a recognition that radiation segregation produces significant chromium depletion near grain boundaries in initially solution annealed materials. These chromium profiles are broadly characteristic of thermal sensitization (Figure 2-7), although they are much narrower and generally not as deep. The similarity in SCC response was demonstrated by comparing normal thermal sensitization profiles with narrow profiles produced by multi-step heat treatments [2-20, 2-21] of unirradiated stainless steel.
- There are observations that increasing yield strength by cold work enhances SCC growth rates in both aerated and deaerated (pure) water, in the absence or presence of sensitization. This is a strong parallel to the response of irradiated stainless steels, which show increased crack growth rates with fluence. In deaerated water, there should be little effect of sensitization, so the enhancement in growth rate is primarily attributable to the increase in yield strength from irradiation.
- The fact that IASCC increases with test temperature in deaerated water from 288°C to 340°C in a similar fashion to unirradiated materials is observed. While better quantification is needed for both unirradiated and irradiated SCC response, Figures 2-11 and 2-12 show strong similarities.
- There is the observation that the corrosion potential inside cracks is always low, even for oxygen-containing water and under both unirradiated and irradiated conditions (except for non-relevant, 3-side open cracks and properly oriented high fluid flow rate [2-22, 2-23]). Thus, the possibility that radiolysis could produce a net oxidizing environment within the crack (and thereby reverse the direction of the potential gradient from the crack mouth to tip) was dispelled by potential measurements in 288°C water [2-1, 2-2] in which no consequential increase in the crack-tip potential occurred at total (gamma and particle) radiation levels even above peak LWR levels.

- Little or no intergranular cracking occurs in inert environments under similar temperature and loading conditions. Also, cracks are generally observed to initiate from the water side of components.

A broader case can be made for the commonality of many high temperature water SCC systems, including the spectrum of iron and nickel weld and base metals [2-18, 2-19]. For example, the tip of propagating cracks in both BWRs and PWRs is always deaerated, with the corrosion potential controlled by the $H_2 - H_2O$ line, and the difference in pH at temperature for various water chemistries is typically limited to about 3 units. Some special factors must be accounted for. Higher H_2 (and lower temperature) increases the stability of Ni metal [2-17, 2-23]. The presence of oxidizing species and the lack of a buffering chemistry provides an opportunity for shifts in crack chemistry.

Both phenomenological interpretation and predictive modeling relies on this evidence in support of a “radiation-enhanced” view of IASCC as a basis to extend our existing understanding and predictive modeling for unirradiated stainless steels to include irradiated effects. This approach does not dismiss the prospect of other contributions but it does relegate them to a secondary role. Therefore it is very appropriate to emphasize the important relationship between water chemistry and the magnitude of the crack growth rate in both unirradiated and irradiated stainless steel.

2.3 Status of Current Understanding of Irradiated Crack Growth Rate Behavior

As stated earlier, all structural materials exhibit an inherent SCC susceptibility in high temperature water. Austenitic materials manifest this susceptibility in the form of IGSCC. Each of the major factors, material susceptibility, stress and environmental parameters control the level of cracking and the growth rates of cracks. Specifically, for stainless steels, cold work, sensitization, neutron fluence, corrosion potential, water purity, temperature, and loading all affect those rates. In that the easiest parameters to control is the coolant environment, it is also important to recognize that the resultant stress corrosion crack growth rates of all BWR structural materials, including unirradiated or irradiated stainless steel, are very strongly affected by corrosion potential. For all of these materials, there is a large benefit of changing to low potential conditions, which can lead to an order of magnitude or more reduction in crack growth rate. This is achieved through the implementation of effective hydrogen water chemistry.

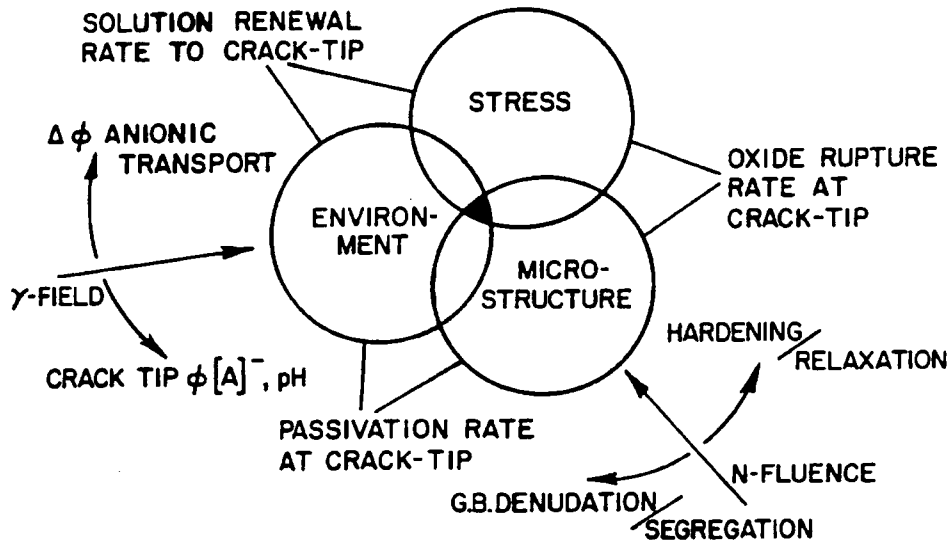


Figure 2-1
 Illustration of engineering factors (stress, environment, and microstructure), underlying fundamental phenomena (mass transport, oxide rupture, and repassivation), and primary effects of radiation on crack advance processes

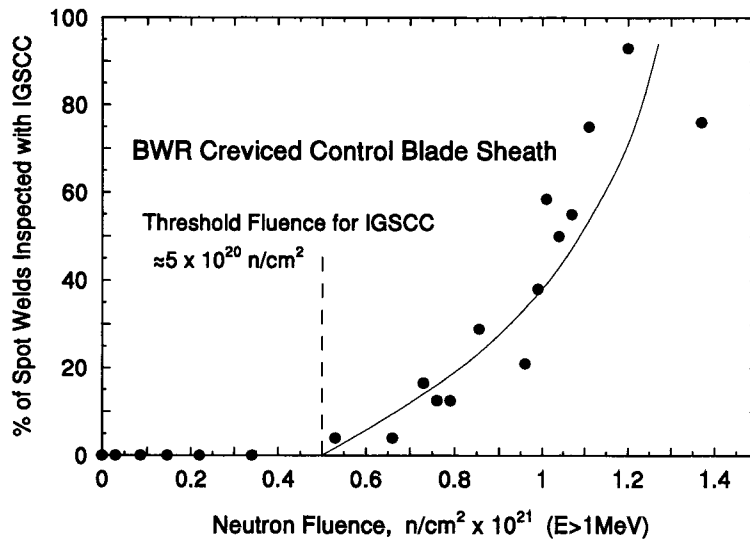


Figure 2-2
 Dependence of IASCC on fast neutron fluence for creviced control blade sheath in high conductivity BWRs [2-10]

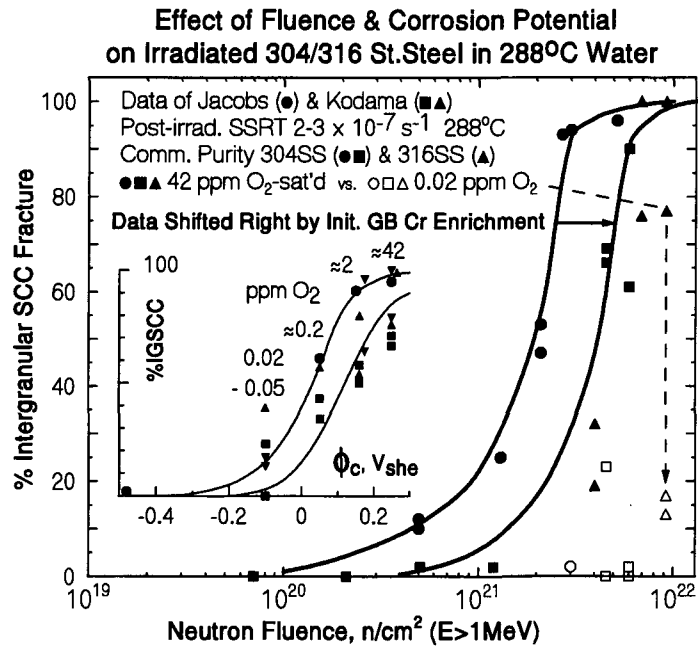


Figure 2-3
 Dependence of IASCC on fast neutron fluence in slow strain tests at $3.7 \times 10^{-7}/s^{-1}$ on pre-irradiated type 304 stainless steel in 288°C water [2-12]. The inset shows the effect of corrosion potential via changes in dissolved oxygen at a fluence of $2 \times 10^{21} n/cm^2$

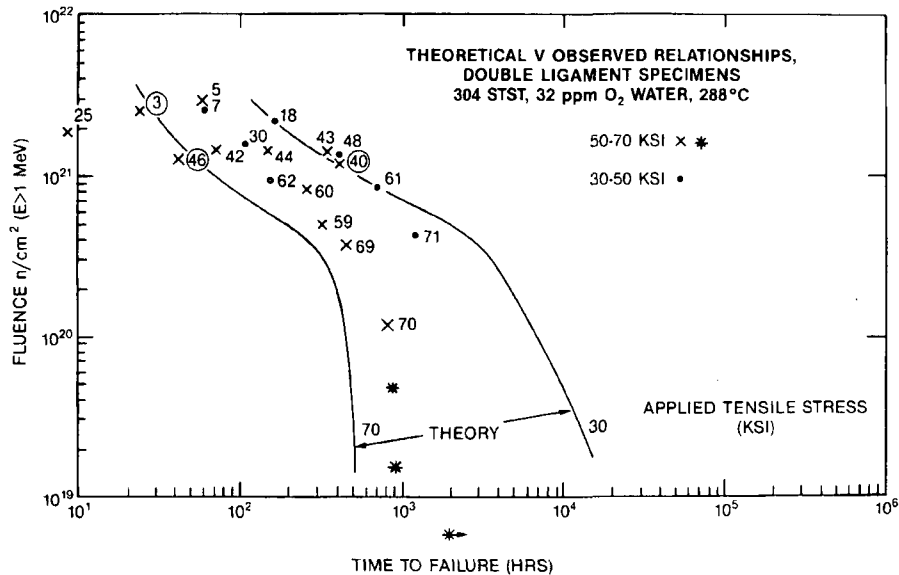


Figure 2-4
 Comparison between observed [2-24] and predicted time-to-failure for the effect of fast neutron fluence on pre-irradiated type 304 stainless steel tested at constant load in the laboratory in oxygen saturated, 288°C water

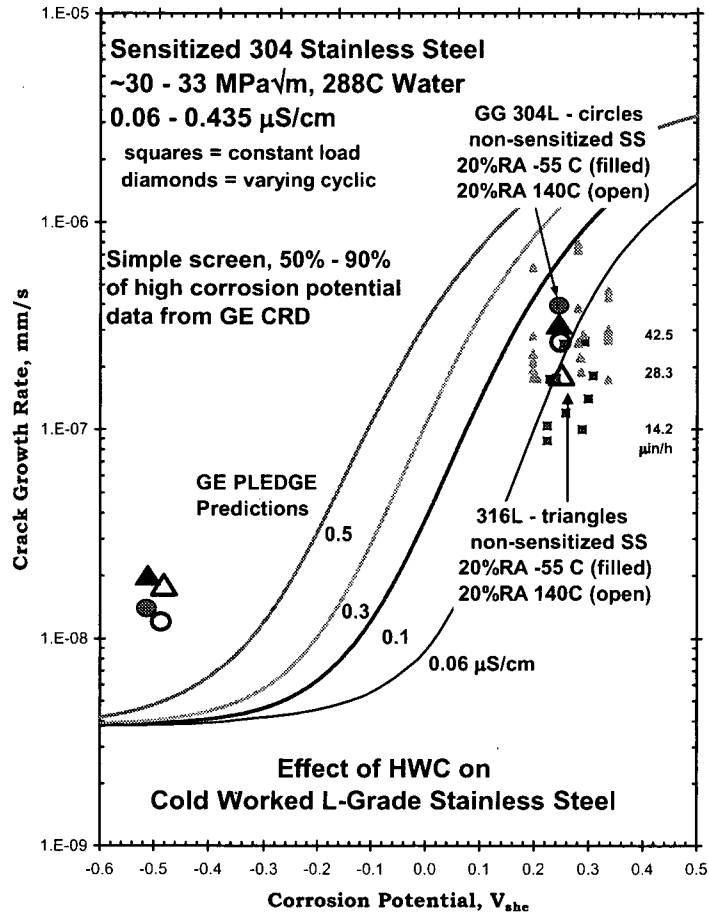


Figure 2-5

The large points show the effect of corrosion potential on the crack growth rate of unsensitized stainless steels in very high purity, 288°C water [2-13, 2-14]. The smaller points are for sensitized type 304 stainless steel under the same test conditions. The curves represent the predicted response of sensitized type 304 stainless steel for different water purity levels

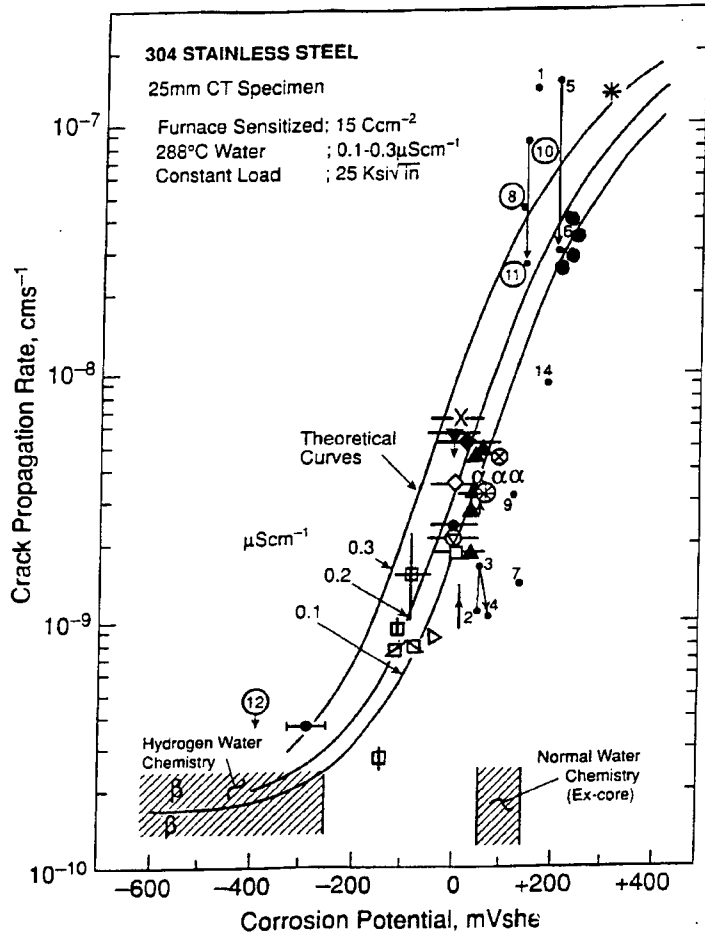


Figure 2-6
 Observed and predicted relationships of crack growth rate vs. Corrosion potential for furnace sensitized type 304 stainless steel at a constant K of $\approx 27.5 \text{ MPa}\sqrt{\text{m}}$. The observed data were obtained in water of conductivity between 0.1 to 0.3 $\mu\text{S}/\text{cm}$. The predicted relationships show the sensitivity of the crack growth rate to changes in combinations of corrosion potential and water purity (0.1 to 0.5 $\mu\text{S}/\text{cm}$) [2-9, 2-10, 2-11]. The circled points above 0.1 V_{she} (and at $-0.42 V_{\text{she}}$) were obtained in-core in a BWR or under proton irradiation simulating BWR core exposure

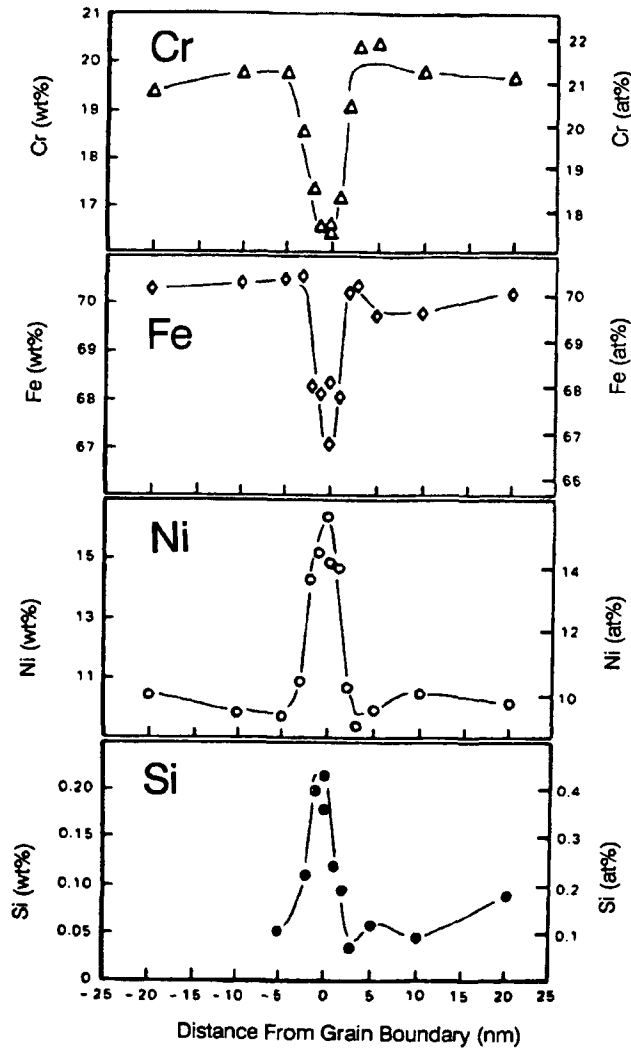


Figure 2-7
 Compositional profiles across grain boundaries obtained by dedicated STEM from a low strain, high purity 348 stainless steel swelling tube specimen irradiated to 3.4×10^{21} n/cm² at 288°C in a BWR [2-25]. The depletion of Cr and Fe, and enrichment of Ni and Si are characteristic of irradiated stainless steels

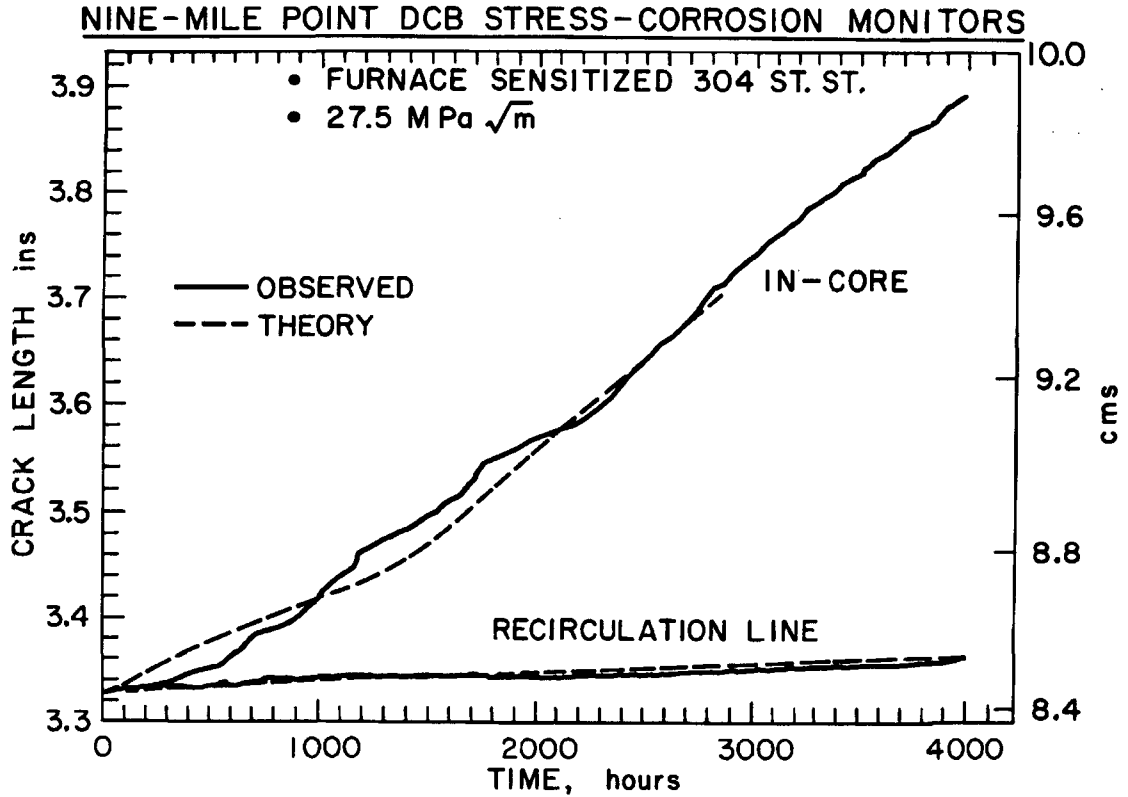


Figure 2-8
 Comparison of predicted and observed crack length vs. time for fracture mechanics specimens of *furnace sensitized* type 304 stainless steel in the peak flux region of the core and in the recirculation line of a commercial BWR [2-1 through 2-3]. The high corrosion potential in core caused significantly higher crack growth rates than in the specimen exposed in the recirculation system (neutron fluence did not reach consequential levels early in core exposure). Specimens were pre-cracked and wedge loaded to an initial stress intensity factor of 27.5 MPa \sqrt{m}

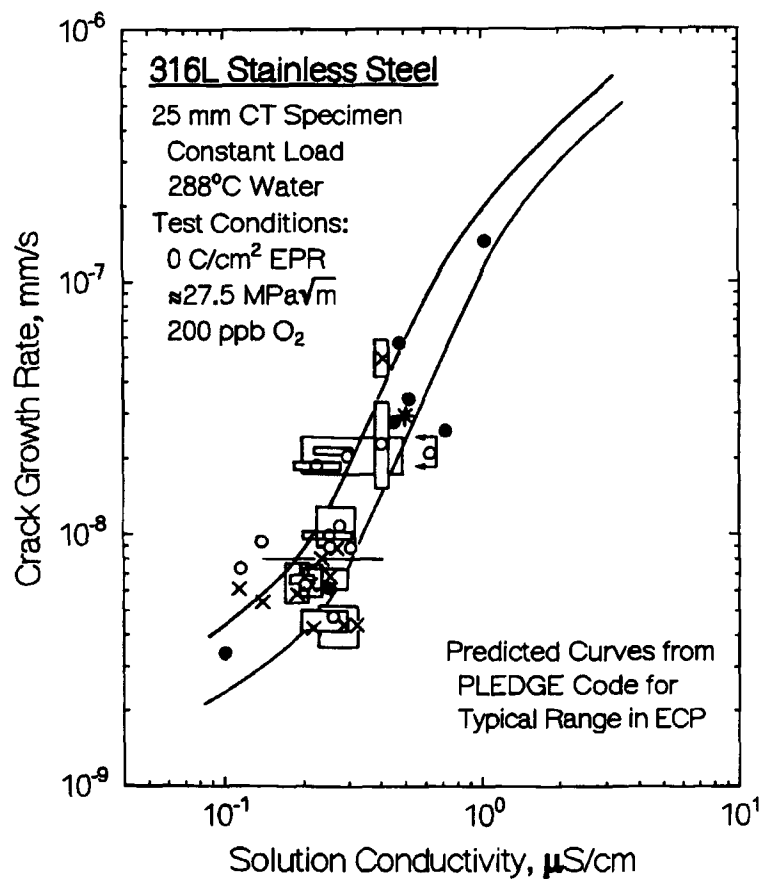


Figure 2-9
 Comparison between observed and predicted crack growth rate vs. solution conductivity for statically loaded type 316L and sensitized type 304 stainless steels in 288°C water containing 200 ppb O₂ [2-16 through 2-18]

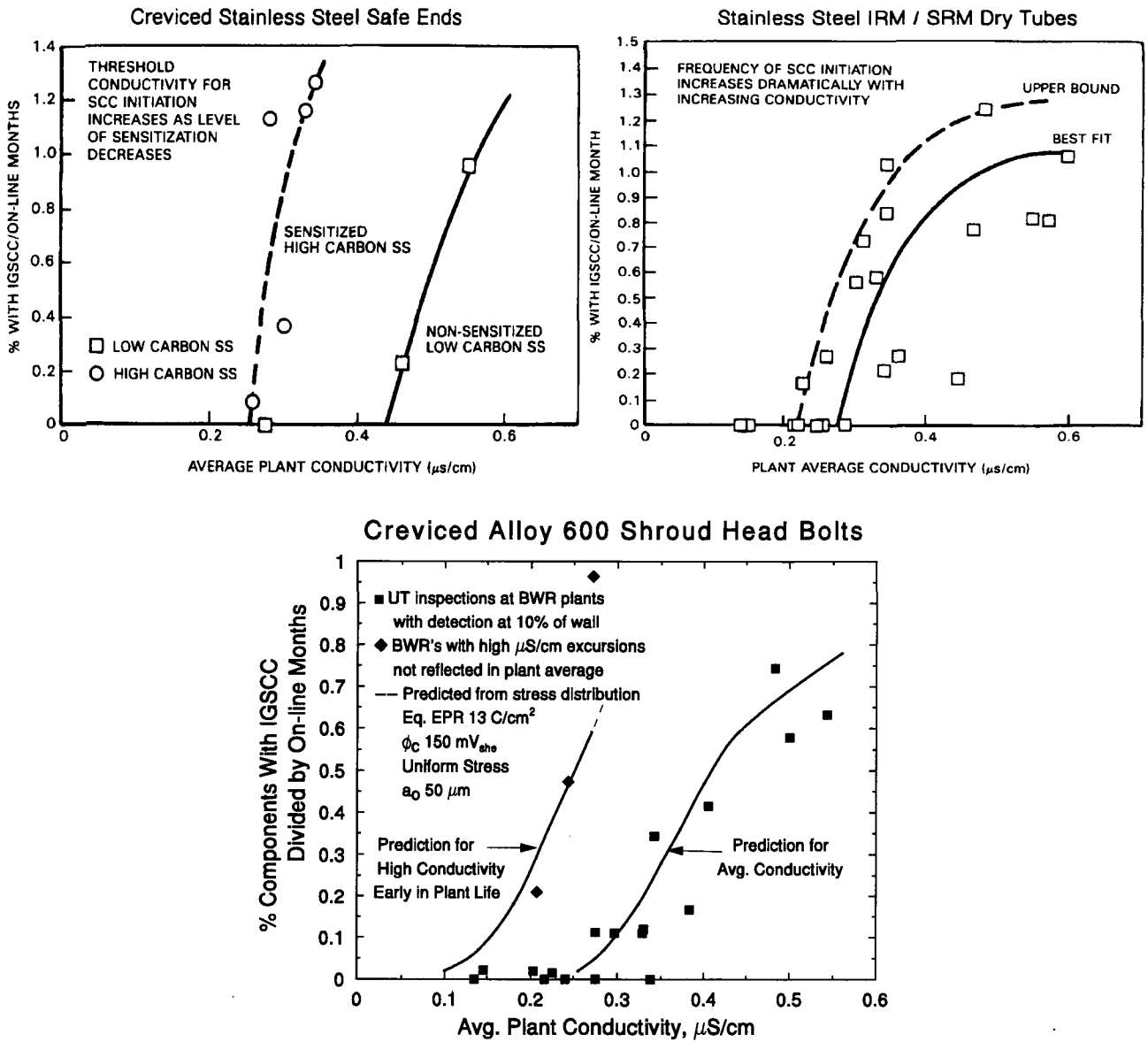


Figure 2-10

The similarity in the effects of solution conductivity for unirradiated and irradiated BWR components is shown in the field correlations of the core component cracking behavior vs. average plant water purity for (a) stainless steel IRM/SRM instrumentation dry tubes, (b) creviced stainless steel safe ends, and (c) creviced inconel 600 shroud head bolts, which also shows the predicted response vs. conductivity [2-11, 2-26]

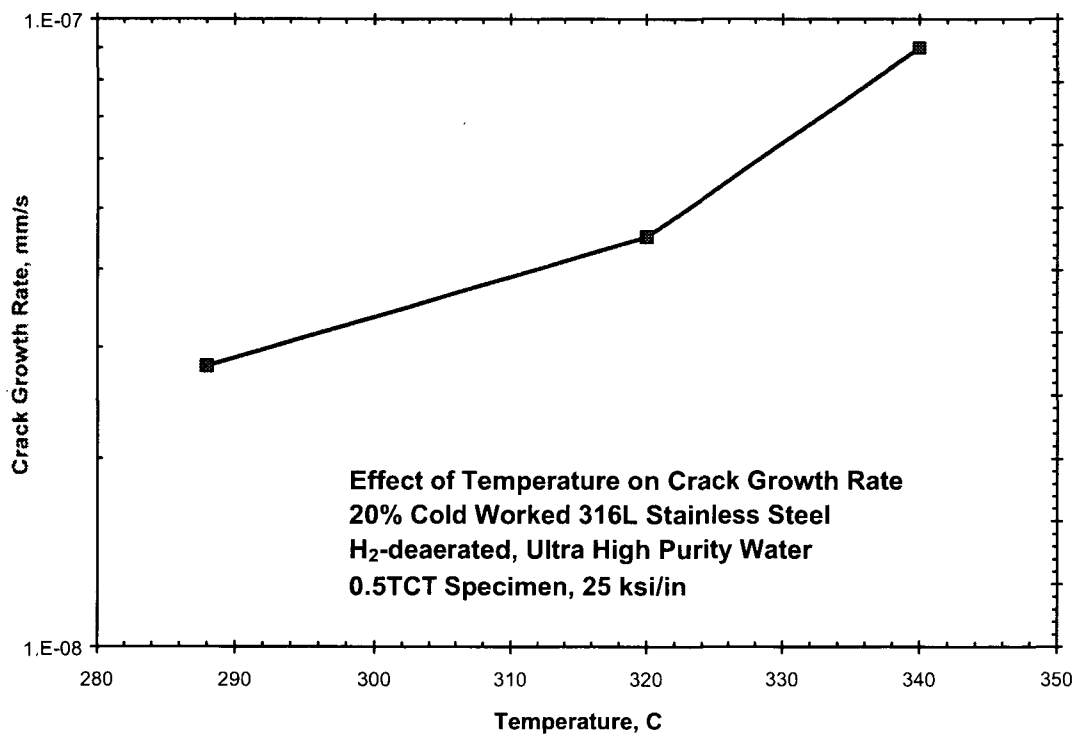


Figure 2-11
Effect of temperature on stress corrosion crack growth rate of stainless steel cool worked by 20% at +140°C and tested in H₂-deaerated, near-theoretical purity water [2-13, 2-14]

**Content Deleted -
EPRI Proprietary Information**

Figure 2-12
Effect of temperature on SCC of irradiated stainless steel in PWR water [2-27]

3

FIELD EVALUATIONS OF CRACK GROWTH RATES IN HIGH FLUENCE STAINLESS STEEL WELDMENTS BASED ON ULTRASONIC MEASUREMENTS

In previous BWRVIP crack growth reports, efforts were undertaken to examine the information available from the field components themselves [1-1, 1-2]. For these earlier efforts and this effort, the only field data that is available must be derived from ultrasonic inspection data. These data can be used to ascertain the depth of cracking at any one inspection period. The data are available from much of the circumference of the shroud. If repeat inspections have been made of the same areas and with similar techniques, the change in depth can be used to determine the amount of growth that occurred between inspections. An average rate can be estimated by dividing the crack growth, Δa , by the hot operating hours. For irradiated stainless steel, the weld locations that are of the greatest interest are those that have been exposed to a high fluence; in particular, the H4 weld. While the number of plants that have performed repeat inspections is limited due to the large number of plants that have installed shroud repairs, there are still several plants that do have this important data. These data are presented in the next sections, along with the overview information regarding the operation of each plant, with the intention of validating the proposed disposition curves and methods given later in this report.

3.1 Background of Field Data Approach

Content Deleted -
EPRI Proprietary Information

3.2 Actual Plant Data

3.2.1 KKM Weld 11 (H4): 1994 through 1995 (from BWRVIP-14)

Content Deleted -
EPRI Proprietary Information

**Content Deleted -
EPRI Proprietary Information**

3.2.2 Susquehanna Unit 1 and Unit 2 Weld H4: 1995 through 2000

**Content Deleted -
EPRI Proprietary Information**

**Content Deleted -
EPRI Proprietary Information**

3.2.3 Peach Bottom Unit 3 Weld H4: 1995 through 1999

**Content Deleted -
EPRI Proprietary Information**

3.2.4 Brunswick Unit 2 Weld H4: 1995 through 1999

**Content Deleted -
EPRI Proprietary Information**

3.3 Summary of Field Data

**Content Deleted -
EPRI Proprietary Information**

**Content Deleted -
EPRI Proprietary Information**

**Content Deleted -
EPRI Proprietary Information**

**Figure 3-1
Comparison of the 1994 and 1995 KKM UT determined crack depths of the different ID indications in weld 11 (H4). (shroud thickness of 31.2 mm equivalent to 1.25 inches)**

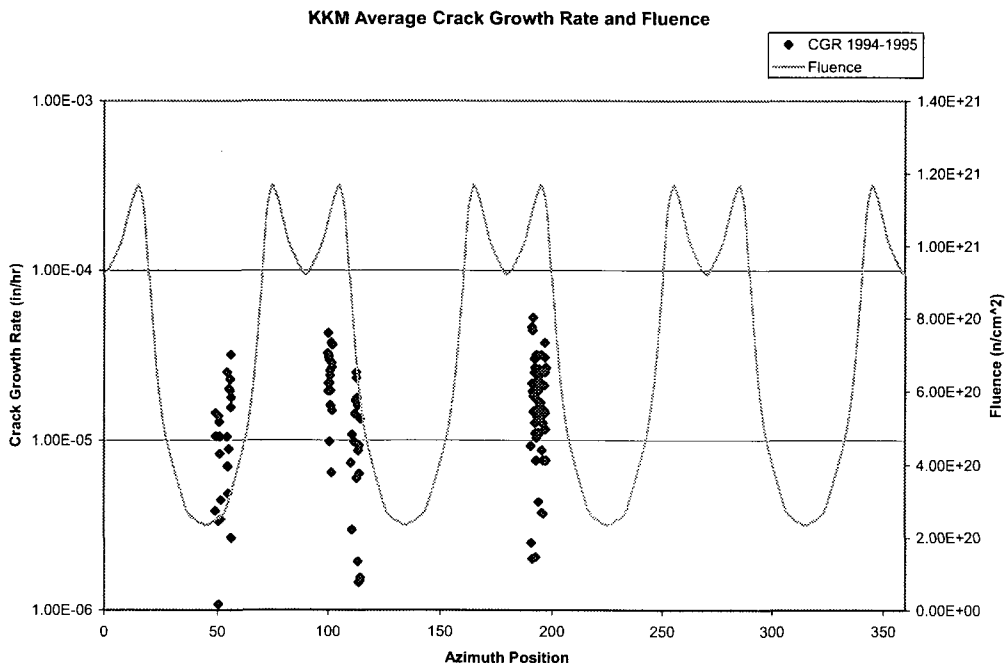


Figure 3-2
Average crack growth rates plotted as a function of azimuthal location along with the predicted fluence levels for KKM weld 11

**Content Deleted -
EPRI Proprietary Information**

Figure 3-3
Average crack growth rates determined from 1994/95 inspections of KKM weld 11 plotted as a function of initial 1994 depth

**Content Deleted -
EPRI Proprietary Information**

Figure 3-4
UT scans for the 1995/96 and 2000 inspections of the lower ID H-4 weld in plant susquehanna unit 1 with relative location and growth shown

**Content Deleted -
EPRI Proprietary Information**

Figure 3-5
Average crack growth rates as a function of azimuthal position are shown along with fluence estimates for the H4 weld in susquehanna unit 1

**Content Deleted -
EPRI Proprietary Information**

figure 3-6
UT scans for the 1995 and 1999 inspections of the lower ID of H-4 weld in susquehanna unit 2 with relative location and growth shown

**Content Deleted -
EPRI Proprietary Information**

Figure 3-7
Average crack growth rates as a function of azimuthal position are shown along with fluence estimates for susquehanna unit 2

**Content Deleted -
EPRI Proprietary Information**

Figure 3-8
Average crack growth rates determined based on UT inspection data for susquehanna units 1 and 2, plotted as a function of initial depth

**Content Deleted -
EPRI Proprietary Information**

Figure 3-9
UT scans for the 1995 and 1999 inspections of the upper and lower ID of H-4 weld in peach bottom unit 3 with relative location and growth shown

**Content Deleted -
EPRI Proprietary Information**

Figure 3-10
Average crack growth rates as a function of azimuthal position for peach bottom unit 3

**Content Deleted -
EPRI Proprietary Information**

Figure 3-11
UT scans for the 1996 and 1999 inspections of the ID of H-4 weld in brunswick unit 2 along with relative location and growth shown

**Content Deleted -
EPRI Proprietary Information**

**Figure 3-12
Average crack growth rates as a function of azimuthal position for brunswick unit 2**

**Content Deleted -
EPRI Proprietary Information**

Figure 3-13

The field derived crack growth rate data is re-plotted based on the average normalized depth crack growth rates decrease with increasing depth

4

SUMMARY OF IRRADIATED CRACK GROWTH RATE DATA FROM LABORATORY TESTING OF IRRADIATED STAINLESS STEEL MATERIALS

The amount of available data developed on LWR neutron irradiated materials is very limited. First, the availability of candidate irradiated materials has been limited by difficulty and cost of removal from operating BWRs or BWR components. This is further complicated by the costs and special requirements associated with the manufacturing of the actual test specimens. Secondly, the ability to perform testing remotely in a hot cell facility, with proper load, crack growth monitoring and water chemistry is limited to a handful of facilities. Therefore, the data that is available has been developed primarily by two testing organizations: GE Nuclear Energy at their Vallecitos Nuclear Center (VNC) and at the Halden Test Reactor in Norway.

Since crack growth rate data on irradiated stainless steel is critical to this effort, the available data must be scrutinized in terms of testing approach, the actual results and the material and test pedigree. The results of these tests and the testing details are proprietary to participating organizations. Therefore the detailed data will be presented in a second and a third supporting report. The second report, designated as the "EPRI/GE Irradiated Crack Growth Data Report," is a joint proprietary EPRI/GE report [1-6]. This report will contain the top level crack growth rate data at Halden and GE. This report will also include the screening and analysis summaries that served as the basis for the proposed disposition curves. The third data report, designated as the "GE Proprietary Data Report" contains more detailed information on all of the actual laboratory tests such as the crack length versus time plots for reference proprietary studies, the water chemistry data and the material pedigree background as well as the source data from GE proprietary efforts [1-6]. This information will support all of the conclusions that are contained in either this BWRVIP document or in the EPRI/GE report. Since this level of detailed evaluation has been necessary to assign crack growth rates and to support the technical foundation for many of the screening decisions, the additional two reference reports provide the important proprietary underpinning of the disposition curves given in this report. Although the details are contained in these other reports, a comprehensive summary of the test efforts and relevant data are given in the next sections.

4.1 GE/JAPEIC Irradiated Crack Growth Testing (GENE-VNC)

As part of a Japan Power Engineering and Inspection Corporation (JAPEIC) sponsored research project defined and conducted by General Electric Nuclear Energy, crack growth testing was performed at GE's Vallecitos Nuclear Center. Two major tasks were performed on highly irradiated Type 304 stainless steel; (i) crack growth tests using CT specimens, and (ii) crack growth tests using slotted 4-point bend specimens that simulated the configuration of the top guide beam in operating BWRs.

The irradiated material crack growth test facility at the General Electric Vallecitos Nuclear Center (GE-VNC) included crack growth data acquisition using the reversing D.C. potential drop method, and a high purity water loop capable of supplying BWR-type environments with various dissolved oxygen and hydrogen levels, and controlled levels of H₂SO₄ impurity additions. Each specimen was subjected to environmental crack growth rate testing at several stress intensity levels in 288°C water containing various concentrations of dissolved oxygen, hydrogen and/or H₂SO₄ impurity.

4.1.1 CT Tests-Specimens

For the CT testing, three specimens were fabricated from control rod blade handle material from a domestic operating BWR that had a fluence of $\sim 3 \times 10^{21}$ n/cm². The specimens were 0.3 inch thickness 0.5T-CTs with the following nominal geometry:

$$B = 7.62 \text{ mm [0.30. inch]}$$

$$B_n = 6.10 \text{ mm [0.24 inch]}$$

$$W = 25.4 \text{ mm [1.00 inch]}$$

$$\text{Initial Notch Depth} = 10.16 \text{ mm [0.40 inch]} \text{ (measured from the load line)}$$

Figure 4-1 shows the details of the CT specimen used at GE.

The irradiated crack growth test facility included (1) a test autoclave and tensile test machine installed in a hot cell of the GE-VNC irradiated materials laboratory, (2) environmental water loop in the hot cell corridor, and (3) computer data acquisition and control instrumentation in the hot cell operating area. The test autoclave and associated load frame was mounted in an MTS Model 810 Materials Testing System servo-hydraulic test machine that was equipped with a Wave Function Generator with computer interface. For each crack growth test a CT specimen was mounted in a load chain that passed through the autoclave head through friction seals. The crack growth tests were conducted under load control, with the load continually monitored by the data acquisition system and controlled to maintain the desired stress intensity level.

After machining of the CT specimens from the control rod material, they were air fatigue precracked, and side grooves were added to better control the crack plane. The precracking was performed at a maximum stress intensity of about 25 MPa-m^{0.5} [22.7 ksi-in^{0.5}], and R-Ratio = 0.1. Crack extension (and the corresponding applied stress intensity) was estimated using specimen compliance measurements. While the nominal crack length after precracking was to be 12.2 mm [0.480 inch], examination of the specimens after environmental testing revealed that the actual precrack lengths were 11.48, 11.35 and 10.72 mm [0.452, 0.447 and 0.422 inch].

The CT specimens were instrumented with platinum wires for reversing D.C. potential data acquisition to monitor crack growth. Duplicate potential probes were installed on each test specimen to provide redundancy in an effort to minimize test interruptions due to data acquisition problems. The crack growth result was estimated from the most stable set of probes, and was adjusted to the actual observed final crack length as determined by post-test fractography by SEM. In all cases, the actual crack growth matched the potential drop measurements within 5-10%.

4.1.2 CT Tests-Experimental

Environmental crack growth tests were conducted on three irradiated specimens over a large range of stress and water chemistry conditions. Three load phases were used during the testing:

1. SCL-Slow Cyclic Load
R-Ratio = 0.75, 90 min/cycle saw tooth.
2. CL₁-Constant Load with Small Cyclic Component
R-Ratio = 0.70, 100 sec/cycle saw tooth every 1000 seconds.
3. CL₂-Constant Load
No Cycling.

The different load phases were used to encourage stable, well-behaved crack growth, but most crack growth results were obtained at constant load (CL₂) or slow cyclic load (SCL).

**Content Deleted -
EPRI Proprietary Information**

4.1.3 Notched 4-Point Bend Tests-Specimens

The notched 4-point bend test specimen was designed to simulate the core top guide cross beam for testing against model predictions of crack growth. Highly irradiated control blade handle material was obtained to fabricate two test specimens. The specimen overall dimensions were 4 inch x 1 inch x 0.3 inch [101.6 mm long by 25.4 mm high by 7.62 mm thick]. A rectangular slot was machined in the specimen to accommodate a simulated crossbeam that produced a crevice region 0.002 inch (0.05 mm) wide in the slot area similar to the top guide beam configuration. A small starter notch was machined at one corner of the slot to facilitate crack initiation. Figure 4-2 shows the details of the notched 4-point bend used at GE.

The stress intensity versus crack length relationship was derived for the 4-point bend specimen geometry using a finite element code. The nodal displacements determined from linear-elastic fracture mechanics (LEFM) was compared to the results predicted by finite element analysis. The analysis technique was first validated using a finite element model for a standard 3-point bend specimen. When the predicted stress intensity factor was found to compare well with the published solution for the three-point bend specimen, the finite element model was modified to accommodate the unique JAPEIC 4-point bend specimen geometry.

Crack growth during environmental testing was monitored using the reversing D.C. potential drop method. Platinum probe wires were welded on the specimen faces using the remote handlers in the hot cell facility prior to specimen installation in the test autoclave. The 4-point bend load fixturing in the autoclave was designed with ceramic insulators that assured electrical isolation of the specimens necessary for reversing D.C. data acquisition. At the completion of each environmental test, the specimen was loaded to final fracture in room temperature air in a 3-point bend assembly so that the fracture surface could be examined by SEM.

4.1.4 Notched 4-Point Bend Tests-Experimental

During crack growth testing the specimen was loaded by the piston of an air actuator mounted on top of the test autoclave head. This piston applied a compressive force to the push rod that passed through low friction seals in the autoclave head, and extended a load on the specimen. The load was usually removed and reapplied manually by the test operator two times a day to facilitate well-behaved crack propagation. The environmental loop was identical to that described in the previous section.

**Content Deleted -
EPRI Proprietary Information**

4.2 HALDEN Irradiated Crack Growth Tests

The focus of the study in the IASCC program at the Halden Project was to use irradiated materials retrieved from commercial reactors for in-core measurement of crack growth rates in representative BWR conditions. Miniature CT specimens were instrumented for monitoring crack growth in-core and on-line variations in applied stress intensity level (by means of pressurized bellows assemblies). Test program IFA 639 focused on generating long term crack growth rate data in four small compact tension specimens prepared from irradiated 304, 347 and 316NG stainless steels with fluences of 9.0, 1.5 and 0.9 x 10²¹ n/cm². Crack growth rates were computed over time intervals as long as possible during exposure to a “high ECP” environment, created by operating the loop with a high (5-6 ppm) oxygen content. The benefits of hydrogen as an IASCC mitigation method were also studied by exposing the specimens to a “low ECP” environment (i.e., HWC with 2 ppm hydrogen).

The main experimental results from IFA 639, obtained over four irradiation cycles are used in this report.

4.2.1 CT Specimens

Four reconstituted bellows loaded CTs were installed in IFA 639. Each CT was prepared by electron beam welding pieces of irradiated material into an unirradiated “host” specimen carrying the external wiring (one current and two probe pairs) for the reversing DC potential drop measurements. The CTs have overall dimensions of 20 x 19.2 x 5 mm, plus unirradiated arm extensions that result in a total length of 55 mm. In order to ensure a straight crack path, the specimens used 10% side grooves, resulting in an effective thickness, B_{eff} of 4.47 mm, and the critical dimensions are

$$B = 5 \text{ mm [0.204 inch]}$$

$$B_n = 4 \text{ mm [0.167 inch]}$$

$$W = 16 \text{ mm [0.630 inch]}$$

Figure 4-3 shows the details of the CT specimen used at Halden.

Two of the CTs in the test matrix were prepared from Wurgassen NPP 347SS top guide material, with reported fluence of 1.5 x 10²¹ n/cm². One specimen was prepared from an Oskarshamn 2 304SS control blade handle material with a reported fluence of 9 x 10²¹ n/cm², and the fourth CT was prepared from irradiated 316 NG (reported fluence of 0.9 x 10²¹ n/cm²) from a DCB used in an earlier study at Halden. The matrix enabled evaluation of reproducibility in the cracking behavior of the two duplicate 347SS. The CT prepared from 316NG allowed evaluation of the behavior of two different materials (347SS vs. 316NG stainless steel) with similar fluences, while the cracking behavior of the highest fluence 304SS could be compared with that of the lower dose materials.

Prior to environmental testing, the CTs were fatigue pre-cracked in air, and the crack length estimated using the compliance method. The pre-crack length in all the specimens was estimated to be 8.1 mm.

Stress intensity was applied to the CTs by means of individually calibrated loading units fitted with bellows assemblies that were pressurized with helium gas through an outer system. During irradiation, the specimens were either subjected to static (constant) load or to load cycling that was implemented to encourage crack advance. The cyclic loading, with $R=0.7$, comprised a fairly rapid unloading and reloading ($0.5 \text{ MPa}\cdot\text{m}^{0.5}/\text{s}$) with a 900 s hold time, and was implemented every 12 hours.

4.2.2 Experimental

The four CTs were located within the high fast neutron flux (booster) region of the test rig in IFA 639. Coolant thermocouples were installed at the inlet and outlet of the in-core test section and in-core pressure sensors were used to monitor the system pressure in close proximity to the CTs. Neutron detectors positioned at two elevations within the booster region enabled the fast neutron flux (and fluence accumulation in the specimens) to be computed. For measuring the ECP of the stainless steel pressure flask, two Pt electrodes (Pt 1 and Pt 2) from a commercial supplier were also installed in the in-core region of IFA 639 with Pt 1 at the inlet to the test section and Pt 2 immediately above the booster rods.

The test rig was connected to a water loop operating under representative BWR conditions. The loop normally operated at ~1320 psi (90 bar) with a coolant temperature of 536°F (280°C). Normal flow through the loop is 50 liter/hr. On exiting from the in-core region, the coolant was cooled, flowed through a purification system and returned to the feed water tank where the dissolved gas content was controlled (or changed) by sparging the tank with oxygen or hydrogen, depending on the experimental requirements. Both inlet and outlet oxygen and hydrogen were measured continuously with Orbisphere sensors. Inlet and outlet solution conductivity was also monitored on-line, as were system temperatures, pressures and flow rates. Grab samples of inlet and outlet water were collected at regular intervals to measure the concentration of ionic species.

During the investigation in IFA 639, the water loop was either operated with Normal Water Chemistry (NWC) (5-6 ppm O₂ measured at the inlet), or with Hydrogen Water Chemistry (HWC) (1-2 ppm H₂ measured at the inlet). IFA 639 was irradiated for four reactor cycles, from March 1999 to October 2000.

During the first irradiation cycle (March to May 1999) crack growth rates were measured in the CTs under static (constant) load conditions over a total of 1150 full power hours (fph) with two interruptions due to reactor shutdowns.

**Content Deleted -
EPRI Proprietary Information**

**Content Deleted -
EPRI Proprietary Information**

4.3 Overview of Other Data

There have been other testing programs directed at determining the crack growth behavior of irradiated material. A significant effort was performed at Nine Mile Point Unit 1 where both annealed and sensitized stainless steel DCB specimens were loaded in an LPRM in-core [4-1]. These data have proven very useful in evaluating the effects of irradiation on crack growth. They have also provided benchmark data on the role of material sensitization on crack growth response in irradiated material. Other laboratory and in-reactor efforts have also been conducted, including earlier work at the Halden test reactor. These data, while not as important as the other summarized, are also addressed in Section 5 as well as in the EPRI/GE Report [1-6].

4.4 Summary of Relevant Data

The crack growth rate data from GE and Halden was evaluated considering the following factors: (1) testing approach; (2) actual results; (3) material pedigree; and (4) test pedigree. For the GENE data the evaluation included examination of the original data acquisition results and test logs. In the case of the Halden crack growth results, some specifics (such as crack length versus time plots) about each test condition were obtained from interim reports and presentations, as well as the final report [3]. However, periods of test operation that did not yield crack growth results, and may have influenced subsequent crack growth behavior were not clearly discussed in the reports.

Each specific test segment of the GE tests (and where possible the Halden tests) was examined to determine if the test design and specimen condition were reasonable for proper crack growth behavior. The segments were examined for steady, well-behaved crack growth as well as constant environmental test conditions. In the case of the GE crack growth data, the specific crack length versus time data points were re-plotted, and re-analyzed for the average crack growth rate and statistical acceptance. This served as a verification of the reported rates originally determined from the laboratory's data acquisition system, and in a few cases improved the data quality.

Other elements that were considered when evaluating the data quality included specimen K-validity (high K or long crack concerns), memory effects due to environmental exposure in the prior test segment, transgranular-to-intergranular transition effects after precracking or during mid-test fatigue bench marking, and potential drop instrumentation problems.

The quality of each crack growth data segment was evaluated, and defined as follows:

The data for the JAPEIC material were derived from measurements on the material taken from end-of-life control rod blades. (Note: The initial fluence data values are listed in Table 4-3). The available data is insufficient to quantify the effect of fluence on crack growth rates.

- (1) "A" – High/Medium Confidence Level
e.g., reasonable design/execution, steady well defined CG, etc.
- (2) "B" – Inconsistent/Missing Information
e.g., in need of supporting fractography, poor comparison with similar data or with itself, crack growth stagnation, etc.
- (3) "C" – Known Bad Data – Flawed Test Execution
e.g., high K late in the test, noisy potential drop measurements, TG/IG transition issues, adverse memory effects from previous conditions etc.
- (4) "D" – Known Bad Data – Flawed Test Design
e.g., high initial K, specimen invalid, etc.

The screening levels for each data segment are shown in Tables 4-1 to 4-4. Only crack growth data that was evaluated as high quality ("A" or "B" data) was used to develop crack growth disposition curves in BWRVIP-99-A.

**Content Deleted -
EPRI Proprietary Information**

Table 4-1
GENE/JAPEIC NWC data measured in type 304 stainless steel irradiated to a fluence of $2.7\text{-}3.0 \times 10^{21}$ n/cm²

**Content Deleted -
EPRI Proprietary Information**

Table 4-2
Initial and updated Halden NWC data measured in types 304, 316 and 347 stainless steel irradiated to a starting fluence of 8×10^{20} to 1.5×10^{21} n/cm²

**Content Deleted -
EPRI Proprietary Information**

Table 4-2
Initial and updated Halden NWC data measured in types 304, 316 and 347 stainless steel irradiated to a starting fluence of 8×10^{20} to 1.5×10^{21} n/cm² (continued)

**Content Deleted -
EPRI Proprietary Information**

Table 4-3
GENE/JAPEIC HWC data measured in type 304 stainless steel irradiated to a fluence of $2.7-3.0 \times 10^{21}$ n/cm²

**Content Deleted -
EPRI Proprietary Information**

Table 4-4
Initial and updated Halden HWC data measured in type 316 and 347 stainless steel irradiated to a starting fluence of 8×10^{20} to 1.0×10^{21} n/cm²

**Content Deleted -
EPRI Proprietary Information**

**Content Deleted -
EPRI Proprietary Information**

Figure 4-1
0.3 X 0.5T – CT specimen used in crack growth tests conducted by GE

**Content Deleted -
EPRI Proprietary Information**

**Figure 4-2
Notched 4-point bend specimen used in crack growth tests conducted by GE**

**Content Deleted -
EPRI Proprietary Information**

**Figure 4-3
CT specimen (with unirradiated arm extensions) used in crack growth tests conducted by Halden**

**Content Deleted -
EPRI Proprietary Information**

Figure 4-4
Updated valid Halden data and the BWRVIP-99 NWC disposition curve (a corrected version of figure 8-2) displayed with the data binned by fluence. The curve also details the position of the data points with respect to the curve. (fluence values in Halden Tests are starting values)

**Content Deleted -
EPRI Proprietary Information**

Figure 4-5
Updated Halden data and the BWRVIP-99 HWC disposition curve displayed with the data binned by fluence. The curve also details the position of the data points with respect to the curve. (fluence values in Halden tests are starting values)

**Content Deleted -
EPRI Proprietary Information**

Figure 4-6
Effect of HWC environment (leading to reduction of oxygen levels to ~0 ppb) on crack growth rates. The rates are reduced by a factor greater than 20

5

IMPORTANCE OF PLASTICITY AND OTHER TESTING FACTORS ON LABORATORY TEST DATA

5.1 Background

The applicability and transferability of cracking behavior (fracture toughness, and fatigue, corrosion fatigue, and stress corrosion crack growth rate) from one situation to another relies on the concept of stress intensity factor *similitude* in linear elastic fracture mechanics. *Similitude* means that the behavior of a crack of a specific geometry in a component or specimen of a given thickness under a specific stressing condition can be related to a crack associated with a different geometry, thickness, and/or stressing condition. Similitude permits SCC growth rates measured in laboratory specimens to be compared with each other and applied to plant components. To maintain stress intensity factor similitude, linear elastic conditions must be maintained.

Linear elastic criteria recognize that a plastic zone always forms at the tip of a sharp crack under load, but are designed to ensure “*predominantly elastic*” conditions with the intention that the *observed* cracking behavior not vary consequentially with specimen size. In simple terms, the plastic zone must be small relative to the specimen dimensions, particularly the thickness and remaining crack ligament.

Linear elastic criteria can be formulated in many ways, but the ASTM standards [5-1 through 5-4] provide the most widely recognized criteria. The boundary between “linear elastic” and “plastic” is a soft one, since a sharp crack under load has an associated plastic zone. The intent of the various criteria/standards is to limit plasticity to acceptable levels, so that the underlying crack behavior is not consequentially altered. The allowable stress intensity K depends on specimen size, and thus the criteria are not fixed for all specimen/crack geometries – and are referred to as K /size criteria.

The original K /size criteria were obtained for fracture toughness testing (ASTM E399 [5-1]), and extended to fatigue (E647 [5-2]), primarily by taking into account the effect of cyclic hardening on plastic zone size. While an ASTM K /size criteria has been written for SCC testing (E1681 [5-4]), it is based on very limited data regarding at what point the SCC behavior becomes different as K increases or size decreases. Interestingly, these most-critical data are probably as comprehensive for irradiated as unirradiated stainless steels in light water environments.

The ASTM specimen K /size criteria are addressed (sometimes differently) in various standards. The most relevant standards for SCC testing are E399, E647, E813, and E1681 [5-1 through 5-4]. The latter specifically addresses “Threshold K for Environmentally Assisted Cracking of Metallic Materials at Constant Load”, and is substantially an amalgam of E399 and E647. Several important elements are addressed in the standards, including the concepts of “effective thickness” and “flow stress.”

In Section 7.1.1 on specimen size, ASTM E399 identifies an “effective thickness” for specimens that are side grooved as a root mean square, or $\sqrt{(B \times B_{sg})}$. It specifies that both the effective width “ W ” and crack length “ a ” (not the remaining ligament $(W-a)$) exceed $2.5 (K_{IC}/\sigma_{YS})^2$; K_{IC} is used in this toughness testing standard because it is the maximum K of the test. It later addresses remaining ligament by saying that the crack length “*shall be between 0.45 and 0.55W*” (Section 7.3.2.1 on fatigue cracking), so “ a ” and $(W-a)$ are about equal. For a 1T CT specimen, “ W ” is the 2-inch distance from the center of the loading holes to the back of the specimen, and “ a ” is the crack length (also measured from the center of the loading holes).

E647 focuses more on the remaining ligament: $(W-a) > (4/\pi) (K/\sigma_{YS})^2$ (Section 7.2.1 on specimen size). In Section 7.2.2.1 it also introduces the concept of “*flow stress*” – the average of the yield and ultimate tensile strength $(\sigma_{YS} + \sigma_{UTS})/2$, and permits the flow stress to be substituted for the yield strength for ductile, work hardening materials. Note that this is somewhat relaxed compared to E399 because the $(4/\pi)$ term is close to half of the 2.5 term in E399 (perhaps for cyclic work hardening), and E647 permits the use of flow stress. It does not very directly address specimen thickness criteria, and Section 7.1.3.1 only indicates a recommended remaining ligament between $W/20$ and $W/4$. This appears to be an oversight, especially since the standard recognizes the need for “*the specimen to be predominantly elastic at all values of applied load*” (Section 7.2 on specimen size). This same section acknowledges that the origin of the requirements “*are empirical results and are specific to specimen configuration*”.

E813 addresses the effect of side grooves, and references E399 in proposing the use of $\sqrt{(B \times B_{sg})}$ for the “*effective thickness*” (Section A2.5.2). This is expressed indirectly in the equation for $K_{(1)}$, which uses $(B B_N W)^{1/2}$, which is equivalent to $(B \times B_{sg})^{1/2} \times (W)^{1/2}$.

E1681 addresses *threshold* K measurements, and specifies (Section 7.2.1.1 on specimen size) that “ *B , a_o and $(W-a_o)$ equal or exceed the quantity $2.5 (K_{IEAC}/\sigma_{YS})^2$* ”. It thus succeeds in “equating” all three size/dimension issues. E1681 also permits the use of a flow stress (Section 7.2.1.2). This standard uses the more stringent requirements in E399 involving the factor of 2.5, but allows the $(4/\pi)$ factor for *non-threshold* measurements.

In summary, the various K /size standards differ somewhat in their completeness, but all share very common themes, including an acknowledgement that the underlying empirical objective is to help ensure identical crack response. These include, with some editorial insertions:

- Both the thickness B and remaining ligament $(W-a)$ should exceed $2.5 (K/\sigma_{YS})^2$ or $(4/\pi) (K/\sigma_{YS})^2$.
- σ_{YS} can be replaced by the flow stress (the average of the yield and ultimate tensile strength $(\sigma_{YS} + \sigma_{UTS})/2$) for *ductile, work hardening* materials (see later discussion on irradiated materials).
- The effective thickness B_{eff} of side-grooved specimens should be calculated as a root mean square, i.e., $\sqrt{(B \times B_{sg})}$. The use side grooves are strongly recommended, with a depth for each side groove of between 5% and 10% of specimen thickness.
- The criteria are generally conservative, so that violating them by a small amount (e.g., 20 – 30% in K) is acceptable (i.e., it should have relatively little effect on the SCC data), but violation by 50 – 100% is very likely to be a problem. Again, the objective is solely to help ensure that K /size effects do not influence the observed SCC growth rate response.

- The K/size standards apply to work hardening materials, and therefore break down markedly for materials irradiated to sufficient fluence so that on a local scale, they don't work harden. This certainly occurs with the onset of dislocation channeling, but may occur at lower fluences.

5.2 Application to Unirradiated Materials

The application of the ASTM K/size criteria to unirradiated materials – or, more specifically, to ductile, work hardening materials – is straightforward. The minimum effective thickness or remaining ligament should, more conservatively, be greater than $2.5 (K/\sigma_{FS})^2$ where flow stress, σ_{FS} , is the average of the yield and ultimate tensile strength $(\sigma_{YS} + \sigma_{UTS})/2$. (E1681 allows the use of $(4/\pi) (K/\sigma_{FS})^2$). For stainless steel at 300°C with yield strength of 25 ksi and an ultimate tensile strength of 75 ksi, the flow stress is 50 ksi. For testing at 30 ksi√in, the size should be greater than $2.5 (30/50)^2 = 0.9$ inch. Thus, a 1T CT specimen of crack length <1.1 inch ($a/W < 0.55$) and an effective thickness of > 0.9 inch (i.e., with 5% side grooves per side, the effective thickness is the square root of $1 \times 0.9 = 0.949$ inch) would be satisfactory. A 1T CT specimen of a material of this strength is not appropriate for testing at 40 ksi√in (size >1.6 inch).

In practice, there is typically little evidence of problems if this K/size criterion is exceeded by perhaps 30%; i.e., testing at ≈ 40 ksi√in does not result in a large increase in crack growth rate. Testing at > 50 ksi√in will likely produce altered SCC growth rate behavior (note that using the $(4/\pi) (K/\sigma_{FS})^2$ criterion, the allowable K is 43.2 ksi√in). However, materials like Alloy 182 weld metal can be tested at these K levels because their yield strength is considerably higher (typically 50 to 60 ksi). Depending on the heat treatment, a 1T CT specimen of Alloy 182 weld metal is K/size valid at 50 – 55 ksi√in rather than 30 ksi√in. Because of the square root dependency, using a 2T CT specimen only increases the valid K by a factor of 1.4.

5.3 Application to Irradiated Materials

The application of these K/size criteria to irradiated materials is not straightforward because the response of irradiated materials is so different. While some investigators blindly apply the ASTM standards to their irradiated crack growth testing, the shortcomings are evident both fundamentally (local work softening occurs) and empirically (there is an onset of excessively high rates as K is increased). These shortcomings are not resolved simply by abandoning the flow stress substitution for yield strength (which makes little difference, because by several dpa of irradiation the yield strength approaches the ultimate tensile strength, so there is minimal benefit of averaging these two values).

Above several dpa (depending on the material composition and its level of prior cold work), deformation does not occur nearly as homogeneously as in unirradiated materials. Radiation produces a very high density of barriers to dislocation motion (e.g., vacancy loops and interstitial loops) that are responsible for the increase in yield strength. As the first dislocation begins to move through a sufficiently highly irradiated material, the very fine-scale barriers are removed, creating a slip band that is a highly preferential “channel” for continued dislocation motion. Channels obviously become wider than a few atomic planes, but remain narrow bands of high localized dislocation activity. On a local scale, as well as on a macroscopic scale, this represents marked work softening. Dislocations pile up at grain boundaries and other large obstacles to dislocation motion, with grain boundary slip accommodation and increased dislocation densities.

The transition from an annealed state to a highly irradiated (pronounced dislocation channeling) state does not occur at a single value of fluence, even for a given material. Thus, it is not yet possible to define a specific fluence above which work softening must be accounted for. This is especially true for cold worked materials, which retain residual dislocation structure to at least several dpa (5 dpa is a reasonable estimate for LWR irradiation).

The preliminary guidelines proposed for moderate to highly irradiated material is to discount the irradiation-induced *increase* in yield strength by 2X, and to not employ the concept of a flow stress. Thus, a moderate to highly irradiated stainless steel of 125 ksi yield strength would be treated as though it had an *effective yield strength* of 75 ksi = (125 + 25 ksi)/2. This guideline was developed following the first SCC growth rate tests performed on LWR irradiated materials in high temperature water [5-5] in 1986. At that time the potential concern for work softening of irradiated materials was recognized, but contact with the experts revealed that this had never been considered in toughness, fatigue, or SCC testing.

**Content Deleted -
EPRI Proprietary Information**

**Content Deleted -
EPRI Proprietary Information**

**Content Deleted -
EPRI Proprietary Information**

Unlike the more gradual deviations in response that develop in unirradiated materials, irradiated materials tend to show a more abrupt deviation as K is increased. This is probably associated with the nature of the plastic zone in a cracked body – on initial formation in an irradiated material, plasticity in the plastic zone near the crack tip work softens that material and causes an increase in the plastic zone dimensions. However, the plastic zone is still constrained by the surrounding elastic material. As the K is increased, the plastic zone continues to grow, but as the dimensions of the plastic zone approach the dimensions of the specimen, work softening coupled with the absence of surrounding constraint in the elastic material produce a rapid expansion of the plastic zone. Thus, the transition from adequately elastic to grossly plastic occurs somewhat auto-catalytically. However, SCC testing has shown itself to be a very complex and subtle process to do reproducibly and accurately, so not all “empirical” observations of behavior can be taken at face value.

**Content Deleted -
EPRI Proprietary Information**

5.4 IASCC Data from Halden Test Reactor

**Content Deleted -
EPRI Proprietary Information**

5.5 Nine Mile Point Unit 1 In-Core IASCC Growth Rate Data

In some cases, IASCC data may be too quickly dismissed. An example is the earliest in-reactor IASCC growth rate data obtained at the Nine Mile Point Unit 1 BWR [5-10, 5-11] in 1986. The specimens placed in the recirculation system were a 7.25-inch long, 1-inch square geometry whose thickness at the base of the side grooves is 0.15 inches. The in-core specimens were a 7.125-inch long, complex geometry whose nominal thickness at the crack plane was ≈ 0.52 inch and whose thickness at the base of the side grooves is 0.092 inches. These geometries yield effective thicknesses of 0.387-inch and 0.219-inch, respectively – but for such deep, narrow side grooves relative to a much more substantial specimen cross-section, this is an overly conservative figure, as discussed earlier in this section. For the recirculation specimens, the allowable K value is about $22 \text{ ksi}\sqrt{\text{in}}$, somewhat below the $25 \text{ ksi}\sqrt{\text{in}}$ value used for testing. However, these specimens were well behaved and exhibited reasonable growth rates (Figures 5-8 through 5-10), consistent with the broad international experience that the unirradiated K/size criteria can be stretched before having a strong effect on crack behavior.

**Content Deleted -
EPRI Proprietary Information**

**Content Deleted -
EPRI Proprietary Information**

Figure 5-1
Example from GE/JAPEIC data of rapid increase in crack growth rate for type 304 stainless steel BWR irradiated to 3×10^{21} n/cm² as the specimen exceeded the K/Size criteria for IASCC testing

**Content Deleted -
EPRI Proprietary Information**

Figure 5-2

The DCB specimen design used in early Halden tests. This GE CRD design was about 4.2 inches long and 0.8 inch nominal thickness, and used a tapered ligament (the side grooves varied with crack depth) and tapered height (1 inch near the initial crack depth) to produce a constant K crack depth on a wedge loaded specimen

**Content Deleted -
EPRI Proprietary Information**

Figure 5-3
Example of crack length vs. time for the wedge-loaded DCB design used in the early Halden test reactor program. The specimens were loaded to about 35 ksi $\sqrt{\text{in}}$, which is a severe violation of the K/Size validity criteria

**Content Deleted -
EPRI Proprietary Information**

Figure 5-4
Example of crack length vs. time for the wedge-loaded DCB design used in the early Halden test reactor program. The specimens were loaded to about 35 ksi/in, which is a severe violation of the K/Size validity criteria

**Content Deleted -
EPRI Proprietary Information**

Figure 5-5
Crack growth rate vs. corrosion potential for the wedge-loaded DCB design used in the early Halden test reactor program. The specimens were loaded to about 35 ksi√in, which is a severe violation of the K/Size validity criteria

**Content Deleted -
EPRI Proprietary Information**

Figure 5-6
SCC growth rate vs. corrosion potential of sensitized and cold worked stainless steel and alloy 600 tested under linear elastic K/Size conditions

**Content Deleted -
EPRI Proprietary Information**

Figure 5-7
Response of irradiated stainless steel tested under valid linear elastic K/Size conditions, as evaluated elsewhere in this report. data cover a range of fluences from 1 – 4 dpa, and differ markedly from irradiated crack growth data where the K/Size criteria are violated

**Content Deleted -
EPRI Proprietary Information**

Figure 5-8
Crack length vs. time response for in-core, wedge-loaded DCB specimens installed in the nine mile point unit 1 BWR

**Content Deleted -
EPRI Proprietary Information**

Figure 5-9
Crack length vs. time response for recirculation, wedge-loaded DCB specimens installed in the nine mile point unit 1 BWR

**Content Deleted -
EPRI Proprietary Information**

Figure 5-10

Crack growth rate vs. corrosion potential for sensitized stainless steel tested in 288°C water at 25 – 30 ksi/in. The solid lines are the predicted response. most data are from laboratory specimens of thermally sensitized CT specimens, but the “Asterisk” points (at about 3.3×10^{-8} and 1.4×10^{-7} mm/s) are shown that represent the nine mile point unit 1 DCB specimens exposed in the recirculation system and in-core

6

SUMMARY OF UN-IRRADIATED STAINLESS STEEL DATA RELEVANT TO IRRADIATED BEHAVIOR

6.1 Introduction

The objective of this section is to show that the qualitative effect on stress corrosion cracking (SCC) of corrosion potential is similar among all iron and nickel alloys in high temperature water and, more specifically, that the benefit of low corrosion potential remains strong on cold worked stainless steel, which simulates the detrimental effects of radiation hardening. This section will summarize and provide detailed examples from studies by General Electric's CR&D of these effects, focusing primarily on sensitized and/or cold worked stainless steel, as well as provide some examples of irradiated stainless steel. The case for a strong effect of corrosion potential is very compelling, and the few isolated cases where a very limited benefit has been observed can be questioned in the light of the overwhelming and compelling evidence of a strong effect. Addressing the mechanistic issues associated with stress corrosion crack advance is also useful in providing confidence that SCC in unirradiated and irradiated materials follows a well-behaved continuum.

The tendency to fragment SCC into small, unique modes with individualized mechanisms and dependencies lives on despite the relative narrowness in alloy compositions and similarity in the environments used in light water reactor systems and many common SCC characteristics [6-1 through 6-7]. Similar stainless steel, nickel alloy and weld metal structural materials as well as RPV steel are used in boiling water reactors (BWR) and pressurized water reactors (PWR) – even across many companies and designs. Since it is now being acknowledged [6-8] that the crack tip is deaerated and at low potential in all cases, the environmental conditions under which crack advance occurs in BWR and PWR primary systems should be considered similar [6-1, 6-2, 6-4 through 6-7], especially with the increasing adoption of hydrogen water chemistry in BWRs. Thus, BWRs and PWRs differ primarily in: coolant additives that shift the pH at temperature from 5.6 to ≈ 7.0 ; H_2 fugacity (≈ 50 vs 3000 ppb H_2); and temperature (most structural materials in a BWR are exposed to 274°C water, whereas PWR primary water is up to 50°C hotter, and 65°C hotter in the PWR pressurizer). Of these factors, temperature has the most pronounced and universal effect on SCC.

The underlying mechanism of SCC advance in closely related systems has also been subjected to subdivisions, with unique interpretations applied. By any view, SCC is a complex phenomenological process which responds to 20 or more important engineering parameters whose inter-dependencies cause the effect of any given parameter to *shift* from strong to subtle as the other parameters change. These shifts – combined with a wide distribution in the adequacy of SCC measurements – are largely responsible for the fragmentation of SCC into multiple sub-modes. Underlying the complex phenomenology and the fragmented view of SCC is residual ambiguity in the causal, mechanistic underpinnings of SCC. Hypotheses of stress corrosion crack

advance range from brittle film cleavage [6-9, 6-10], to internal oxidation [6-11], to adsorption – decohesion [6-12], to enhanced surface mobility [6-13], to creep rupture, to film rupture/slip oxidation [6-1 to 6-7, 6-14], to hydrogen assisted cracking [6-12, 6-15 to 6-17], and beyond. Of these, the latter two are widely regarded as the most promising general descriptions of SCC in hot water environments, and one objective of this section is to evaluate hydrogen assisted crack advance mechanisms by evaluating several factors (martensite, yield strength, hydrogen fugacity, temperature) and phenomena (crack growth rate, hydrogen permeation) that should be strongly influential.

6.2 Experiments

Tests were performed to better understand the SCC process, particularly the role of increased yield strength. Compact type (0.5T for cold worked materials, and 1T for the annealed materials) crack growth specimens were machined with 5% side grooves on each side. Linear elastic fracture mechanics criteria were fully satisfied for the stress intensity – specimen size – yield strength conditions employed. Solution annealing was typically performed at 1050°C (1100°C for alloy 600) for 30 minutes followed by a water quench. Deformation was typically introduced by heating the plate material to +140°C (or cooling to –55°C; alloy 600 was rolled at 25°C) and rolling about half of the total reduction in each direction. Rolling at +140°C (termed “cool work”) produces much less deformation-induced martensite in these stainless steels than rolling at –55°C (termed “cold work”). Some materials were worked by forging. No deformation-induced martensite forms in alloy 600. Optical metallography of etched or ferrofluid stained structures was used to evaluate martensite levels.

CT specimens were instrumented with platinum current and potential probe leads for dc potential drop measurements of crack length. In this technique, current flow through the sample is reversed about once per second primarily to reduce measurement errors associated with thermocouple effects and amplifier offsets. The computer control of current reversal, data acquisition, data averaging techniques, and the relationship between measured potential and crack length have been presented previously [6-18 to 6-22]. Data are typically stored in a permanent disk file typically once every 1.5 hours. In addition to the data record number, total elapsed and incremental time, and crack length, the system measures and stores the temperature, current, corrosion potential, dissolved gases, influent and effluent conductivity, load and time/date. Additionally, both operator and automated program messages describing changes in test conditions and test status are a permanent part of the data record.

Hydrogen permeation measurements were made using closed-end 0.25-inch (6.4 mm) outside diameter (0.18-inch ID) stainless steel tubes inserted into the autoclave through a Swagelock fitting. The tubes were abraded on the inside and outside; the inside was exposed only to vacuum and hydrogen after heating. Hydrogen permeation into the tube was recorded by monitoring the increase in pressure to a maximum of 10 torr (10,000 microns) using an MKS Baratron Model 660 with a Model 622A11TCE pressure transducer. He leak checking was used to confirm the absence of leaks, and the system was operated at 150°C and 288°C under N₂ deaerated conditions to confirm its leak-tightness under system operating conditions. These measurements were similar to those performed on Alloy 600 [6-23], although the former had an equivalent gage length about 1.5 times longer, but a total gas volume of ≈ 19 cc vs. 24.8 cc for the Alloy 600 data.

6.3 Results and Discussion

Among the many areas of misunderstanding of SCC in stainless steels is the belief in immunity and thresholds, which are addressed in some detail elsewhere [6-24]. While it is not possible to refute all variants of immunity and threshold behavior, it is instructive to address the issue of sensitization, corrosion potential, and water purity. Figure 6-1 shows data (and predictions) for sensitized and unsensitized stainless steel in moderate to high purity 288°C water. Figures 6-1b and 6-1c shows the data from the SKI/EPRI round robin [6-25] (the smaller symbols at about +150 to +200 mV_{she}); Figure 6-1b also includes data (larger symbols) under carefully controlled changes in potential and at low potential. Figures 6-1c and 6-2 show that unsensitized (annealed) stainless steel is not immune to SCC – rather, the figures emphasize that if significant care is used transitioning from a transgranular fatigue crack to intergranular SCC, crack growth will occur. Figures 6-1c and 6-3 show that SCC readily occurs in unsensitized stainless steels in ultra high purity deaerated water. Cracks in all cases are intergranular [6-26, 6-27]. These are a few of many examples that show that unsensitized (i.e., zero fluence) stainless steels of many grades are not immune to SCC, even in theoretical purity deaerated water – thus, there can be no meaning to a *threshold* in *sensitization*, *neutron fluence*, *water purity*, *corrosion potential*, etc. Disproving that a threshold stress intensity factor, K (K_{ISCC}) exists is a challenge, because testing at very low stress intensity levels (i.e., approaching zero) is impractical. However, real cracks grow from smooth surfaces, and therefore must traverse the low K regime. The lack of a K -threshold is supported by recent data on crack growth in unsensitized stainless steel at 10 ksi $\sqrt{\text{in}}$ (Figure 6-4).

The technique by which the transition is made from the transgranular fatigue pre-crack to intergranular SCC is critical, as are a host of other testing controls and techniques [6-28]. The net result is the ability to reproducibly and accurately measure SCC growth rates under a wide variety of conditions, even at quite low rates. Reproducibility is a key consideration, and returning to identical test conditions to establish similar rates is an important measure of data quality (Figure 6-2).

Other key examples of the environmental crack growth rate response of worked stainless steels are shown in Figures 6-5 through 6-9. Figure 6-5 shows the response of a type 316L stainless steel that was more heavily worked than that shown in Figure 6-2, which leads to somewhat high crack growth rates, both at high and low corrosion potentials. While this specimen shows very well behaved response as loading conditions are changed in 288 °C water containing 2000 ppb O₂, it exhibits an initially lower growth rate at low potential, which slowly rises by 2.5X with time. (Note that this “constant K ” testing is done by (only) load shedding after every 0.001 change in a/W . Typically this represents a slow load shed of about 5 pounds (out of 1400 pounds total) every 20 hours (in the high potential regime)).

Crack growth rate data in Figure 6-6 on Type 347 stainless steel with 20% cold work shows the transition to static K response as increasingly gentle cyclic loading conditions are used. The growth rates are essentially identical to those observed on similarly worked types 304L and 316L stainless steel, indicating that the subtle changes in composition associated with $\approx 0.5\%$ Nb or $\approx 2.5\%$ Mo do not have a consequential effect on SCC behavior, although they can have a significant effect on sensitization behavior (which would produce differences in SCC).

Figure 6-7 shows a different heat of Type 304 stainless steel tested under similar conditions to prior heats. This material exhibited a factor of $\approx 2X$ higher crack growth rate at high potential than other materials (e.g., Figure 6-5), but was only slightly higher in growth rate at low potential. Nonetheless, the growth rates at low potential are relatively high, roughly equivalent to the historical rates on sensitized stainless steel piping (Figure 6-1a, at moderate potential). A repeat test on this material is showing similar response at high potential of 6.7×10^{-7} mm/s under constant K conditions. Figure 6-8 shows the response of another heat of type 316L stainless steel also tested under conditions similar to prior tests. It showed a well-behaved transition from gentle cycling to constant K conditions (although a somewhat higher growth rate was observed), as well as a sudden reduction in rate on shifting to low potential. In this heat, both high and low potential growth rates are somewhat lower than observed in 304 stainless steel (Figure 6-7), although this is not a general pattern – among all observations made to date, there is no consistent difference between the common grades of stainless steel for a given condition (sensitized, cold worked, etc.)

For comparison purposes, Figure 6-9 shows the response of 20% cold worked (by cross-rolling at 25°C) alloy 600 under similar test conditions. The growth rate at both high and low corrosion potential is very similar to the observations on stainless steels. The fractography on all stainless steel and alloy 600 specimens tested is intergranular (Figure 6-10).

The crack growth rate response in 288°C water of stainless steels and alloy 600 (and alloy 182 weld metal) is quite similar when comparisons are separately made for the sensitized, the unsensitized, or the cold worked (Figure 6-1) conditions [6-26, 6-29, 6-30]. There is clearly a strong effect of elevated corrosion potential (200 or 2000 ppb dissolved O_2) under all conditions. However, at low potential, there is no evidence of any difference in crack growth rate of stainless steel with smaller changes in potential associated with variations in the dissolved H_2 concentration. Here the changes in potential are limited to ≈ 56 mV per decade change in H_2 at 288°C; as the H_2 level is changed from 95 ppb (about 1.06 cc/kg) to 1580 ppb (17.7 cc/kg), the change in potential is only about 68 mV (vs. a 600 – 700 mV potential change for 2000 ppb O_2). The important distinction is that, unlike O_2 , H_2 is not consumed in the crack, so no potential gradient is formed. However, such small changes in potential can be important for nickel alloys, because (unlike iron alloys) the transition from NiO (or spinel) stability to Ni metal stability occurs in this potential regime [6-31, 6-32].

Hydrogen permeation data were obtained for stainless steel and for alloy 600 [6-23]. All data were very linear and highly reproducible (Figure 6-11), and show that hydrogen permeation is primarily controlled by the coolant H_2 fugacity (Figure 6-12), temperature, and material (alloy 600 is about twice as permeable to hydrogen at a given temperature). Thus, the H_2 fugacity in the coolant (not corrosion reactions, transmutation, radiolytic proton injection into the metal, etc.) dominates hydrogen permeation through the metal, following (as expected) a square root dependency on H_2 fugacity over the temperature range studied (≈ 200 to 360°C). Also interesting is that the effective surface fugacity of H_2 becomes very low in O_2 -containing solutions, as reflected in a rapid drop in H_2 partial pressure in the tube [6-27]. Clearly the H_2 gas in the tube readily dissociates to adsorbed hydrogen on the tube ID.

The crack growth rate data obtained on unsensitized, cold worked stainless steels and alloy 600 are remarkably similar, and inconsistent with a hydrogen dominated crack advance mechanism in high temperature water. Considering only the crack growth rate data, the similarity in crack growth rates for Types 304L and 316L stainless steel and alloy 600 under both aerated and deaerated 288°C water (Figure 6-1) conditions show that martensite per se does not influence crack growth rates. This is reinforced in Figures 6-13 and 6-14 which plot SCC growth rate vs. yield strength for high potential and low potential conditions, respectively (specimens with extremely high or low martensite are identified). Martensite is present only Type 304L stainless steel that was cold worked at -55°C. Prior studies [6-12, 6-15, 6-16] have shown a large effect of martensite on SCC of stainless steels at temperatures below about 125°C.

The data also show no correlation between stress corrosion crack growth rates and hydrogen permeation rate (Figure 6-12). Very high hydrogen permeation rates occur as the coolant H₂ level is increased, but the growth rate is unchanged whether deaeration (low corrosion potential conditions) is achieved using N₂, 95 ppb H₂, or 1580 ppb H₂ – a range which produces more than 200X change in hydrogen permeation rate at 288°C. It is also important to note that the fairly thick oxides (typically 0.1 – 0.5 μm) of varying structure that form under high and low potential conditions seem to have little effect on hydrogen permeation, and that permeation both in and out of the tube occurs readily (Figure 6-11).

The role of H in irradiation assisted SCC of stainless steels can also be addressed, including under conditions where H is formed by transmutation. The H concentration in irradiated stainless steels typically saturates in the vicinity of 15 – 25 wppm [6-33, 6-34], although the formation of voids (which occurs readily above 320°C, and can occur to a limited extent at < 300°C) correlates with dramatically higher concentrations of H [6-35]. However, the rate of formation of H by transmutation (or the rate of proton injection from radiolysis) is many orders of magnitude lower than the permeation rates measured in this study. Note that BWR and PWR primary coolants always have hydrogen present, from as low as 10 ppb H₂ in BWRs under “normal water chemistry”, to 50 – 100 ppb H₂ under “hydrogen water chemistry” or NobleChem™ operation, to about 3000 ppb in PWR primary systems. In turn, these studies have shown that H₂ is not readily “trapped” in a void (or tube), but readily dissociates and diffuses. Thus, the fugacity of H in the metal remains in equilibrium with the coolant H₂, except perhaps in the rare case of rapid temperature changes. In turn, it is hard to imagine that the highly elevated (e.g., 50 wppm, or 2800 appm) H concentrations measured in irradiated stainless steel [6-35] are anything but a reflection of additional “storage” sites in the microstructure (i.e., it is not hydrogen that is microstructurally active). Such H cannot be attributed to transmutation or corrosion reactions when the permeability of H from the coolant is orders of magnitude higher. In turn, the effect of lowering the potential by decreasing the dissolved O₂ has a pronounced beneficial effect on IASCC of even highly irradiated stainless steel, just as in unirradiated materials.

A pronounced role of H on higher strength iron and nickel base alloys is well accepted for tests below ≈ 130°C. The importance of martensite in exacerbating hydrogen effects is highlighted in reference [6-16], where the correlation between severe hydrogen embrittlement (that induced highly intergranular fracture) and martensite content of Type 304 stainless steel was *very* strong, in contrast to these results. It is certainly possible that some effects of H on dislocation mobility in metals persist to higher temperatures, although thermally activated dislocation motion increases with temperature. Also, the ubiquitous nature of H in metals exposed to hot water

(most achieve 2 – 5 wppm levels within days of exposure) raises the question of whether there is a unique/distinguishable contribution of hydrogen that varies from differences in coolant fugacity that pragmatically vary by <300X (10 ppb to 3000 ppb) – especially since high hydrogen permeation rates are recorded even at the lowest fugacity levels. Other findings such as the absence of detrimental effects of applying Pt-group catalysts to the surface, high crack propagation rates (only) at low temperature of high strength nickel alloys [6-36, 6-37], and other evidence against a causal role for hydrogen in SCC in hot water is discussed in reference [6-34]. However, it should also be noted that there is evidence in the corrosion fatigue literature that reduced life is observed when high coolant H₂ fugacity conditions exist [6-38]. This may be related to some “residual” effect of H on the reversed slip processes at 290°C, although it may also be caused by the differences in film properties and general corrosion rate (about 10X higher in deaerated water). It is interesting that some strong effects of gentle cyclic loading have been observed on high yield strength materials (Figure 6-15), although similar effects are observed both at high and low potential, indicating that H is most unlikely not a major factor.

The PLEDGE predicted responses of yield strength, corrosion potential, and sensitization effects are shown in Figures 6-1, 6-13 and 6-14. These include the effects of corrosion potential, sensitization, stress intensity, and water purity (specific anion concentrations) that have long been well understood along with the effects of yield strength from cold work and irradiation (as well as other irradiation effects) that has been more recently modeled. There is a strong equivalence of cold work and irradiation contributions to yield strength in terms of enhancing SCC. The amount of published crack growth data on irradiated stainless steel at low corrosion potential (where radiation induced Cr depletion plays a small role) is limited, but growth rates (at somewhat lower K values of 20 – 25 MPa√m, the limit of the LEM K/size validity for the specimen sizes tested) are in the vicinity of 1 – 3 x 10⁻⁸ mm/s at 288°C for irradiation doses that produce a yield strength of 700 – 850 MPa. Higher growth rates will be observed at higher temperatures (e.g., Figure 6-3). (Note that the K/size validity is not well treated by the ASTM standards because irradiated materials undergo local and macroscopic work softening as the first dislocations sweep out the “point” defect damage, thereby creating localized “channels” of high dislocation activity.) Experience with SCC of irradiated materials suggests that when increased yield strength occurs by irradiation (vs. from initially cold worked materials that slowly convert to a purely irradiated microstructure), the average of the *annealed* and irradiated yield strengths should be used as effective yield strength.

A major factor in assimilating the role of increased yield strength in SCC is the recognition that it comes not only from bulk cold work or irradiation, but also from surface cold work and from residual strain adjacent to weld heat affected zones (HAZ). While there has been much recognition that weld residual stresses are important (and sensitization from welding), the role of weld residual strain has only recently surfaced [6-26, 6-29, 6-39]. New techniques for measuring strains reveal that most weld HAZs have 8 – 20% equivalent room temperature tensile strain, and SCC measurements show enhanced growth rates in the unsensitized HAZ region.

6.4 Relevance to IASCC and Supporting Evidence for Corrosion Potential Benefits

There is a growing recognition that irradiation by the first neutron (or first 10^{21} neutrons/cm²) does not transform the SCC into an entirely new phenomenon with no link to its “past”. Indeed, most investigators accept that the dominant contributions of light water reactor irradiation fall into four categories:

- Increased corrosion potential (on the surface, not in the crack) from radiolysis, at least for dissolved H₂ levels below about 500 ppb.
- Radiation induced segregation (RIS) at grain boundaries, leading to Cr and Fe depletion, and enrichment in Ni, Si, P, etc.
- Radiation hardening (RH), which produces a pronounced increase in yield and ultimate tensile strength, typically exceeding 100 ksi within a few dpa.
- Radiation creep relaxation, which produces dynamic strain under load and relaxes constant displacement stresses, e.g., associated with weld residual stresses.

It is therefore not surprising that factors that have a significant effect on SCC growth rate of unirradiated materials also have a significant effect on irradiated materials. Of such factors, the effect of corrosion potential is of the greatest pragmatic importance, because it has a large effect on growth rates and can be reduced on almost all wetted surfaces in a BWR.

The many examples of the effect of corrosion potential that have been shown on unirradiated materials of many types and conditions represent a small fraction of the total available data. These effects observed on unirradiated stainless steel show excellent consistency and continuity with the behavior of irradiated stainless steels, as summarized in Section 2. While some partly contradictory data do exist, the benefit in reducing SCC growth rate by lowering the corrosion potential is very consistently observed over a wide range of fluence, materials, and testing techniques. The benefit remains even under conditions that are very aggressive, including slow strain rate testing and crack growth testing where the stress intensity employed is significantly in excess of that allowed for a given specimen size.

6.5 Summary

Many stress corrosion crack growth rate studies have been performed in high temperature, ultra high purity water on unsensitized stainless steels and alloy 600 as a function of type and heat of material, yield strength, martensite, corrosion potential, temperature, and hydrogen fugacity. SCC is strongly influenced by yield strength, corrosion potential, and temperature, and was essentially independent of the martensite content per se, the type and heat of material, the hydrogen fugacity, the hydrogen permeation rate (which was controlled by the H₂ fugacity in the coolant). These observations are inconsistent with a hydrogen-controlled mechanism of crack advance, and erode the argument that corrosion-based sources of hydrogen can play a consequential role. The behaviors of various grades of stainless steel and Alloy 600 at 20% cold work are essentially identical at both low and high corrosion potential. The SCC response was

similar for cold worked and irradiated materials of similar YS levels tested at low potential (where radiation induced Cr depletion plays a minimal role). Finally, the effect on SCC growth rates of yield strength, corrosion potential, alloy type/heat, sensitization, and other factors are accurately predicted by the GE PLEDGE model as well.

These effects observed on unirradiated stainless steel show excellent consistency and continuity with the behavior of irradiated stainless steels. The effects of radiation hardening (increased yield strength) on crack growth are well simulated by cold work, and the effects of radiation induced segregation by Cr depletion. While some partly contradictory data do exist, the benefit in reducing SCC growth rate by lowering the corrosion potential is very consistently observed over a wide range of fluence, materials, and testing techniques. The benefit remains even under conditions that are very aggressive, including slow strain rate testing and crack growth testing where the stress intensity employed is significantly in excess of that allowed for a given specimen size.

It should always be recognized that the factor of improvement in crack growth rate associated with any change in material, stress / stress intensity, water chemistry, temperature, etc. will depend (sometimes very markedly) on every other condition. For example, at moderate to high potential, small levels of impurities make a big difference while at low potentials, even 10X higher levels in impurities make no difference whatsoever. Sensitization has a big effect at high potential, but little or no effect at low potential – etc. For sensitized materials, a large benefit in growth rate is commonly observed on shifting from high to low potential, but these observations are typically at a fairly high stress intensity of typically 30 ksi√in. As the K is decreased the benefit rises.

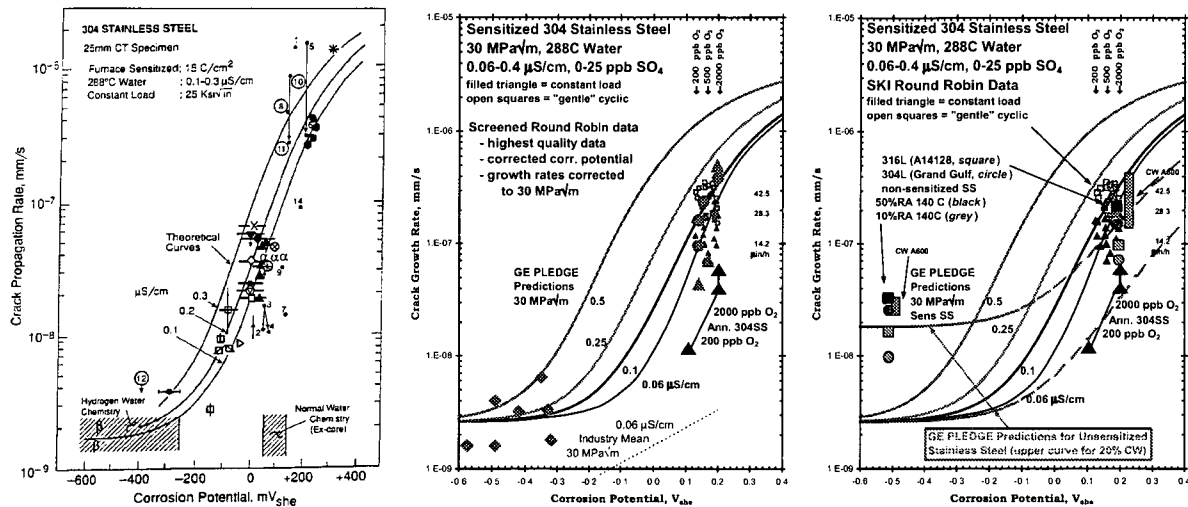


Figure 6-1
SCC growth rate vs. corrosion potential for stainless steels tested in 288°C high purity water containing 2000 ppb O₂ and 95 – 3000 ppb H₂

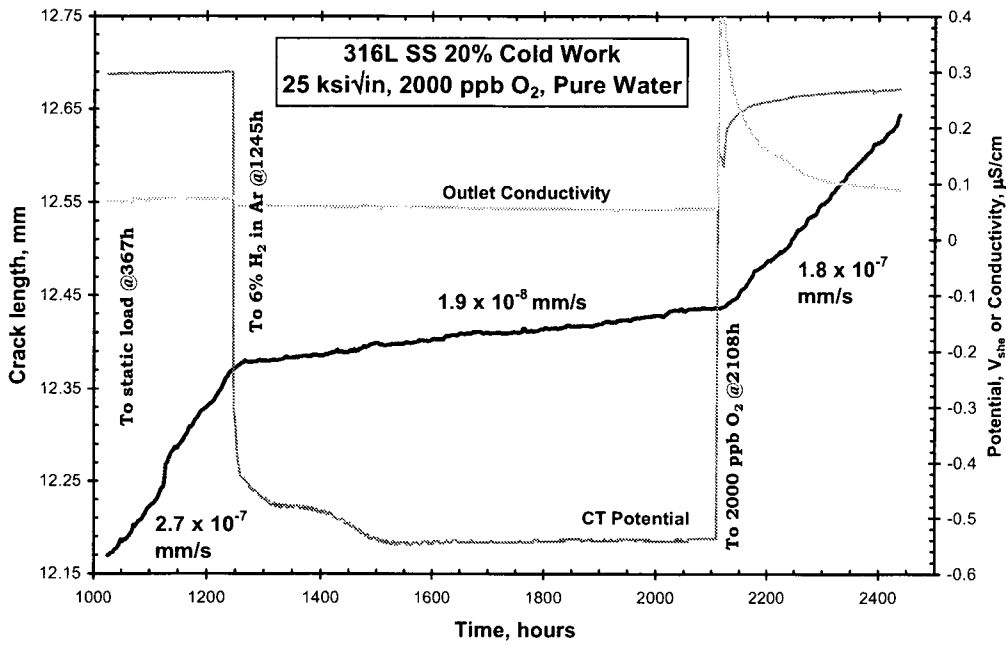


Figure 6-2
Crack length vs. time for a 0.5TCT specimen of unsensitized type 316L stainless steel “Cold” worked at -55°C to 20% reduction in area

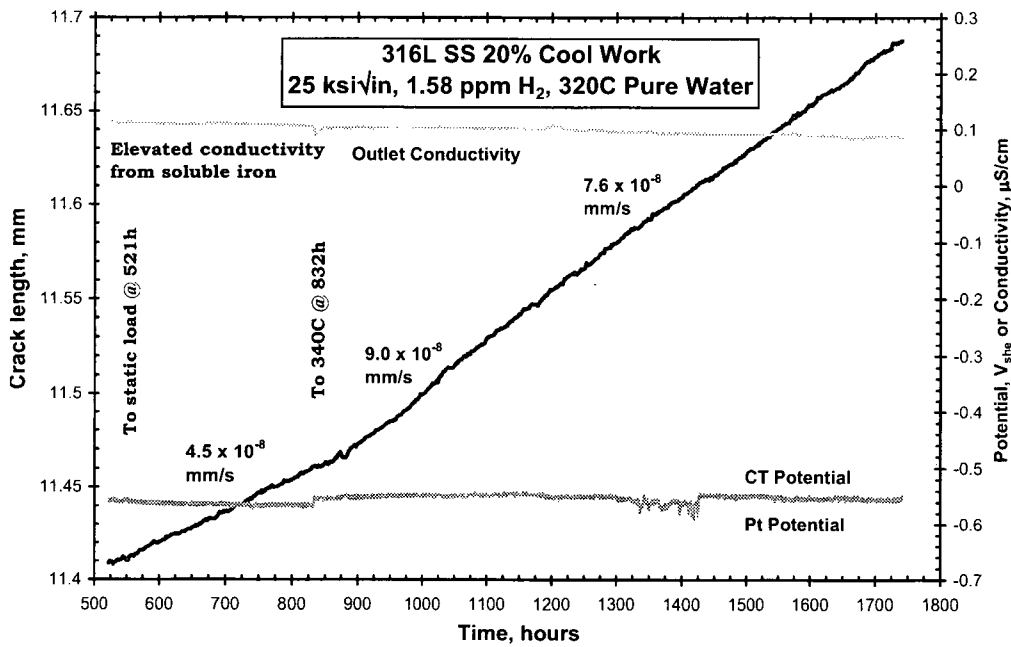


Figure 6-3
Crack length vs. time for a 0.5TCT specimen of unsensitized type 316L stainless steel “Cool” worked at $+140^{\circ}\text{C}$ to 20% reduction in area

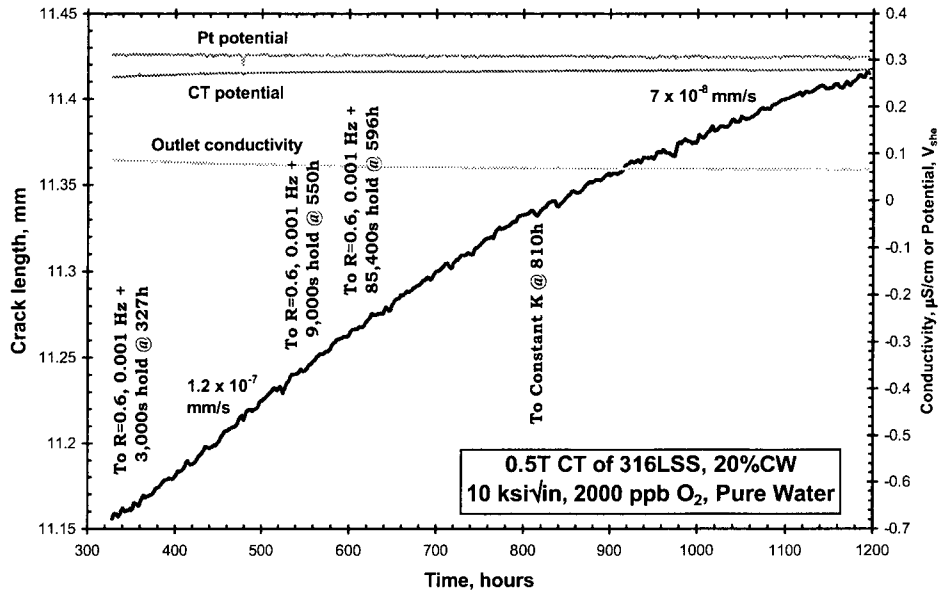


Figure 6-4
Crack length vs. time for a 0.5TCT specimen of unsensitized type 316L stainless steel "Cool" worked at +140°C to 20% reduction in area

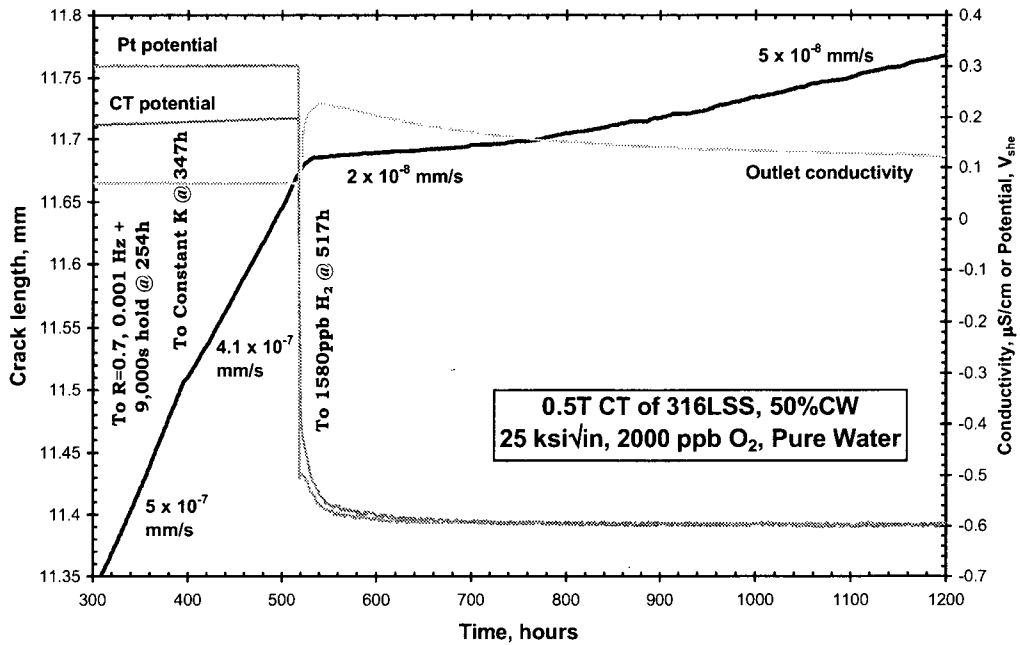


Figure 6-5
Crack length vs. time for a 0.5TCT specimen of unsensitized type 316L stainless steel "Cool" worked at +140°C to 50% reduction in area

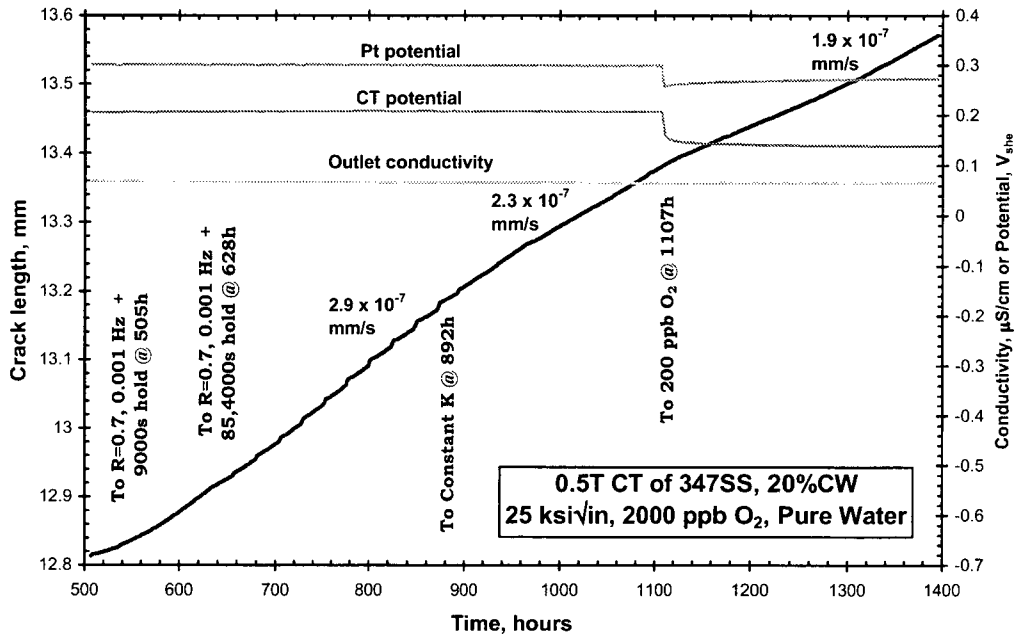


Figure 6-6
Crack length vs. time for a 0.5TCT specimen of unsensitized type 347 stainless steel "Cool" worked at 140°C to 20% RA

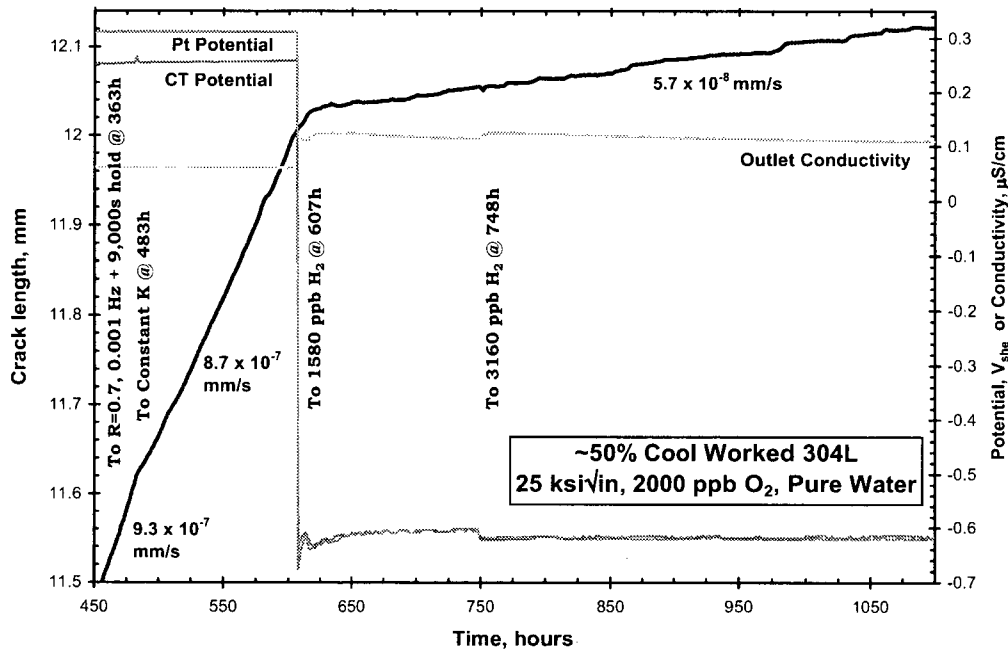


Figure 6-7
Crack length vs. time for a 0.5TCT specimen of unsensitized type 304L stainless steel "Cool" worked to ≈50%

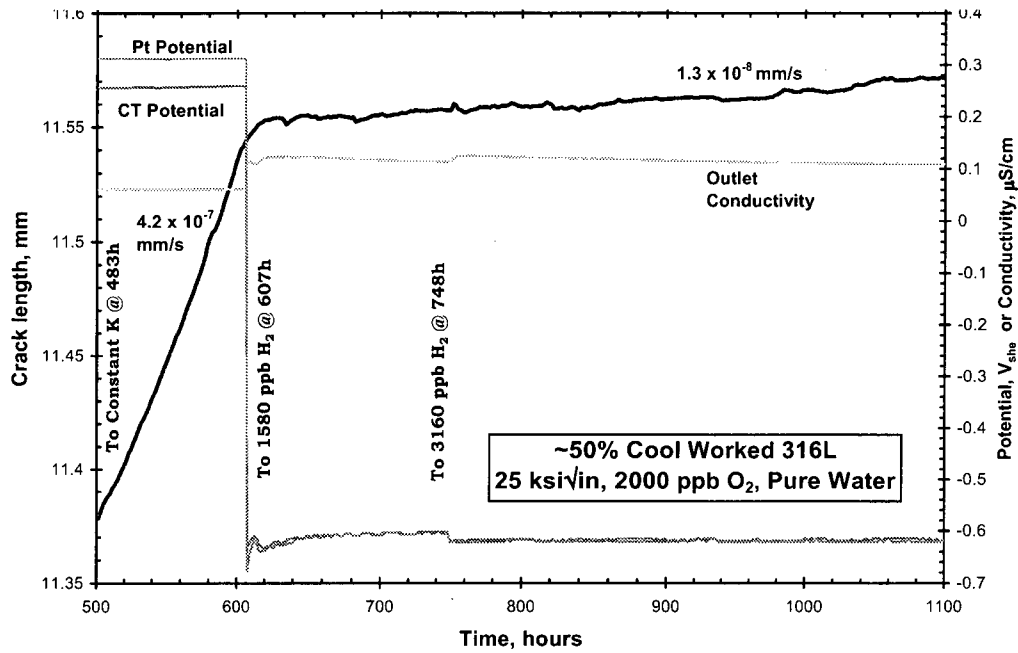


Figure 6-8
Crack length vs. time for a 0.5TCT specimen of unsensitized type 316L stainless steel "Cool" worked to $\approx 50\%$

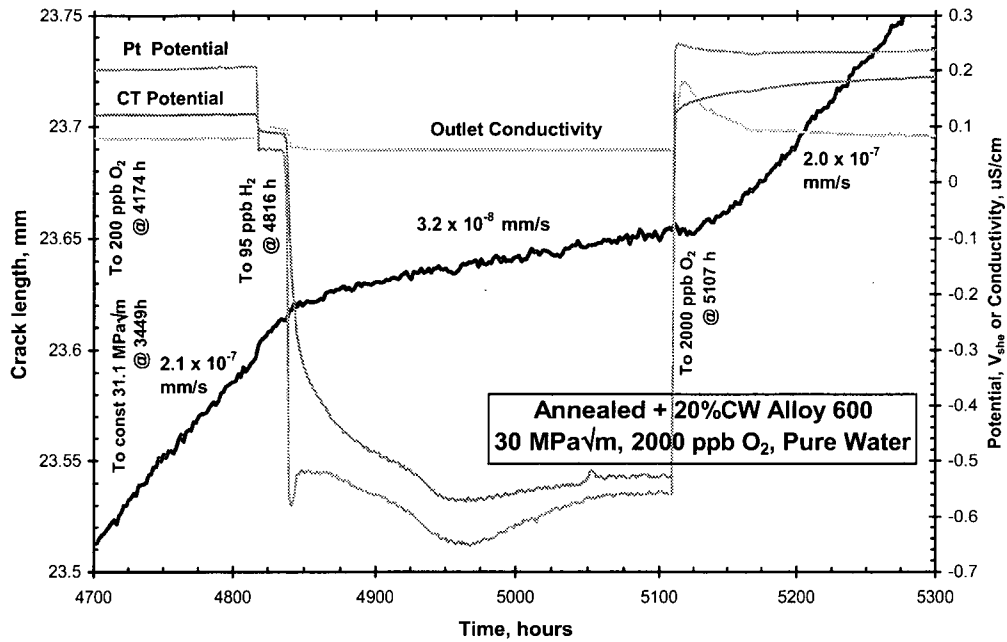


Figure 6-9
Crack length vs. time for a 1TCT specimen of unsensitized alloy 600 cold worked at 25°C to 20% reduction in area

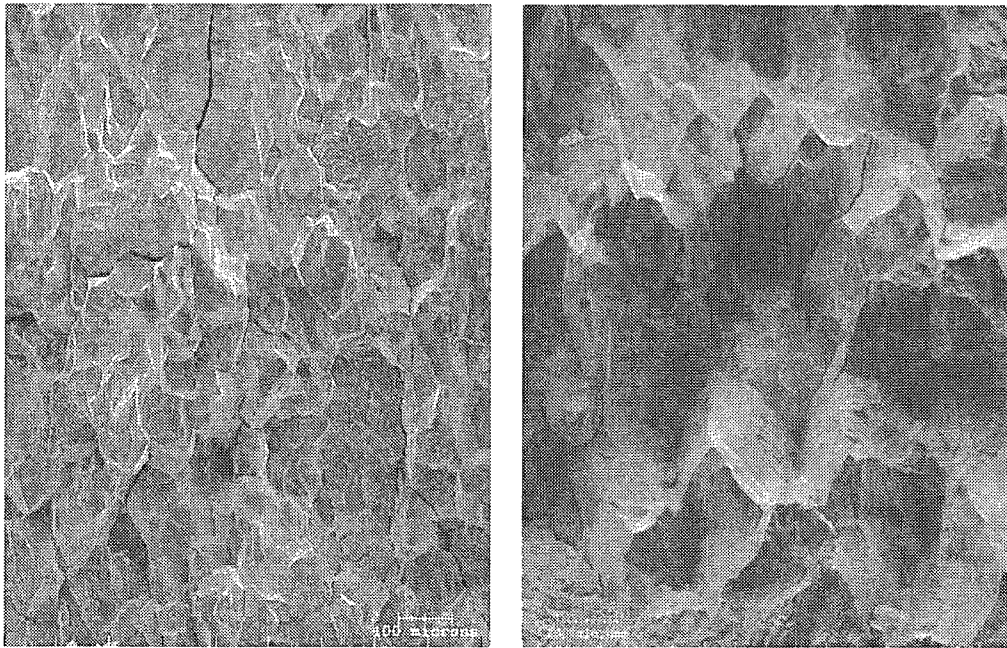


Figure 6-10
IG morphology observed in cold worked materials. (a) annealed + 20% cold work (-55°C) type 304L SS. (b) annealed + 20% cold work alloy 600

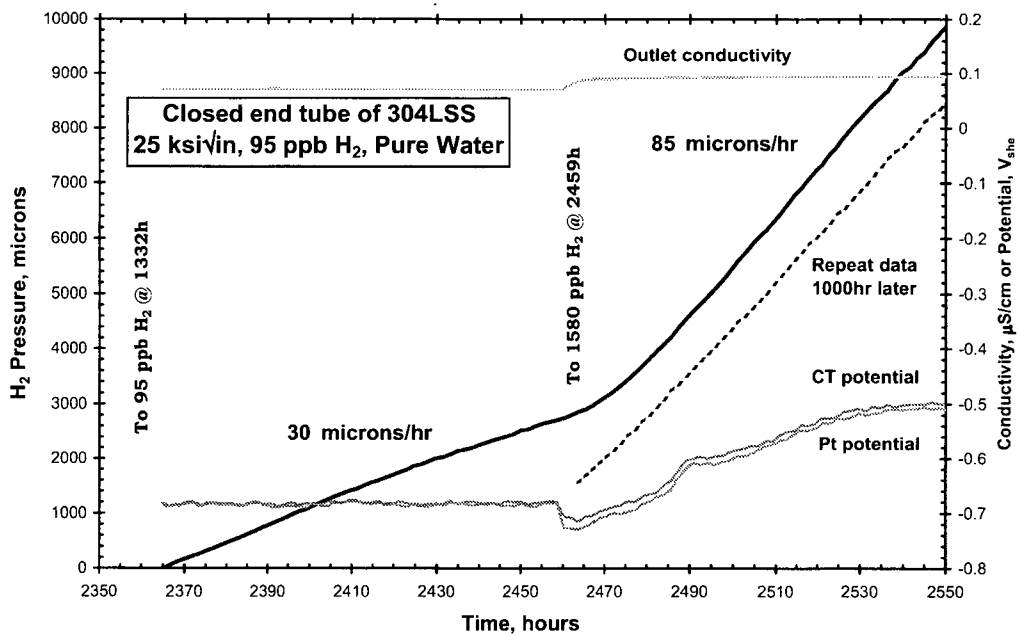


Figure 6-11
Hydrogen permeation vs. time and coolant H_2 fugacity unsensitized type 304L stainless steel

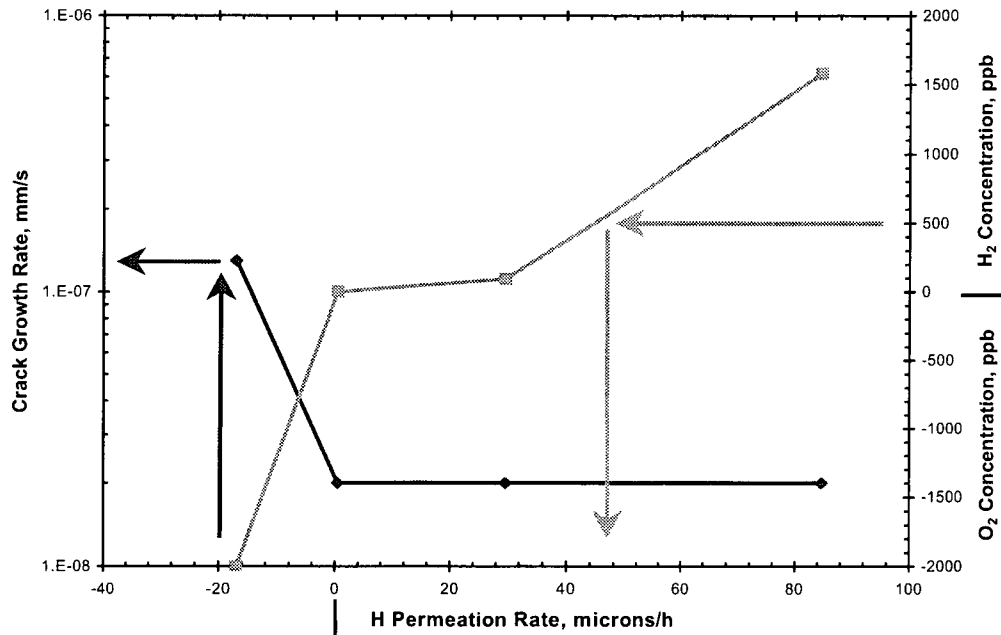


Figure 6-12
 Hydrogen permeation rate (measured as a pressure increase or decrease) vs. crack growth rate and vs. coolant H₂ (and O₂) concentration in unsensitized 304L SS

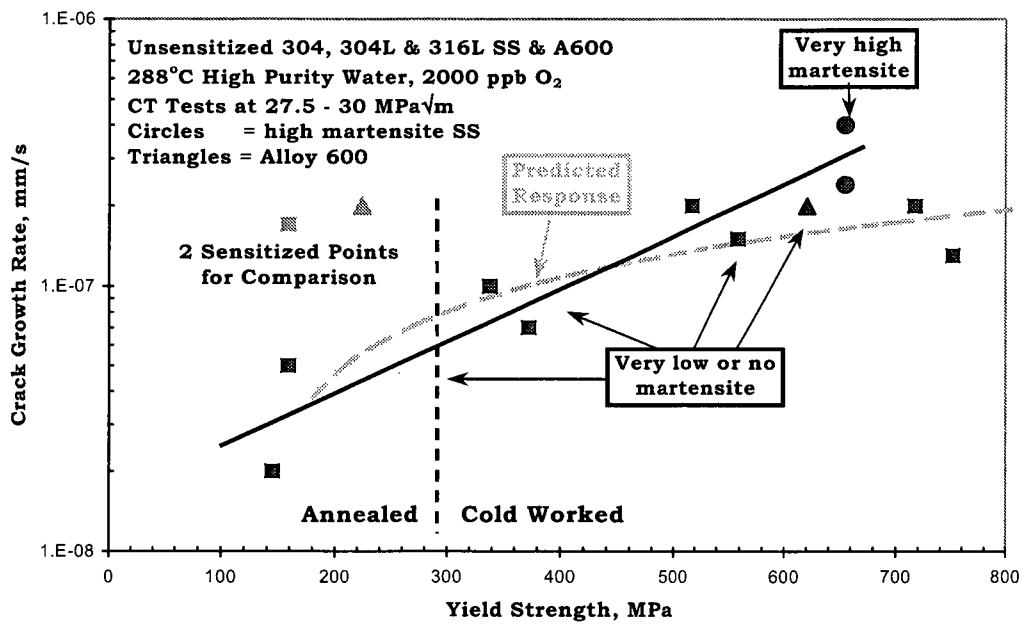


Figure 6-13
 Effect of yield strength and martensite on the stress corrosion crack growth rate on stainless steel and alloy 600 in 288°C, high purity water (<0.10 μS/cm outlet) containing 2000 ppb O₂

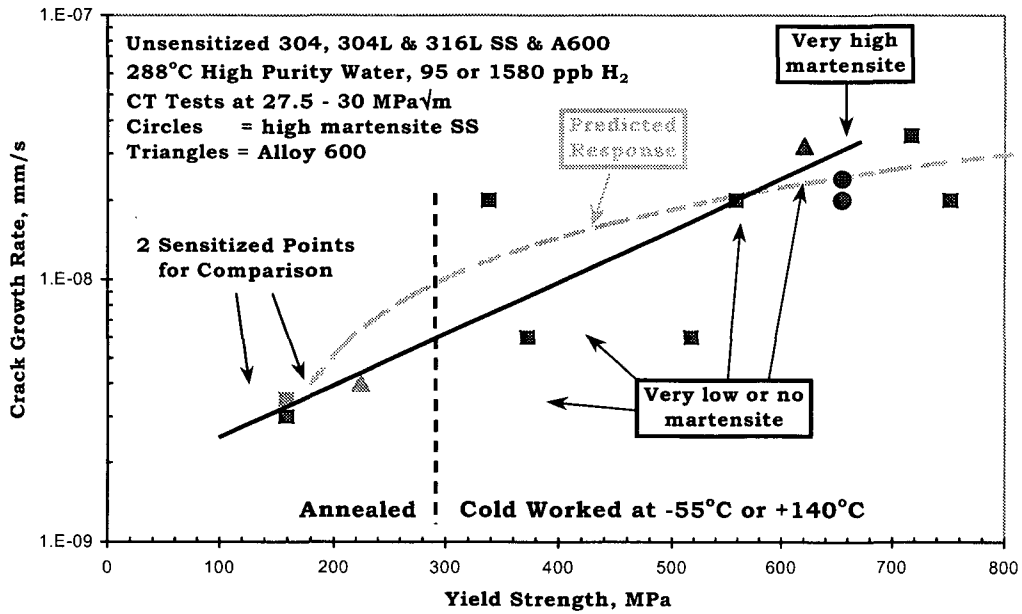


Figure 6-14 Effect of yield strength and martensite on the stress corrosion crack growth rate on stainless steel and alloy 600 in 288°C, high purity water ($\approx 0.06 \mu\text{S/cm}$ outlet) containing 95 or 1580 ppb H₂

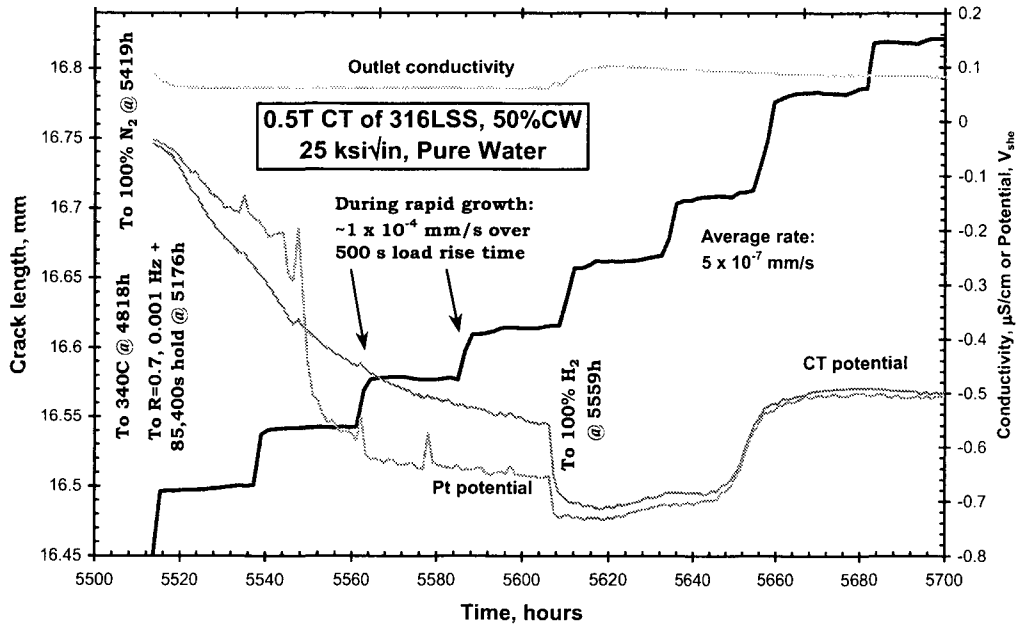


Figure 6-15 Effect of gentle unloading cycles on environmental crack advance on stainless steel whose yield strength is elevated by cold work

7

DEPENDENCY OF SCC ON STRESS INTENSITY AND THE ROLE OF RADIATION CREEP RELAXATION

7.1 Background

To interpret the historical trajectory by which cracks developed, or to project their future growth, the nature of the residual stress profile and the associated change in stress intensity factor with crack advance is important. This section will address the importance of residual stress profiles, their relaxation by radiation creep, and the effect of stress intensity on SCC growth rate.

**Content Deleted -
EPRI Proprietary Information**

Radiation produces a number of simultaneous and related displacement damage effects in materials. When high energy particles interact with materials, atoms are displaced from their original lattice locations to relatively distant locations, generally producing a cascade of secondary displacement damage. While the efficiency of generating displacement damage is much less than 100% (vacancies and interstitials recombine), a large number of new interstitial atoms (i.e., the displaced atoms) and vacancies are created, and these coalesce to form interstitial and vacancy loops, or migrate to grain boundaries. Thus, the processes that produce radiation segregation (a product of the vacancy and interstitial flux to the grain boundary), radiation hardening (e.g., the development of the interstitial and vacancy loops), and radiation creep relaxation (migration and interaction of the continuously generated interstitials and vacancies with dislocations under stress) occur in concert – it is not possible to have the damaging elements (segregation and hardening) without the beneficial elements.

There are relatively few studies where the effect of stress intensity has been evaluated in high quality, definitive experiments. Probably the most voluminous studies have been performed by Speidel [7-2 to 7-3], but the quality of this data is widely called into question for many reasons, including the use of wedge-loaded specimens; uncertain precision in the wedge loading procedures; lack of side grooves and associated out-of-plane cracking and extensive crack branching; use of thin specimens that often severely violate ASTM K/size validity criteria; very poor control of testing conditions exemplified by the nearly consistent use of static autoclaves; absence of continuous crack measurement capability (depth is determined destructively after the test); poor reproducibility of much of the data; etc.

In other work, the SCC growth rate response is sufficiently noisy and irreproducible (e.g., Figure 7-3) that determining a stress intensity response is impossible. A primary source of the scatter in such data is the use of poor testing procedures [7-4 to 7-7], especially the assumption that a transgranular fatigue precrack can be treated as though it were an intergranular stress corrosion crack, so that subsequent behavior on loading will be representative of “SCC”. Additionally, highly uneven crack fronts often develop for this and other reasons which complicate the reporting, correction and interpretation of data.

It has been proposed [7-7 to 7-11] that environmentally assisted crack advance in hot water occurs by a slip oxidation mechanism, which attributes primary importance to the protective oxide film that forms on engineering materials. As dynamic strain produces slip offsets that cause rupture of this protective film, rapid corrosion and film reformation occurs – that is, the environmental component of crack advance is “Faradaically” linked to the oxidation / corrosion process. The intergranular path is preferred either because there is a chemical preference (associated, e.g., with Cr depletion) or because deformation occurs preferentially along the grain boundary (e.g., from slip accommodation from the adjacent grains).

The conceptual framework of this model has been embodied in a simple expression that relates the crack velocity, V , with the deformation (crack tip strain) rate, $\dot{\epsilon}_{ct}$, and the rate at which the film reforms (the repassivation rate, $-n$): $V = f(n) (\dot{\epsilon}_{ct})^n$. [2-16] It is accepted that $\dot{\epsilon}_{ct}$ has a dependence on K and “ n ” which varies with the water chemistry and material chemistry at the crack tip, but typically varies between 0.3 and 1.0. For modern BWR operating conditions models as well as field data [1-1] predict a K dependence of between K^2 to $K^{2.5}$ (for normal water chemistry conditions) and K^3 to $K^{3.5}$ (for low potential conditions).

7.2 Observed K Dependencies in Unirradiated and Irradiated Data

This range of predicted K dependence is observed in many categories of data. In early BWR operation, represented by sensitized stainless steel and higher conductivity (impurity levels), the NRC disposition line and associated supporting data were close to a K^2 dependency (Figure 7-4). However, this dependency (the slope) varies with material and water chemistry conditions, as shown in Figures 7-4 and 7-5. The effect of very aggressive water chemistry conditions in creating a shallow dependency on stress intensity is also evident in Figure 7-6, which shows the predicted and observed response for Alloy 182 weld metal with 100 ppb sulfate as H_2SO_4 .

The effect of stress intensity on unsensitized, 20% cold worked 316L stainless steel in pure water at high corrosion potential is shown in Figure 7-7 a dependency of $K^{2.3}$ is shown. The quality of the supporting crack length vs. time data for each of the low stress intensity data is also shown in Figure 7-7. Well-behaved SCC growth data has not been that difficult to obtain provided careful transitioning phases are used to shift from transgranular fatigue precracking to static load intergranular stress corrosion cracking.

A very similar stress intensity dependency is observed in well behaved data on irradiated stainless steel of various types (e.g., Figures 7-8 and 7-9). In these figures, some of the crack growth data obtained early or late in the test are differentiated. The problems of obtaining reliable data early in the test are complicated by the need to transition from TG to IG

morphology along the entire crack front, which was not done in these tests. The subsequent data with increasing K appears to be very well behaved. This is not the case in Figure 7-10. At low K values the apparent K dependency is astronomically high at $\approx K^{16}$. This can be attributed to testing where the specimen probably did not transition to a fully IG crack front and had an uneven crack front, both of which would lead to anomalously low crack growth rates. The subsequent straightening of the crack front produced very high growth rates later in the test.

7.3 Summary of Stress Intensity Dependency

The stress intensity dependency is controlled by material properties (esp. Cr depletion), water purity, corrosion potential, etc. While there is no shortage of confusing and somewhat contradictory data, there is a compelling case to be made for a stress intensity dependency on stress corrosion crack growth rate of $\approx K^{2.0}$ to $K^{2.5}$ under high purity water conditions at high corrosion potential. Under low corrosion potential conditions in reasonable purity water, a stress intensity dependency of $\approx K^{3.2}$ to $K^{3.6}$ is appropriate.

7.4 Radiation Creep Relaxation

High energy radiation produces a number of simultaneous effects in materials, most originating with the displacement of atoms from their original lattice position to relatively distant locations, usually as an interstitial. The interstitial atoms and the associated vacancies group into interstitial and vacancy clusters (hardening), migrate to grain boundaries (producing changes in grain boundary chemistry), and relax constant displacement (e.g., weld residual) stresses with interaction with and absorption by dislocations.

**Content Deleted -
EPRI Proprietary Information**

**Content Deleted -
EPRI Proprietary Information**

7.5 Proposed Stress Intensity Dependency and Weld Residual Stress Relaxation Levels

**Content Deleted -
EPRI Proprietary Information**

**Content Deleted -
EPRI Proprietary Information**

Figure 7-1

Calculated default residual stress profile for BWR core shroud belt-line weld based on alternate side welding passes (a ≈ 0.5 ksi stress from differential pressure also exists). some local shifts in this average residual stress profile must exist because of fit-up stresses, location of the last welding pass, statistical deviations in residual stresses, etc.

**OBSERVED RESIDUAL STRESS PROFILES
IN HAZ OF 24"-28" DIA. SCH. 80 PIPING**

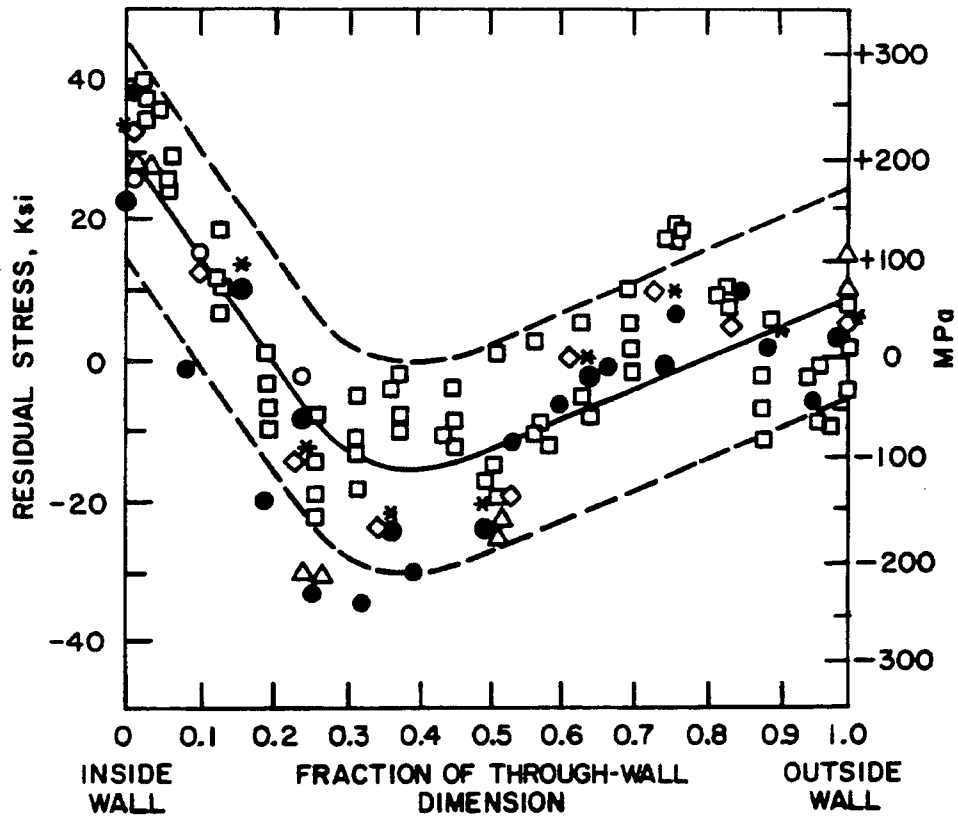


Figure 7-2
Measured residual stress data for large diameter BWR pipe weld. variations about the average may be associated with fit-up stresses, location of the last welding pass, statistical deviations in residual stresses, etc.

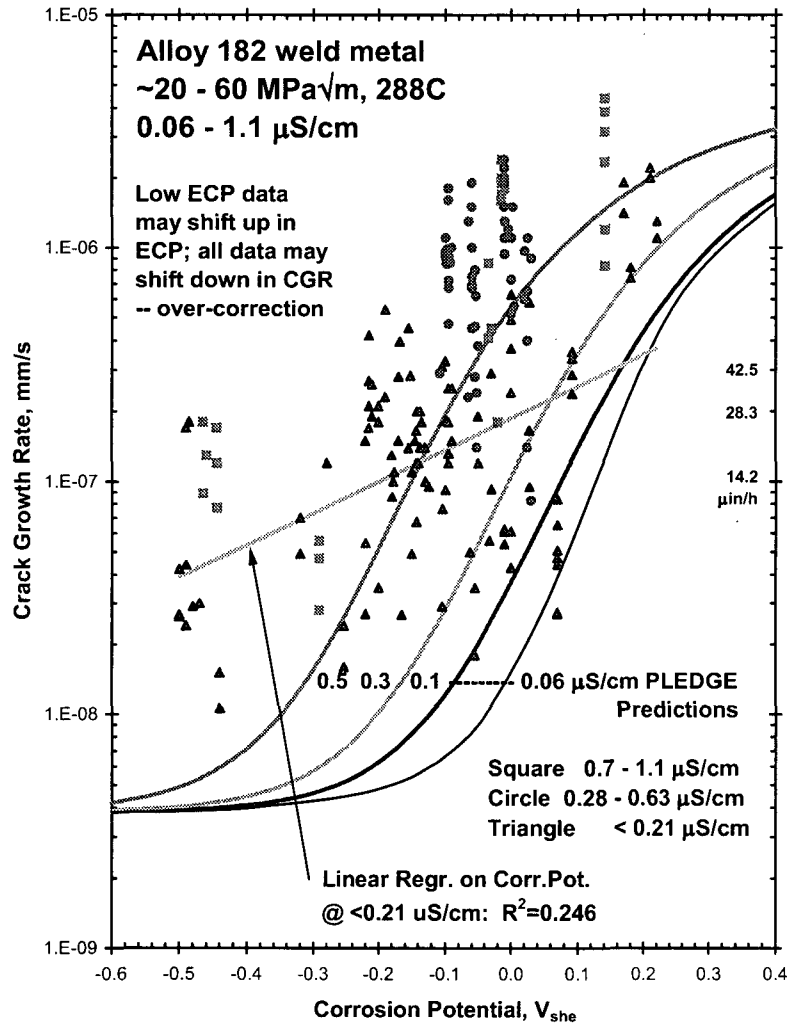


Figure 7-3
 Stress corrosion crack growth rate data for alloy 182 weld metal from the literature [7-4, 7-7]. Similar examples of irreproducible SCC data exist for stainless steel, low alloy steel, and irradiated stainless steel, and are due primarily to flaws in testing

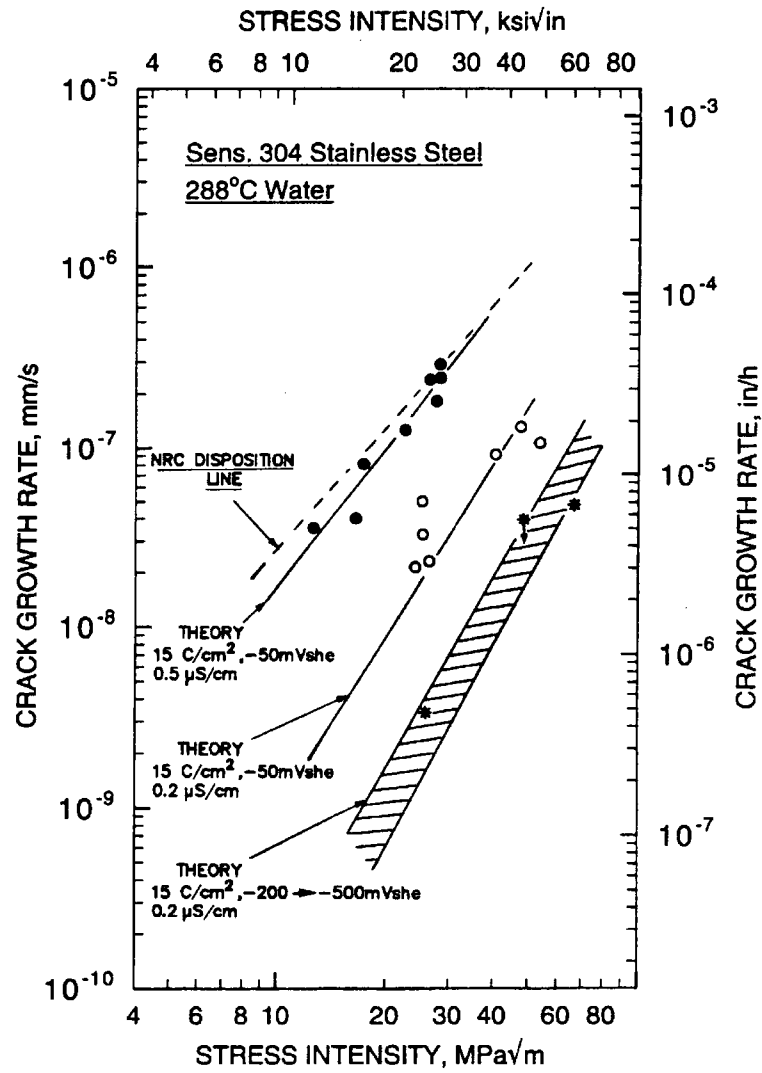


Figure 7-4
Crack growth rate vs. stress intensity for sensitized stainless steel in water of varying purity and corrosion potential. These variations change the K dependency from about K^2 to over K^3

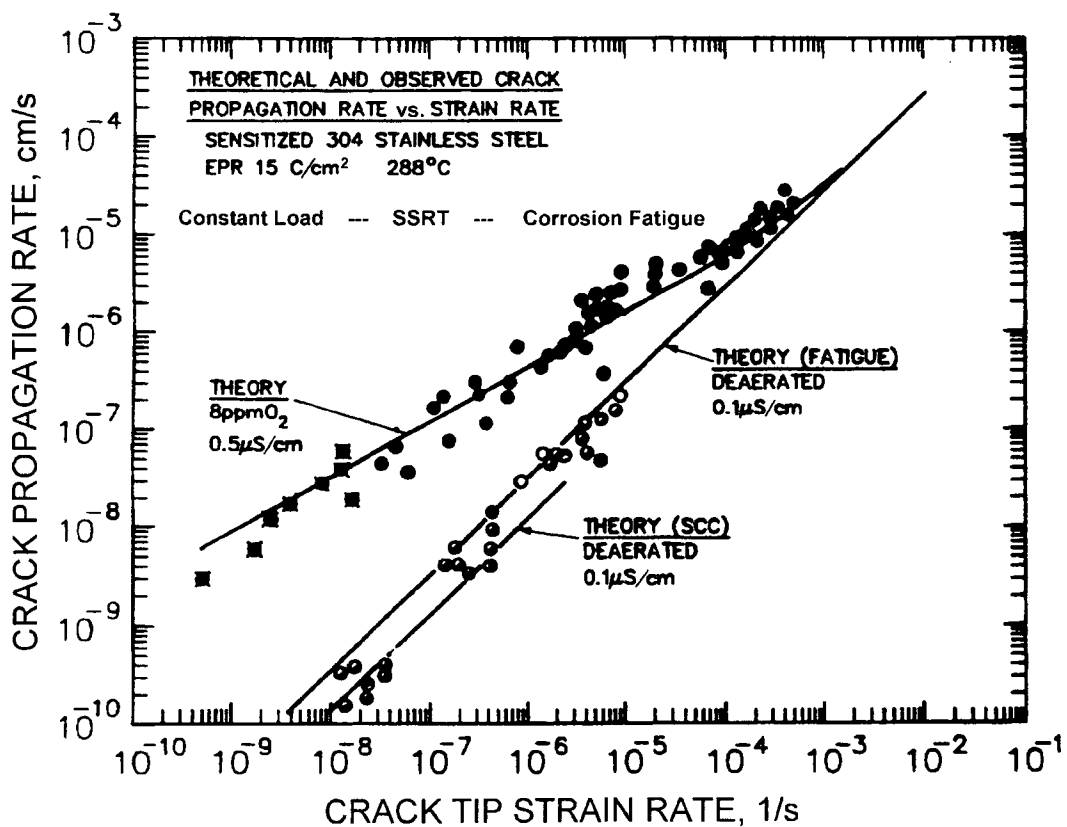


Figure 7-5
 Crack growth rate vs. crack tip strain rate (proportional to K^4) for sensitized stainless steel in water of varying purity. This variation changes the dependency on crack tip strain Rate (i.e., stress intensity) markedly

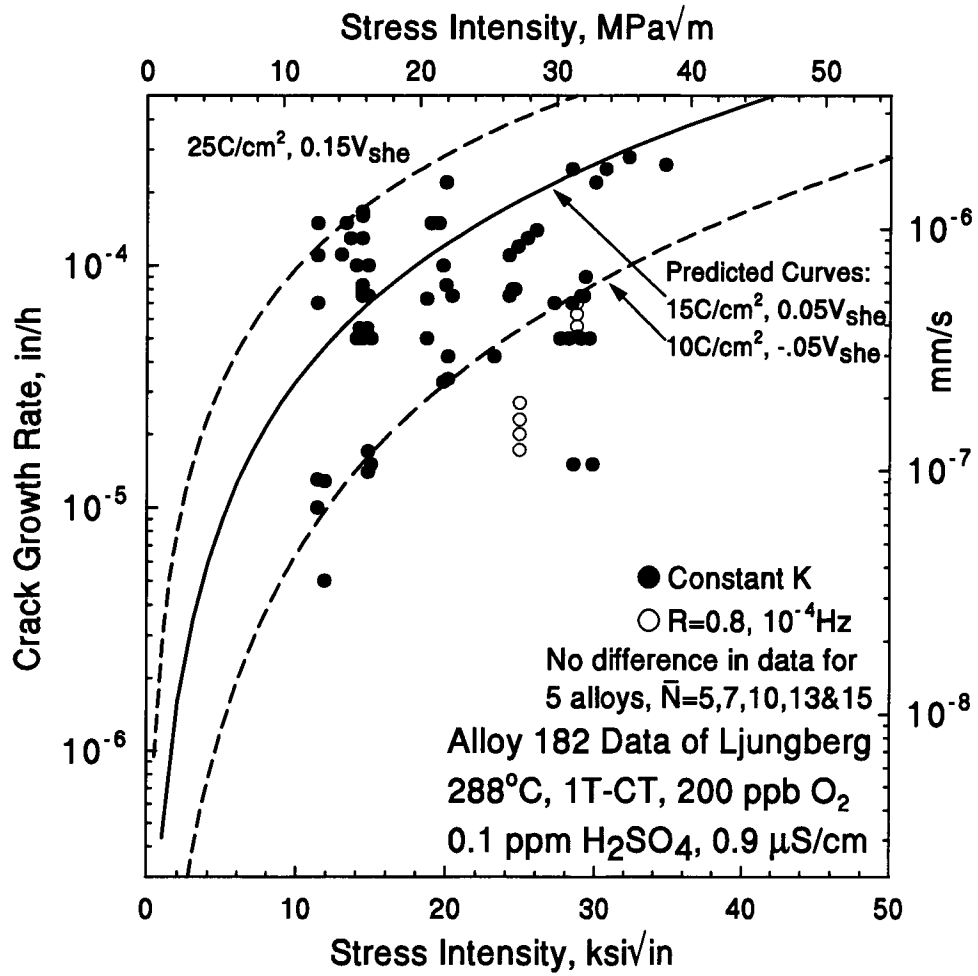


Figure 7-6
The effect of stress intensity on SCC growth rate of alloy 182 weld metal in 288°C water containing 100 ppb sulfate as H₂SO₄, [7-12]

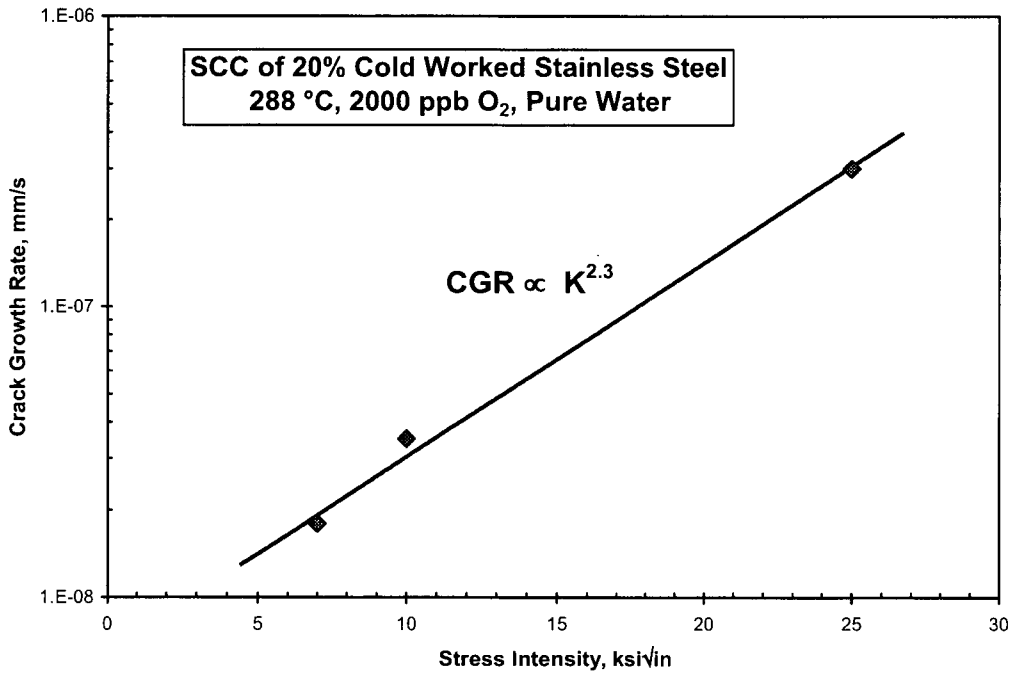
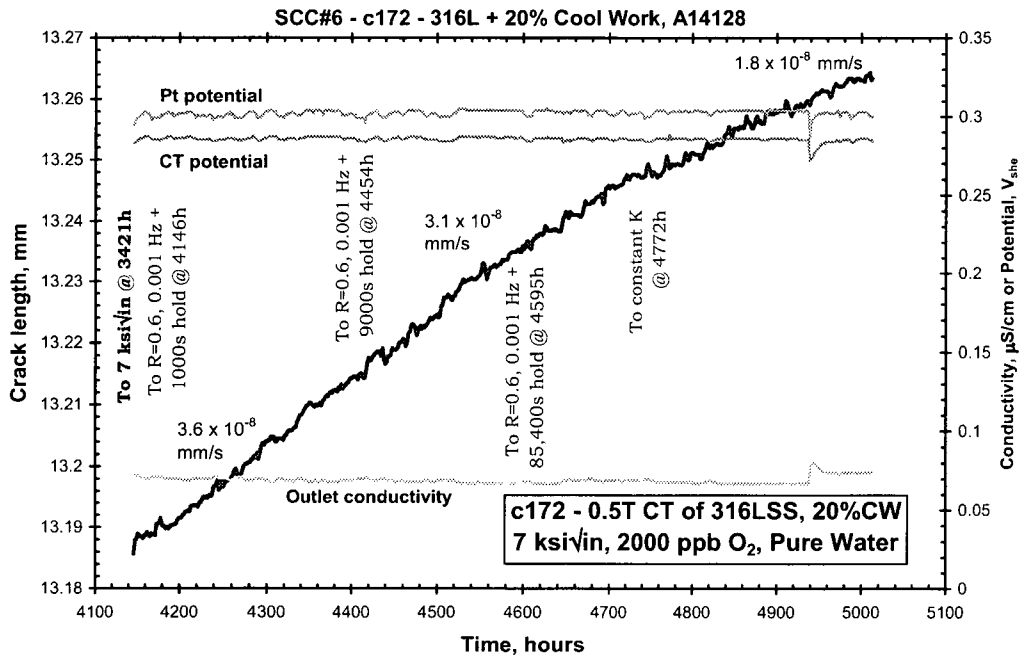


Figure 7-7
Crack length vs. time and the effect of stress intensity on SCC growth rate of cold worked 316L stainless steel in 288°C pure water at high corrosion potential [7-7, 7-13,7-14]

**Content Deleted -
EPRI Proprietary Information**

Figure 7-8
The effect of stress intensity on SCC growth rate of 316NG stainless steel irradiated to 0.9×10^{21} n/cm² in 288°C pure water at high corrosion potential [7-15, 7-16]

**Content Deleted -
EPRI Proprietary Information**

Figure 7-9
The effect of stress intensity on SCC growth rate of 347 stainless steel irradiated to 1.5×10^{21} n/cm² in 288°C pure water at high corrosion potential [7-15, 7-16]

Content Deleted -
EPRI Proprietary Information

Figure 7-10
The effect of stress intensity on SCC growth rate of 304 stainless steel irradiated to 9×10^{21} n/cm^2 in 288°C pure water at high corrosion potential [7-15,7-16]

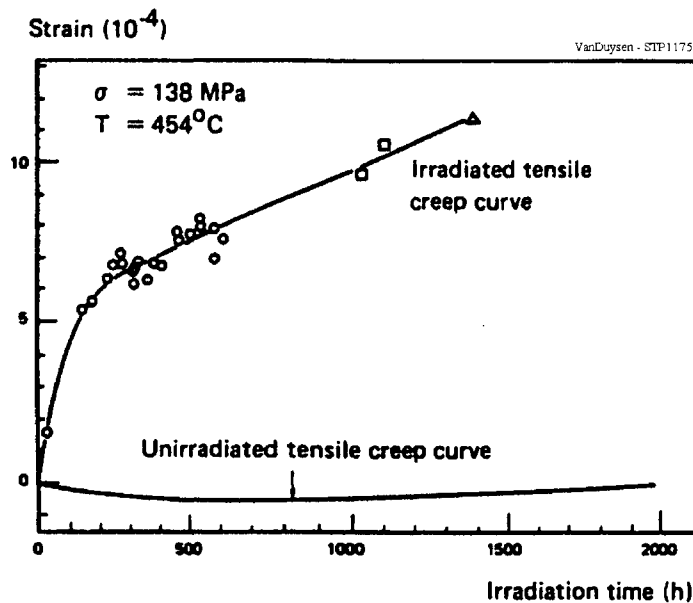


Figure 7-11
Creep strain of 20% cold worked 316 stainless steel with and without radiation (about 10^{15} $n/cm^2\text{-s}$, $E > 0.1 \text{ MeV}$) [7-8, 7-19]. Following a short-term transient, the creep strain at constant load is very linear with fluence (integrated flux over time)

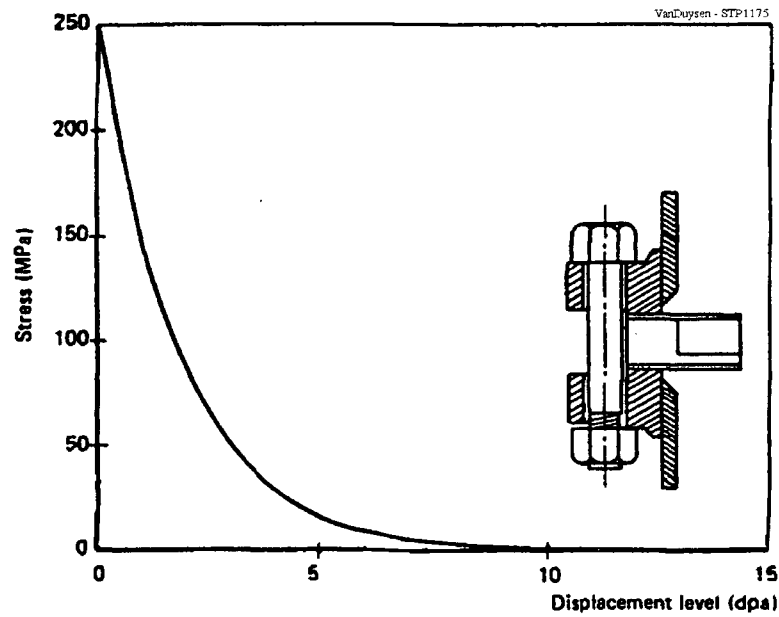


Figure 7-12
Stress relaxation in bolts of 20% cold worked 316 stainless steel initially stressed to 250 MPa and exposed at temperatures between 60 and 400°C [7-19, 7-20]

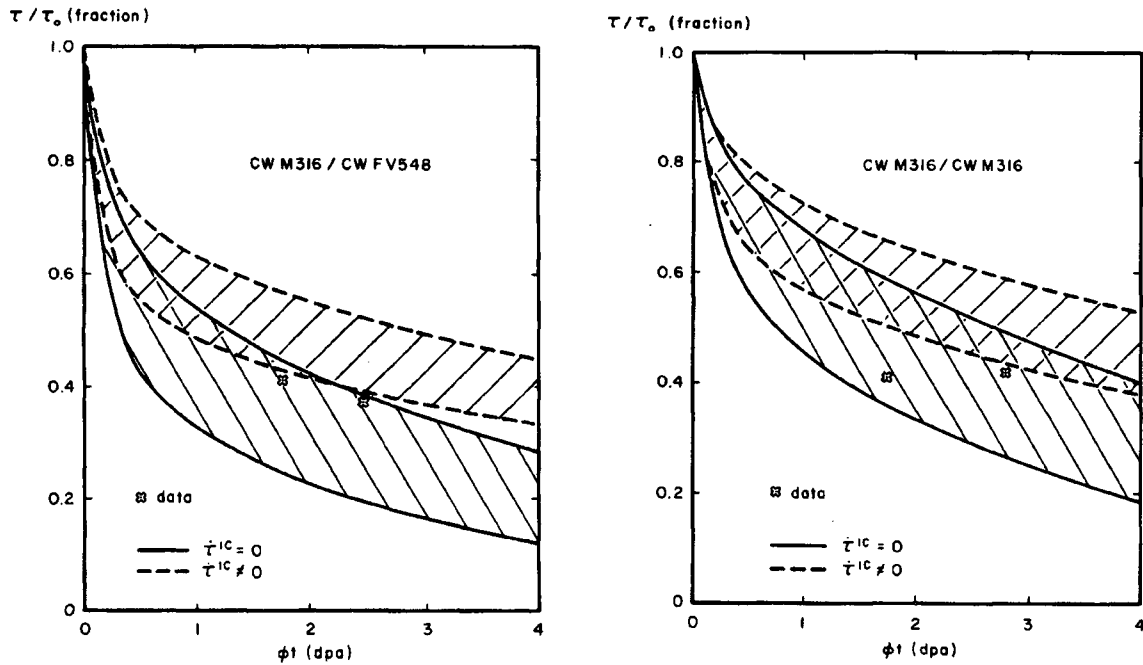


Figure 7-13
Radiation creep relaxation of shear stresses in springs of 20% cold worked 316 stainless steel, along with modeling curves [7-21]

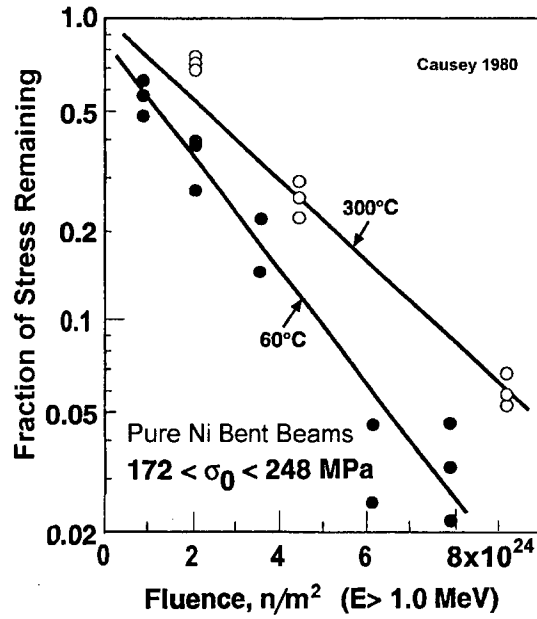


Figure 7-14
Constant curvature bent beams exposed at 60 – 300°C in the chalk river reactor on pure nickel with 50% relaxation occurring at or before the 1 dpa point

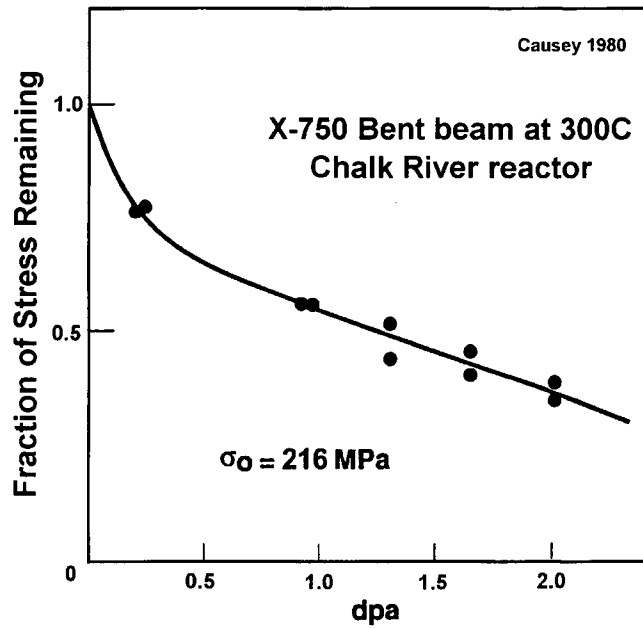


Figure 7-15
Constant curvature bent beams of X-750 exposed at 60 – 300°C in the chalk river reactor

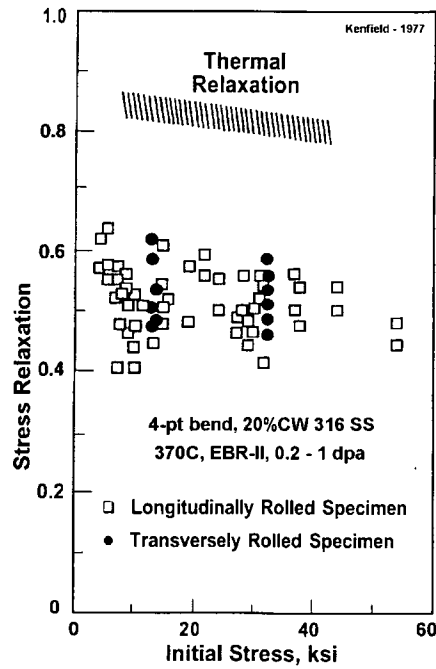


Figure 7-16
stress relaxation in 20% cold worked 316 stainless steel four-point bend beams at 370°C in EBR-II ranging from 4 to 54 ksi and up to 1 dpa. relaxation is independent of stress level

**Content Deleted -
EPRI Proprietary Information**

Figure 7-17
Stress relaxation in wedge-loaded DCB specimens at Halden that exhibited minimal or no crack growth [7-22]

8

PROPOSED DISPOSITION RATES AS A FUNCTION OF FLUENCE AND WATER CHEMISTRY

Beginning in the late 1970s and continuing to the present, General Electric Nuclear Energy (GENE) and the industry have performed crack growth rate studies on the behavior of Type 304 stainless steels. While the majority of these studies were directed at un-irradiated materials, efforts in the 1980s were also conducted in hot cells using irradiated material taken for actual BWR components. These tests were initiated with the objective of developing the ability to disposition crack indications in irradiated BWR in-core components. The previous sections of the report have been focused on presenting the understanding of IGSCC in irradiated materials along with supporting crack growth and field data to provide the underpinnings for the crack growth rates to be used to predict the behavior of materials irradiated above 5×10^{20} n/cm². The report has also provided key field data and laboratory test data to be used in validating the growth rates. Finally, the report has presented technical discussion to support the important role of corrosion potential (ECP), K and stress relaxation in reducing the magnitude of residual stresses that were induced by welding during fabrication. The formulation of the crack growth rate disposition curves that will be used is given in this section along with comparison to the different available data. These curves will be used to predict the rate of crack deepening through the shroud thickness. This section will first describe the approach used in developing the curves. It will then compare the curves to the data, establishing that they bound the large majority of them. Finally, it will define the range of fluence over which these curves are to be used.

8.1 Review of Approach to Disposition Curves

In all previous GENE and BWRVIP efforts to quantify stress corrosion crack growth rates for BWR structural materials, the proposed curves have been related to the stress state, the water chemistry parameters and the material susceptibility. The bases for these dependencies have been discussed in detail by Andresen and Ford in conjunction with others [2-1, 2-9, 2-16, 2-17] in the technical community. These bases, importantly, are broadly accepted. As discussed in Section 2, the behavior of irradiated stainless steel is a natural extension of IGSCC of un-irradiated stainless steel. Therefore, the approach will necessarily include water chemistry and stress dependencies. While it is known that there are material changes that occur with fluence, these are hard to quantify or verify given the very limited set of crack growth rate data on irradiated material. There is also evidence that the levels of sensitization and radiation hardening (the parameters that influence the material susceptibility) will saturate at fluences in the range of 3×10^{21} n/cm² (other factors may surface at or above $\sim 10^{22}$ n/cm² or at higher temperature). The approach in this report follows that used in BWRVIP-59 for austenitic nickel base alloys. The proposed rates focus on each of the two main environments: (1) the high corrosion potential NWC environment present under normal operating conditions and (2) the low corrosion potential HWC environment, applicable to plants with adequate hydrogen injection levels to reduce core oxidizing species so

that the corrosion potential is below -230 mV, SHE (best ensured by using NMCA). Discussion of these curves follow.

8.2 Applicable Range of Fluence

**Content Deleted -
EPRI Proprietary Information**

8.3 Proposed Disposition Curves

**Content Deleted -
EPRI Proprietary Information**

8.3.1 Normal Water Chemistry (NWC)

**Content Deleted -
EPRI Proprietary Information**

**Content Deleted -
EPRI Proprietary Information**

8.3.2 Hydrogen Water Chemistry (HWC)

**Content Deleted -
EPRI Proprietary Information**

8.4 Comparison with Field derived data

**Content Deleted -
EPRI Proprietary Information**

**Content Deleted -
EPRI Proprietary Information**

8.5 Summary

**Content Deleted -
EPRI Proprietary Information**

**Content Deleted -
EPRI Proprietary Information**

Figure 8-1
Proposed NWC curve for stainless steel irradiated between 5×10^{20} to 3×10^{21} n/cm². Applicable to normal operation at or below action level 1 parameters limits

**Content Deleted -
EPRI Proprietary Information**

Figure 8-2
Proposed HWC curve for stainless steel irradiated between 5×10^{20} to 3×10^{21} n/cm². Applicable to normal operation with verified reduction in corrosion potential at or below action level 1 parameter limit

**Content Deleted -
EPRI Proprietary Information**

Figure 8-3
Comparison of calculated K-dependent rates as a function of average normalized depth with the field data plotted against average depth. Note that the K level varies based on the actual shroud thickness. The legend indicates the core shroud thickness

9

EXAMPLE EVALUATIONS OF CRACK GROWTH ASSESSMENT: CORE SHROUD MATERIAL IRRADIATED TO A FLUENCE BETWEEN 5×10^{20} N/CM² AND 3×10^{21} N/CM²

The information developed in the prior sections of this report along with the data from the earlier assessments of crack growth assessment in core shrouds [1-1, 1-2] is utilized in this section to illustrate the manner in which a crack growth analysis will be performed in an H4 weld in a typical BWR core shroud that has been irradiated in a range of 5×10^{20} n/cm² to 3×10^{21} n/cm². This section describes evaluation examples for each of the two key environments: NWC and HWC. The procedures for core shroud crack growth analysis follow those used throughout the industry and presented in BWRVIP-14. Section 9.1 reviews the procedures for determining the amount of through-wall deepening and Sections 9.2 and 9.3 provide examples that illustrate the predicted trajectory of crack deepening with time.

9.1 Evaluation Procedure Review

**Content Deleted -
EPRI Proprietary Information**

9.2 Examples of Crack Growth Depth Predictions in a Irradiated Core Shroud H4 Weld for NWC, Action Level 1 Operating Conditions

The first example employs the NWC curve (Figure 8-1). The parameters used in this example are as follows: the shroud thickness is set at 1.5 inches and a full 360 degrees circumferential, ID flaw is assumed. The initial depth is 0.05 inches, thus allowing one to determine the times required to reach any range of depths. Table 9-1 along with Figure 9-3 present the results for the recommended stress intensity factor (K) distribution shown in Figure 9-1.

9.3 Examples of Crack Growth Depth Predictions in a Irradiated Core Shroud H4 Weld for HWC, Action Level 1 Operating Conditions

The second example employs the proposed HWC curve (Figure 8-2), which is based on a FOI of three reduction in growth rate from the NWC curve. Again, the initial depth is 0.05 inches, thus allowing one to determine times required to reach any range of depths. Tables 9-2 along with Figure 9-3 present the results for this evaluation for the recommended stress intensity factor (K) distribution shown in Figure 9-1.

Table 9-1

**Depth versus time for NWC crack growth rates and recommended K conditions for 1.5
inch thick shroud**

**Content Deleted -
EPRI Proprietary Information**

Table 9-1
Depth versus time for NWC crack growth rates and recommended K conditions for 1.5 inch thick shroud (continued)

**Content Deleted -
EPRI Proprietary Information**

Table 9-2

**Depth versus time for HWC (FOI=3) crack growth rates and recommended K conditions for
1.5 inch thick shroud**

**Content Deleted -
EPRI Proprietary Information**

**Content Deleted -
EPRI Proprietary Information**

Figure 9-1

Stress intensity profile for a 1.5 in thick core shroud based on combined stress distribution which serves as the basis for the crack growth rate determination in example evaluations shown in figure 9-2

Example Evaluations of Crack Growth Assessment: Core Shroud Material Irradiated to a Fluence Between 5×10^{20} N/CM² and 3×10^{21} N/CM²

**Content Deleted -
EPRI Proprietary Information**

Figure 9-2
Normalized stress intensity profile for a core shroud versus normalized crack depth

Example Evaluations of Crack Growth Assessment: Core Shroud Material Irradiated to a Fluence Between 5×10^{20} N/CM² and 3×10^{21} N/CM²

**Content Deleted -
EPRI Proprietary Information**

Figure 9-3
Predictions for crack deepening under NWC and HWC conditions. Calculations made for recommended stress intensity distributions based on (1) combination of 1.6 ksi membrane and BWRVIP-NRC agreed upon weld residual stresses which are relaxed 30%. Predictions are applicable over 5×10^{20} to 3×10^{21} n/cm² fluence range

10

SUMMARY AND CONCLUSIONS

This report achieves its objective of providing new crack growth rates that can be used for irradiated stainless steel that has been subjected to a fluence greater than 5×10^{20} n/cm². In support of that objective, the report provides technical and engineering data as well as specific proposed disposition curves. Key outputs from the report are as follows.

- The report provides an overview of the fundamental basis for the effects of irradiation on crack growth behavior and the benefits of reducing the corrosion potential of the core environment. This is directly tied to the fundamental understanding of stress corrosion cracking processes in austenitic structural materials.
- The report presents supporting data from crack growth measurements made on H4 core shrouds through ultrasonic inspections.
- A summary of relevant laboratory crack growth rate data measured in irradiated stainless steel is given. This data is used as the basis for the proposed disposition curves. These data, developed by GENE and Halden test facilities in BWR-type environments, establish the effects of stress and environment on the measured rates.
- The report also provides a discussion of the importance of plasticity effects on measured crack growth rates. This understanding is needed to effectively screen the existing test data on irradiated stainless steel.
- The report provides a summary of other test data conducted on unirradiated stainless steel. These data strong evidence for the benefits of HWC.
- The report also provides important data and discussion in support of defining the K dependence of the proposed disposition curves.
- The final technical topic discussed is the very important role of irradiation-induced stress relaxation. This factor significantly reduces the driving force for crack growth in irradiated components where the residual stresses make up the main stress component.
- The report proposes two disposition crack growth rate curves for use with stainless steel core components such as the beltline H4 core shroud weld irradiated in the range of 5×10^{20} to 3×10^{21} n/cm². One curve is applicable to NWC conditions (Figure 8-1) and one is applicable to effective HWC condition (Figure 8-2).
- The field data is also used to benchmark the stress distribution that is proposed for use in evaluation efforts of irradiated crack growth.

The disposition curves are used in example calculations to predict crack depth versus time in a H4 core shroud weld for both NWC and HWC environments.

11

REFERENCES

- 1-1 *BWR Vessel and Internals Project, Evaluation of Crack Growth in BWR Stainless Steel RPV Internals (BWRVIP-14)*. March 1996. EPRI Report TR-105873.
- 1-2 *BWR Vessel and Internals Project, Evaluation of Crack Growth in BWR Nickel Base Austenitic Alloys in RPV Internals (BWRVIP-59)*. December 1998. EPRI Report TR-108710.
- 1-3 Safety Evaluation of EPRI Topical Report TR-105873: *BWR Vessel and Internals Project, Evaluation of Crack Growth In BWR Stainless Steel Internals, (BWRVIP-14)*. June 8, 1998.
- 1-4 Final Safety Evaluation of EPRI Topical Report TR-105873: “BWR Vessel and Internals Project, Evaluation of Crack Growth In BWR Stainless Steel Internals, (BWRVIP-14)” (TAC No. M94975), dated December 3, 1999.
- 1-5 *Letter from William A. Eaton to Meena Khanna, PROJECT NO. 704 – BWRVIP Response to NRC Request for Additional Information on BWRVIP-99 dated September 21, 2004 (BWRVIP Correspondence File Number 204-410)*.
- 1-6 EPRI/General Electric Nuclear Energy: Summary of Irradiated Crack Growth Rate Data from Laboratory Testing of Irradiated Stainless Steel Materials, June 2002.
- 2-1 P.L. Andresen, “Irradiation Assisted Stress Corrosion Cracking”, in *Stress Corrosion Cracking: Materials Performance and Evaluation*, Ed. R.H. Jones, ASM, Materials Park, 1992, p.181-210.
- 2-2 P.L. Andresen, F.P. Ford, S.M. Murphy & J.M. Perks, “State of Knowledge of Radiation Effects on Environmental Cracking in Light Water Reactor Core Materials”, *Proc. 4th Int. Conf. on Environmental Degradation of Materials in Nuclear Power Systems - Water Reactors, NACE*, p.1-83 to 1-121, 1990.
- 2-3 F.P. Ford, P.L. Andresen & A.J. Jacobs, “Life Prediction of Irradiated Components Subject to Environmentally Assisted Cracking”, *Int. Symp. On Plant Aging & Life Prediction of Corrodible Structures Sapporo, Japan*, May 15-18, 1995.
- 2-4 International Cooperative Group on Irradiation Assisted Stress Corrosion Cracking (IGC-IASCC), L.J. Nelson, Vice-Chairman, EPRI, Palo Alto, CA.
- 2-5 G.S. Was & P.L. Andresen, “Irradiation Assisted Stress Corrosion Cracking in Austenitic Alloys”, *Journal of Metals*, Vol. 44, No. 2, p. 8-13, April 1992.

References

- 2-6 A.J. Jacobs & G.P. Wozadlo, "Irradiation Assisted Stress Corrosion Cracking As a Factor in Nuclear Power Plant Aging", Proc. Int. Conf. on Nuclear Power Plant Aging, Availability Factor and Reliability Analysis, San Diego, CA, ASM, p.173, 1985.
- 2-7 F. Garzarolli, H. Rubel & E. Steinberg, "Behavior of Water Reactor Core Materials with Respect to Corrosion Attack", Proc. First Int. Symp. on Environmental Degradation of Materials in Nuclear Power Systems - Water Reactors, NACE, 1984, p.1-24.
- 2-8 H. Hanninen & I. Aho-Mantila, "Environment-Sensitive Cracking of Reactor Internals", Proc. Third Int. Symp. on Environmental Degradation of Materials in Nuclear Power Systems - Water Reactors, AIME, 1987, p.77-92.
- 2-9 G.M. Gordon & K.S. Brown, "Dependence of Creviced BWR Component IGSCC Behavior on Coolant Chemistry", Proc. 4th Int. Conf. on Environmental Degradation of Materials in Nuclear Power Systems - Water Reactors, NACE, p.14-46 to 14-62, 1990.
- 2-10 K.S. Brown & G.M. Gordon, "Effects of BWR Coolant Chemistry on the Propensity for IGSCC Initiation and Growth in Creviced Reactor Internals Components", Proc. Environmental Degradation of Materials in Nuclear Power Systems - Water Reactors, AIME, p.243-248, 1987.
- 2-11 A.J. Jacobs, D.A. Hale & M. Siegler, Unpublished Data, GE Nuclear Energy, San Jose, CA, January 1986.
- 2-12 T.M. Angeliu, P.L. Andresen, J.A. Sutliff and R.M. Horn, "Intergranular Stress Corrosion Cracking of Unsensitized Stainless Steels in BWR Environments", Proc. Ninth Int. Symp. on Environmental Degradation of Materials in Nuclear Power Systems - Water Reactors, AIME, 1999.
- 2-13 P.L. Andresen, T.M. Angeliu, W.R. Catlin, L.M. Young and R.M. Horn, "Effect of Deformation on SCC of Unsensitized Stainless Steel", Corrosion/2000, Paper 00203, NACE, 2000.
- 2-14 "Standard Test Method for Plane Strain Fracture Toughness of Metallic Materials", E399-90 (re-approved 1997), 1997 Annual Book of ASTM Standards, Volume 03.01, ASTM, 1997. Also, "Standard Test Method for Constant Load Amplitude Fatigue Crack Growth Rates Above 10^{-8} m/cycle", E647-95a, 1997 Annual Book of ASTM Standards, Volume 03.01, ASTM, 1997. Other ASTM standards also apply.
- 2-15 F.P. Ford, D.F. Taylor, P.L. Andresen & R.G. Ballinger, *Corrosion Assisted Cracking of Stainless and Low Alloy Steels in LWR Environments*. EPRI Contract RP2006-6, February 1987. Report NP5064M.
- 2-16 P.L. Andresen & F.P. Ford, "Life Prediction by Mechanistic Modelling and System Monitoring of Environmental Cracking of Fe and Ni Alloys in Aqueous Systems", *Mat'l's Sci. and Eng.*, A103, p.167-183, 1988.

- 2-17 F.P. Ford & P.L. Andresen, "Corrosion in Nuclear Systems: Environmentally Assisted Cracking in LWRs", in Corrosion Mechanisms, Ed. P. Marcus & J. Ouder, Marcel Dekker, p.501-546, 1994.
- 2-18 P.L. Andresen, "Conceptual Similarities and Common Predictive Approaches for SCC in High Temperature Water Systems", Paper 96258, Corrosion/96, NACE, 1996.
- 2-19 P.L. Andresen, "Effect of Noble Metal Coating & Alloying on the Stress Corrosion Crack Growth Rate of Stainless Steel in 288 C Water", Proc. Sixth Int. Symp. on Environmental Degradation of Materials in Nuclear Power Systems - Water Reactors, AIME, 1994, p.245-253.
- 2-20 S.M. Bruemmer, B.W. Arey & L.A. Charlot, "Grain Boundary Chromium Concentration Effects on the IGSCC and IASCC of Austenitic Steels", Proc. Sixth Int. Symp. on Environmental Degradation of Materials in Nuclear Power Systems - Water Reactors, AIME, 1994, p.277-285.
- 2-21 P.L. Andresen & L.M. Young, "Characterization of the Roles of Electrochemistry, Convection & Crack Chemistry in SCC", Proc. Seventh Int. Symp. on Environmental Degradation of Materials in Nuclear Power Systems - Water Reactors, NACE, p.579-596, 1995.
- 2-22 P.L. Andresen, "Effects of Flow Rate on SCC Growth Rate Behavior in BWR Water", 8th Int. Symp. on Environmental Degradation of Materials in Nuclear Power Systems - Water Reactors, ANS, 1997.
- 2-23 A.J. Jacobs & G.P. Wozadlo, "Stress Corrosion Testing of Irradiated Type 304 Stainless Steel Under Constant Load", Paper #41, Corrosion/91, NACE, Houston, 1991.
- 2-24 A.J. Jacobs, R.E. Clausing, M.K. Miller & C. Shepherd, "Influence of Grain Boundary Composition on the IASCC Susceptibility of Type 348 Stainless Steel", Proc. Fourth Int. Conf. on Environmental Degradation of Materials in Nuclear Power Systems - Water Reactors, NACE, p.14-21 to 14-45, 1990.
- 2-25 K.S. Brown, G.M. Gordon, and P.L. Andresen, "Modeling of Creviced Alloy 600 Shroud Head Bolt SCC Field Experience", Proc. Life Prediction of Corrodible Structures, Hawaii, November 1991, NACE, Houston.
- 2-26 T. Yonezawa et al., "SCC Susceptibility of Irradiated Austenitic Stainless Steels for PWR", Proc. Eighth Int. Symp. on Environmental Degradation of Materials in Nuclear Power Systems - Water Reactors, ANS, p.823, 1997.
- 2-27 "In-reactor Stress Corrosion Monitor Prototype Development, Installation and Operation", Final Report by GENE/GECRD, EP85-37, ESEERCO, Feb. 1988. (NEDC 31319).
- 4-1 EPRI NP-7200 SL, dated March 1991.

References

- 4-2 *BWR Vessel and Internals Project, BWR Water Chemistry Guidelines-2000 Revision, (BWRVIP-79)*. February 2000. EPRI Report TR-103515-R2.
- 5-1 ASTM “Standard Test Method for Plane Strain Fracture Toughness of Metallic Materials”, E399-90 (re-approved 1997), 1997 Annual Book of ASTM Standards, Volume 03.01, ASTM, 1997.
- 5-2 “Standard Test Method for Constant Load Amplitude Fatigue Crack Growth Rates Above 10^{-8} m/cycle”, E647-95a, 1997 Annual Book of ASTM Standards, Volume 03.01, ASTM, 1997.
- 5-3 “Standard Test Method for J_{IC} , a Measure of Fracture Toughness”, E813-89, 1997 Annual Book of ASTM Standards, Volume 03.01, ASTM, 1997.
- 5-4 “Standard Test Method for Determining a Threshold Stress Intensity Factor for Environment-Assisted Cracking of Metallic Materials Under Constant Load”, E1681-95, 1997 Annual Book of ASTM Standards, Volume 03.01, ASTM, 1997.
- 5-5 GE Proprietary IASCC Growth Rate Data on Irradiated Type 304 Stainless Steel, “Prediction Methodology for Stress Corrosion Cracking of BWR Core Components”, 1988.
- 5-6 T.M. Karlsen and E. Hauso, “Qualification and Application of Instrumented Specimens for In-core Studies on Cracking Behavior of Austenitic Stainless Steels”, Proc. 9th Int. Symp. On Environmental Degradation of Materials in Nuclear Power System – Water Reactors, TMS, p. 951, 1999.
- 5-7 Proprietary Halden Test Reactor Report HWR-473, “Final report on IFA-586, 605; water chemistry and crack behavior”, April 1996. See also Report HWR-427, “Analysis of irradiated steel from IASCC rigs IFA-586, 605”, September 1995.
- 5-8 Proprietary Halden Test Reactor Report HWR-630, “Analysis of CGR data from IFA-586, 605, 611”, February 2000.
- 5-9 Proprietary Halden Test Reactor Report HWR-675, “Crack growth behavior of irradiated specimens in IFA-639”, February 2001.
- 5-10 “In-reactor Stress Corrosion Monitor Prototype Development, Installation and Operation”, Final Report by GENE/GECD, EP85-37, ESEERCO, Feb. 1988. (NEDC 31319).
- 5-11 P.L. Andresen and F.P. Ford, “Modeling of Irradiation Effects on Stress Corrosion Crack Growth Rates”, Paper 89497, Corrosion/89, NACE, 1989.

- 5-12 P.L. Andresen, F.P. Ford, S.M. Murphy, J.M. Perks, "State of Knowledge of Radiation Effects on Environmental Cracking in Light Water Reactor Core Materials", Invited Review Paper, Proc. Fourth International Symposium on Environmental Degradation of Materials in Nuclear Power Systems – Water Reactors, NACE, pp. 1-83 to 1-121, 1990.
- 5-13 P.L. Andresen, "Irradiation Assisted Stress Corrosion Cracking", in Stress Corrosion Cracking: Materials Performance and Evaluation, Ed. R.H. Jones, ASM, p.181-210, 1992.
- 5-14 S.M. Bruemmer et al, Final Report on Cooperative IASCC Research Program, 2000.
- 5-15 G.R. Odett and G.E. Lucas, "The Effects of Intermediate Temperature Irradiation on the Mechanical Behavior of 300-Series Austenitic Stainless Steels", J of Nuclear Mat'ls 179-181, p.572-576, 1991.
- 6-1 F.P. Ford and P.L. Andresen, "Corrosion in Nuclear Systems: Environmentally Assisted Cracking in Light Water Reactors", in Corrosion Mechanisms, Ed. P. Marcus and J. Ouder, Marcel Dekker, p.501-546, 1994.
- 6-2 P.L. Andresen and F.P. Ford, "Life Prediction by Mechanistic Modelling and System Monitoring of Environmental Cracking of Fe and Ni Alloys in Aqueous Systems", Materials Science and Engineering, A103, pp.167-183, 1988.
- 6-3 F.P. Ford, D.F. Taylor, P.L. Andresen and R.G. Ballinger, *Corrosion Assisted Cracking of Stainless and Low Alloy Steels in LWR Environments*. EPRI Contract RP2006-6, February 1987. Report NP5064M.
- 6-4 P.L. Andresen, "Conceptual Similarities and Common Predictive Approaches for SCC in High Temperature Water Systems", Paper 96258, Corrosion/96, NACE, 1996.
- 6-5 P.L. Andresen, F.P. Ford, S.M. Murphy, J.M. Perks, "State of Knowledge of Radiation Effects on Environmental Cracking in Light Water Reactor Core Materials", Proc. 4th Int. Symp. on Environmental Degradation of Materials in Nuclear Power Systems – Water Reactors, NACE, pp. 1-83 to 1-121, 1990.
- 6-6 P.L. Andresen and L.M. Young, "Characterization of the Roles of Electrochemistry, Convection and Crack Chemistry in Stress Corrosion Cracking", Proc. 7th Int. Symp. on Environmental Degradation of Materials in Nuclear Power Systems - Water Reactors, NACE, p.579-596, 1995.
- 6-7 P.L. Andresen and F.P. Ford, "Response to 'On the Modeling of Stress Corrosion Cracking of Iron and Nickel Base Alloys in High Temperature Aqueous Environments' ", Corrosion Science Vol. 38, p.1011-1016, 1996.
- 6-8 G.R. Engelhardt, D.D. Macdonald, and M. Urquidi- Macdonald, "Development of Fast Algorithms for Estimating Stress Corrosion Crack Growth Rate", Corrosion Science 41, p. 2267-2302, 1999 (see p.2288).

References

- 6-9 R.C. Newman, "Stress Corrosion of Austenitic Steels", Proc. of 1st Int. Conf. on "Environment Induced Cracking of Metals", Kohler, NACE, pp. 489-510, 1988.
- 6-10 K. Sieradzki, "Atomistic and Micromechanical Aspects of Environment Induced Cracking of Metals", Kohler, NACE, p 125-138, 1988.
- 6-11 P.M. Scott, "An Overview of Internal Oxidation as a Possible Explanation of Intergranular SCC of Alloy 600 in PWRs", Proc. Ninth Int. Symp. on Environmental Degradation of Materials in Nuclear Power Systems - Water Reactors, AIME, p.3-14, 1999.
- 6-12 Hydrogen Degradation of Ferrous Alloys, Eds. R.A. Oriani, J.P. Hirth & M. Smialowski, Noyes Publ., 1985.
- 6-13 J.R. Galvele, "Surface Mobility Mechanism of SCC", Parkins Symp. on "Fundamental Aspects of Stress Corrosion Cracking", Ed. by S.M. Bruemmer et al., AIME, p.85-102, 1992.
- 6-14 R.N. Parkins, "Mechanistic Aspects of SCC", Parkins Symp. on "Fundamental Aspects of Stress Corrosion Cracking", Ed. by S.M. Bruemmer et al., AIME, p.3-42, 1992.
- 6-15 Hydrogen Effects in Metals, Eds. I.M. Bernstein and A.W. Thompson, TMS-AIME, 1981.
- 6-16 C.L. Briant, "Hydrogen Assisted Cracking of Type 304 Stainless Steel", Met Trans A, 10A, p.181, 1979.
- 6-17 D. Symons, "Effect of Hydrogen on Fracture Toughness of Alloy X750 at Elevated Temperature," J. of Nuclear Materials, Vol. 265, No. 3, p.225-231, 1999.
- 6-18 P.L. Andresen and C.L. Briant, "Environmentally Assisted Cracking of Types 304L/316L/316NG Stainless Steel in 288°C Water," Corrosion, Vol. 45, pp. 448-463, 1989.
- 6-19 P.L. Andresen and C.L. Briant, "Role of S, P and N Segregation on Intergranular Environmental Cracking of Stainless Steels in High Temperature Water," Proc. 3rd Int. Symp. on Environmental Degradation of Materials in Nuclear Power Systems - Water Reactors, AIME, pp. 371-382, 1988.
- 6-20 P.L. Andresen, "Environmentally Assisted Growth Rate Response of Nonsensitized AISI 316 Grade Stainless Steels in High Temperature Water," Corrosion 44, 7, p. 450, 1988.
- 6-21 P.L. Andresen, "The Effects of Aqueous Impurities on Intergranular Stress Corrosion Cracking of Sensitized Type 304 Stainless Steel," Final Report NP3384 Contract T115-3, EPRI, 1983. See also, "Innovations in Experimental Techniques for Testing in High Temperature Aqueous Environments," Report No. 81CRD088, GE-CRD, Schenectady, New York, 1981.

- 6-22 L.W. Niedrach, "A New Membrane Type pH Sensor for Use in High Temperature High Pressure Water", J. Electrochem. Soc. 127, p. 2122, 1980.
- 6-23 D.S. Morton, S.A. Attanasio, G.A. Young, P.L. Andresen, and T.M. Angeliu, "The Influence of Dissolved Hydrogen on Nickel Alloy SCC: A Window to Fundamental Insight", Corrosion, Paper 01117, NACE, 2001.
- 6-24 P.L. Andresen, T.M. Angeliu and L.M. Young, "Immunity, Thresholds, and Other SCC Fiction", Proc. Staehle Symp. on Chemistry and Electrochemistry of Corrosion and SCC, TMS, Feb. 2001.
- 6-25 P.L. Andresen, K. Gott and J.L. Nelson, "Stress Corrosion Cracking of Sensitized Type 304 Stainless Steel in 288C Water: A Five Laboratory Round Robin", Proc. Ninth Int. Symp. on Environmental Degradation of Materials in Nuclear Power Systems - Water Reactors, AIME, 1999.
- 6-26 P.L. Andresen, T.M. Angeliu, W.R. Catlin, L.M. Young and R.M. Horn, "Effect of Deformation on SCC of Unsensitized Stainless Steel", Corrosion/2000, Paper 00203, NACE, 2000.
- 6-27 P.L. Andresen, T.M. Angeliu and L.M. Young, "Effect of Martensite & Hydrogen on SCC of Stainless Steels", Paper #01228, Corrosion/01, NACE, 2001.
- 6-28 P.L. Andresen, "SCC Testing and Data Quality Considerations", Ninth Int. Symp on Environmental Degradation of Materials in Nuclear Power Systems - Water Reactors, AIME, 1999. See also, P.L. Andresen, "Experimental Quality Guidelines for SCC Testing", GE CRD, January 30, 1998.
- 6-29 T.M. Angeliu, P.L. Andresen, J.A. Sutliff and R.M. Horn, "Intergranular Stress Corrosion Cracking of Unsensitized Stainless Steels in BWR Environments", Proc. 9th Int. Symp. on Environmental Degradation of Materials in Nuclear Power Systems - Water Reactors, AIME, p.311-318, 1999.
- 6-30 P.L. Andresen, T.M. Angeliu, P.W. Emigh, L.M. Young and R.M. Horn, "Crack Growth Rate Behavior of Ni Alloys", Corrosion/2000, Paper 00202, NACE, 2000.
- 6-31 T.M. Angeliu, P.L. Andresen, and M.L. Pollick, "Repassivation and Crack Propagation of Alloy 600 in 288°C Water", Corrosion 53, p.114, 1997.
- 6-32 D.S. Morton, S.A. Attanasio, J.S. Fish, and M.K. Schurman, "Influence of Dissolved Hydrogen on Nickel Alloy SCC in High Temperature Water", Corrosion/99, Paper 99447, NACE, 1999.
- 6-33 A.J. Jacobs, "Hydrogen Buildup in Irradiated Type 304 Stainless Steel", 13th Symp. Radiation Induced Changes in Microstructure, Eds. F.A. Garner, N.H. Packan & A.S. Kumar, STP 956, Vol. II, ASTM, Phila., 1985, p.239.

References

- 6-34 P.L. Andresen and T.M. Angeliu, "Evaluation of the Role of Hydrogen in SCC in Hot Water", Paper #97197, Corrosion/97, NACE, 1997.
- 6-35 F. Garner, personal communication, Battelle Pacific Northwest National Lab, Richland, WA, May 2000.
- 6-36 C.A. Grove and L.D. Petzold, "Mechanism of SCC of Alloy X750 in High Purity Water", J. of Materials for Energy Systems, Vol. 7, No. 2, p.147-162, Sept 1985.
- 6-37 L.D. Petzold and C.A. Grove, "Mechanism of SCC of Alloy X750 in High Purity Water", Proc. of Corrosion of Nickel Alloys, Ed. R.C. Scarberry, ASM, 1985, p.165.
- 6-38 K. Tsutsumi, et al, "Fatigue Life Reduction in PWR Water Environments for Stainless Steel", PVP Conf. Volume 410-2, ASME, p.23-34, 2000.
- 6-39 T.M. Angeliu, P.L. Andresen, E. Hall, J.A. Sutliff, S. Sitzman, "Strain and Microstructure Characterization of Austenitic Stainless Steel Weld HAZs", Corrosion/2000, Paper 00186, NACE, 2000.
- 7-1 "Technical Report on Materials Selection and Processing Guidelines for BWR Coolant Boundary Piping - Final Report," NUREG-0313, Rev. 2, U.S. Nuclear Regulatory Commission, January 1988.
- 7-2 R. Magdowski and M.O. Speidel, "Effect of Cold Work on the Growth Rates of SCC in Structural Materials of Nuclear Systems", Paper #112, Corrosion/96, NACE, 1996.
- 7-3 M.O. Speidel and R. Magdowski, "SCC of Nickel Base Alloys in High Temperature Water", Proc. Sixth Int. Symp. on Environmental Degradation of Materials in Nuclear Power Systems – Water Reactors, NACE, p.361, 1993.
- 7-4 P.L. Andresen, "SCC Testing and Data Quality Consideration", Proc. Ninth Int. Symp. on Environmental Degradation of Materials in Nuclear Power Systems –Water Reactors, AIME, 1999.
- 7-5 P.L. Andresen, K. Gott and J.L. Nelson, "Stress Corrosion Cracking of Sensitized Type 304 Stainless Steel in 288C Water: A Five Laboratory Round Robin", Proc. Ninth Int. Symp. on Environmental Degradation of Materials in Nuclear Power Systems – Water Reactors, AIME, 1999.
- 7-6 P.L. Andresen, "Experimental Quality Guidelines for SCC Testing", GE CRD, January 30, 1998.
- 7-7 P.L. Andresen, "Perspective and Direction of Stress Corrosion Cracking in Hot Water", Proc. Tenth Int. Symp. on Environmental Degradation of Materials in Nuclear Power Systems - Water Reactors, NACE, 2001.

- 7-8 F.P. Ford and P.L. Andresen, "Corrosion in Nuclear Systems: Environmentally Assisted Cracking in Light Water Reactors", in *Corrosion Mechanisms*, Ed. P. Marcus and J. Ouder, Marcel Dekker, p.501-546, 1994.
- 7-9 P.L. Andresen and F.P. Ford, "Life Prediction by Mechanistic Modelling and System Monitoring of Environmental Cracking of Fe and Ni Alloys in Aqueous Systems", *Mat'l Sci. & Eng.*, A103, p.167-183, 1988.
- 7-10 F.P. Ford, D.F. Taylor, P.L. Andresen and R.G. Ballinger, "Corrosion Assisted Cracking of Stainless and Low Alloy Steels in LWR Environments", EPRI Contract RP2006-6, Report NP5064M, February 1987.
- 7-11 P.L. Andresen, F.P. Ford, S.M. Murphy, J.M. Perks, "State of Knowledge of Radiation Effects on Environmental Cracking in Light Water Reactor Core Materials", Proc. 4th Int. Symp. on Environmental Degradation of Materials in Nuclear Power Systems – Water Reactors, NACE, pp. 1-83 to 1-121, 1990.
- 7-12 L. G. Ljungberg, D. Cubicciotti, and M. Trolle, "Crack Propagation in Alloys 600 and 182 in Simulated BWR Environment", Eighth Int. Symp. on Environmental Degradation of Materials in Nuclear Power Systems – Water Reactors, ANS, p.226, 1997. See also L. G. Ljungberg, "Stress Corrosion Cracking of Alloys 600 and 182 in BWRs, Volume 1," SD 94-1103, ABB Atom Interim Report, September 1994.
- 7-13 P.L. Andresen, T.M. Angeliu and L.M. Young, "Immunity, Thresholds, and Other SCC Fiction", Proc. Staehle Symp. on Chemistry and Electrochemistry of Corrosion and SCC, TMS, Feb. 2001.
- 7-14 P.L. Andresen, T.M. Angeliu, L.M. Young, W.R. Catlin, and R.M. Horn, "Mechanisms and Kinetics of SCC in Stainless Steels", Proc. Tenth Int. Symp. on Environmental Degradation of Materials in Nuclear Power Systems – Water Reactors, NACE, 2001.
- 7-15 "Crack Growth Behavior Of Irradiated Specimens in IFA-639", Proprietary Report HWR-675, Halden, February 2001
- 7-16 "Minutes Of IASCC Meeting 25 May 2000", Proprietary Report HWR-631, Halden, June 2000.
- 7-17 R.B. Davis, "Crack Growth of Irradiated Stainless Steel in 288°C to 340°C Water", Final Report, EPRI/CIR Program, to be completed in 2001.
- 7-18 E.R. Gilbert, D.C. Kaulitz, and J.J. Holmer, Proc of BNES Conf. On Embrittlement and Creep in Fuel Cladding and Box Components, BNES, London, p.239, 1972.
- 7-19 J.C. Van Duysen, P. Todeschini and Guy Zacharie, "Effects of Neutron Irradiations at Temperatures below 500°C on the Properties of Cold Worked 316 Stainless Steels: A Review", Proc. *Effects of Radiation on Materials: 16th Int. Symp*, ASTM 1175, p.747, 1993.

References

- 7-20 M.L. Brossbeck and L.K. Mansur, *J of Nuclear Materials*, Vol. 179-181, p.130, 1991.
- 7-21 J.P. Foster, "Analysis of In-reactor Stress Relaxation Using Irradiation Creep Models", *Proc. Irradiation Effects on the Microstructure and Properties of Metals*, ASTM STP611, p.32, 1976.
- 7-22 "Final Report On IFA-586, 605; Water Chemistry And Crack Behavior", Proprietary Final Report HWR-473, Halden, April 1996.
- 8-1 Letter from Carl Terry (BWRVIP Chairman) to Meena Khanna (NRC), Project 704-Errata Sheet and Revised Figures for BWRVIP-99 dated August 6, 2002 (BWRVIP Correspondence File Number 2002-219).

A

NRC SAFETY EVALUATION

**Enter Appendix Deleted -
EPRI Proprietary Information**

B

RECORD OF REVISIONS

BWRVIP-99-A	<p>Information from the following documents was used in preparing the changes included in this report:</p> <ol style="list-style-type: none">1. <i>BWRVIP-99: BWR Vessel and Internals Project, Crack Growth Rates in Irradiated Stainless Steels in BWR Internal Components</i>. EPRI, Palo Alto, CA: 2001. 1003018.2. Letter from Carl Terry (BWRVIP Chairman) to Meena Khanna (NRC), Project 704- Errata Sheet and Revised Figures for BWRVIP-99 dated August 6, 2002 (BWRVIP Correspondence File Number 2002-219)3. Letter from Meena Khanna (NRC) to Carl Terry (BWRVIP Chairman), "Proprietary Request for Additional Information – Review of BWR Vessel and Internals Project Reports, BWRVIP-96, -97, -99, and -100 (TAC NOS. MB3947, MD3948, MB3951, and MB3946)," dated January 8, 2003 (BWRVIP Correspondence File Number 2003-022)4. Letter from William A. Eaton to Meena Khanna, PROJECT NO. 704 – BWRVIP Response to NRC Request for Additional Information on BWRVIP-99 dated September 21, 2004 (BWRVIP Correspondence File Number 2004-410).5. Letter from William H. Bateman (NRC) to Bill Eaton (BWRVIP Chairman), "Proprietary Safety Evaluation of EPRI Report, BWR Vessel and Internals Project, Growth Rates in Irradiated Stainless Steels in BWR Internal Components (BWRVIP-99)" (TAC NO. MB3951)", dated August 5, 2005, (BWRVIP Correspondence File Number 2005-295A). <p>Details of the revisions can be found in Table B-1.</p>
-------------	--

Table B-1
Revision details

Required Revision	Source of Requirement for Revision	Description of Revision Implementation
Revised Report Summary	Editorial	Revised lead paragraph and referenced NRC Safety Evaluation and edited Results section.
Revised Executive Summary	Editorial	Revised lead paragraph and referenced NRC Safety Evaluation
Revised text in Section 3.3 and revised Figure 3-13	RAI 99-4	Data in Figure 3-13 were reported based on average normalized depth instead of initial normalized depth as requested in the RAI.
Revised text in Section 4.4, added data Tables 4-1, 4-2, 4-3 and 4-4 and revised Figures 4-4 and 4-5.	RAI 99-1	<p>Added discussion of criteria used to screen data.</p> <p>As noted in the RAI response (BWRVIP Correspondence File Number 2004-410) the data include corrections that were transmitted via BWRVIP Correspondence File Number 2002-219 as well as post test corrections based on fractography performed on Halden specimens.</p> <p>Added data tables summarizing the fluence levels, material, environmental and loading conditions used in the crack growth tests on irradiated materials.</p> <p>Provided the fluence levels for the corrected data shown in Figures 4-4 and 4-5.</p>
Revised Figure 5-7	RAI 99-1	Provided the fluence levels for the corrected data shown in Figure 5-7. (same as Figure 4-4).
Revised text in Section 8.3	RAI 99-3	Revised text to explain the basis for the proposed step function response of crack growth rates to fluence levels below 5.0×10^{20} n/cm ² and in the range of $5 - 30 \times 10^{20}$ n/cm ²
Revised text in Section 8.3.1	RAI 99-2	Revised text to compare the corrected crack growth rate data with the proposed disposition curve.
Revised text in Section 8.3.2	RAI 99-2	Revised text to compare the corrected crack growth rate data with the proposed disposition curve.

Table B-1
Revision details (continued)

Required Revision	Source of Requirement for Revision	Description of Revision Implementation
Revised text in Section 8.4, revised Figures 8-1, 8-2 and 8-3.	99-4	<p>Figures 8-1 and 8-2 are identical to Figures 4-4 and 4-5 and include the fluence levels and data corrections discussed in the RAI response 2004-410.</p> <p style="text-align: center;">Content Deleted – EPRI Proprietary Information</p>
Revised text in Section 9.1 and added Figure 9-1a.	99-5	Added new Figure 9-1a to show the stress intensity (K) profile for a 1.5 in thick core shroud which was the basis for the crack growth rate determination in the example shown in Figure 9-3 (which is the same as Figure 9-2 in the original report).
Revised Table 9-1.	99-5	The revised Table 9-1 shows the K distribution and crack depths for a 1.5 inch thick core shroud and is consistent with Figure 9-3. It corrects Table 9-1 in the original report. Table 9-2 and Figure 9-2 of the original report are unchanged.
Revised text in Section 9.2	Editorial	Referenced new Figure 9-1.
Revised text in Section 9.2	Editorial	Referenced new Figure 9-1.


The Electric Power Research Institute (EPRI), with major locations in Palo Alto, California; Charlotte, North Carolina; and Knoxville, Tennessee, was established in 1973 as an independent, nonprofit center for public interest energy and environmental research. EPRI brings together members, participants, the Institute's scientists and engineers, and other leading experts to work collaboratively on solutions to the challenges of electric power. These solutions span nearly every area of electricity generation, delivery, and use, including health, safety, and environment. EPRI's members represent over 90% of the electricity generated in the United States. International participation represents nearly 15% of EPRI's total research, development, and demonstration program.

Together...Shaping the Future of Electricity

Program:

Nuclear Power

© 2007 Electric Power Research Institute (EPRI), Inc. All rights reserved. Electric Power Research Institute, EPRI, and TOGETHER...SHAPING THE FUTURE OF ELECTRICITY are registered service marks of the Electric Power Research Institute, Inc.

 Printed on recycled paper in the United States of America

1016566NP

Electric Power Research Institute

3420 Hillview Avenue, Palo Alto, California 94304-1338 • PO Box 10412, Palo Alto, California 94303-0813 USA
800.313.3774 • 650.855.2121 • askepri@epri.com • www.epri.com